Thevenin Impedance for voltage stability

Estimation of the Thevenin Impedance in Power Transmission Systems

Master thesis

Institut für Elektrische Anlagen
Technische Universität Graz

Vorgelegt von
Stefan Polster

Betreuer/BetreuerIn
Ao. Univ.-Prof. DI Dr. techn. Herwig Renner(TU Graz)
Univ.-Prof. MSc PhD Kjetil Uhlen(NTNU, Trondheim)

Head of Institute: Univ.-Prof. DI Dr.techn. Lothar Fickert

A - 8010 Graz, Inffeldgasse 18-I
Telefon: (+43 316) 873 – 7551
Telefax: (+43 316) 873 – 7553
http://www.ifea.tugraz.at
http://www.tugraz.at

Graz / March – 2016

TU Graz

NTNU

Acknowledgments

I would like to thank Professor Herwig Renner and Professor Kjetil Uhlen for giving me the opportunity to write this thesis in Trondheim and for their guidance. I would also like to thank PhD candidate Dinh Thuc Duong for the helpful discussions throughout the work for this thesis and his points of view on the tasks.

Special thanks to my family for supporting me over the whole duration of my studies.

I also owe my friends and fellow students many thanks for having a good time together.

Karin, thank you for being always there for me and making me happy.

Eidesstattliche Erklärung

Ich erkläre an Eides statt, dass ich die vorliegende Arbeit selbstständig verfasst, andere als die angegebenen Quellen/Hilfsmittel nicht benutzt, und die den benutzten Quellen wörtlich und inhaltlich entnommenen Stellen als solche kenntlich gemacht habe.

Graz, am 14.03.2016

Stefan Polster

Abstract

Increasing energy consumption and the declared intention to meet it with renewable energy sources and smart grid solutions require transmission and distribution grids to be more flexible and better monitored than in former times to be able to withstand fast changes in generation and load. Due to the often long distances between generation units and load centers it is essential to monitor the voltage stability of the system as one of its limiting factors. So far, research on voltage stability focused on providing solutions for off-line applications.

The possibility to acquire real time data from phasor measurement units (PMUs) in concerned buses provides the basic means to develop a real time monitoring of the voltage stability by using the Thevenin theorem to estimate the possible maximum power. A simple stability indicator can be found by comparing the actual load power with the estimated maximum power. The advantage of the proposed algorithm is that, apart from the data from PMUs, only the topology of the examined subsystem and the operational status of included generators must be known. In this work a solution is developed to estimate the Thevenin impedance of a simple network topology, which takes the operational borders of the generators into account. The algorithm is validated by simulating a test network. Moreover, a feasible way to reduce the real time measurements needed and to evolve the algorithm to suit general network topologies is proposed.

Kurzfassung

Der steigende Energieverbrauch und der Wille diesen mit erneuerbaren Energiequellen und dem Einsatz von Smart-Grid-Anwendungen zu befriedigen machen es notwendig, dass der Betrieb von Übertragungs- und Verteilnetzen immer flexibler gestaltet und besser überwacht werden muss um schnelle Last- und Erzeugungsänderungen zu bewältigen. Durch die nun oft langen Distanzen zwischen Erzeugungs- und Verbraucherschwerpunkten ist es essentiell die Blindleistungsstabilität als einen limitierenden Faktor zu überwachen. Der Fokus der Forschung lag in diesem Bereich bisher auf Lösungen für Off-Line-Anwendungen.

Die Möglichkeiten Echtzeitdaten aller gewünschten Abgänge mittels PMUs zu erhalten ist die Grundvoraussetzung, um eine Echtzeitüberwachung der Blindleistungsstabilität, welche auf der durch die Thevenintheorie berechneten maximalen Übertragungsleistung basiert, zu entwickeln. Der Vorteil dieses Algorithmus ist, dass er neben den Daten aus den PMUs nur die Struktur des betreffenden Netzabschnittes und die Betriebszustände der einspeisenden Generatoren benötigt. In dieser Arbeit wird eine Lösung untersucht, um die Theveninimpedanz in einem einfachen Netzwerk mit gesättigten Generatoren zu ermitteln. Der dabei verwendete Algorithmus wird mittels Simulation eines Testnetzes überprüft. Des Weiteren wird die Möglichkeit einer Weiterentwicklung des verwendeten Algorithmus diskutiert, welche die nötigen gemessenen Daten reduziert und auch für allgemeine Netze angewendet werden kann.

List of Symbols

E, E_Q	steady-state internal emf
E_d	d-axis component of the steady-state internal emf
E_f	excitation emf proportional to the excitation voltage V_f
E_q	q-axis component of the steady-state internal emf
E_{th}	equivalent Thevenin emf
E'	transient internal emf
E_d'	d-axis component of the transient internal emf
E_q'	q-axis component of the transient internal emf
E''	subtransient internal emf
E_d''	d-axis component of the subtransient internal emf
E_q''	q-axis component of the subtransient internal emf
f	mains frequency
f_n	rated frequency
H	inertia constant
I_G	armature current
I_d, I_q	d- and q-axis component of the armature current
I_f	field current
I_{inj}	injected current
I_N	equivalent Norton current
J	inertia
k_Q	security index based on voltage stability criteria
M	torque
P	Park transformation matrix
p	number of pole pairs
P_e	electrical active power of the generator
P_G	active power of a generator
P_L	active power of the load
P_m	mechanical power applied to the generator
P_T	turbine power
Q_G	reactive power of a generator
Q_L	reactive power of the load
Q_S	reactive power of a source
R	resistor
R_N	Norton resistor
R_{TH}	Thevenin resistor
S_G	apparent power of a generator
S_L	apparent power of the load
s	Laplace operator
T	transformation matrix dq-system
T_{d0}', T_{d0}''	open-circuit d-axis transient and subtransient time constants
T_{q0}', T_{q0}''	open-circuit q-axis transient and subtransient time constants
V	voltage
v	voltage in p.u. system
V_C	compensated voltage for AVR
V_G	voltage at generator terminal

V_L	voltage at load terminal
V_{ref}	reference voltage
X	reactance
X_d, X_d', X_d''	d-axis synchronous, transient and subtransient reactance
X_{ref}	reactance between generator and infinite stiff bus
X_T	reactance of a transformer
X_q, X_q', X_q''	q-axis synchronous, transient and subtransient reactance
$X_{virtual}$	additional virtual impedance between generator and stiff bus
Y	admittance matrix
Z	impedance
Z_C	compensation impedance
Z_G	impedance of a generator
Z_L	load impedance
Z_T	impedance of a transformer
Z_{TH}	Thevenin impedance
δ	power (or rotor) angle
Δω	rotor speed deviation
σ	static of governor
φ	power factor angle
ω	electrical angular velocity
ω_m	mechanical angular velocity

Abbreviations

AVR	Automatic Voltage Regulator
emf	electro-motive force
PMU	Phasor measurement Unit

Content

1 Introduction

The combination of increasing energy consumption and the boost of renewable energy sources requires a paradigm shift for transmission and distribution grids in Europe. It becomes necessary to be more flexible and better informed of the system status in power system operations, especially due to the unbundling of the former vertical integrated energy supply companies into independent energy production and transmission companies. As a result no direct link between power grid status and the control of energy production units is existing anymore. Altogether, this leads to the need of a real time identification of the transmission limits and given operation margins to be able to react fast enough to maintain a sufficient supply reliability.

The voltage stability becomes more and more a limiting factor, since generation and load centers are often connected with long and heavily loaded transmission lines. Most of previous research done on voltage stability focused on off-line solutions like the continuation power flow [1] or the analysis of the sensitivity of the Jacobian matrix [2]. However, with the increasing use of phasor measurement units (PMUs) a different approach to the voltage stability monitoring became possible by using the estimated Thevenin impedance [3]. The main advantage of this application is, that only the measured data of the PMUs and the topology of the examined subsystem must be known.

This thesis focused on the effects of the operational borders of synchronous generators. The aim is to find an extension to the existing algorithm, which takes the change of the Thevenin impedance, caused by the limits of the generators, into account and can be realized with as little knowledge of the generator parameters as possible. A possible implementation has to be validated by a simulation of a simple network topology. The first step is to build a Simulink model of the examined theoretical topology. The generators will be modelled to include their dynamic behavior and operational borders. The implementation of the load will be done by an impedance with an optionally controlled value to model a constant power load. To evaluate the accuracy of the altered algorithm, the results are compared with the original algorithm and general voltage stability criteria.

The necessary theory for voltage stability, operational borders of the generators and back ground knowledge for the model are described in chapter 2. An overview of simulations and their results are shown in the chapter 3 and are discussed in 4. A brief presentation of an idea how to evolve the algorithm for general networks and what can be the further steps to implement it on actual systems is included in the last one. The detailed description of the model and test cases to validate it are shown in the appendix. Moreover the appendix contains the full parameter list for all simulations and all simulation results.

2 Theory and Methods

2.1 Theoretical Background

2.1.1 Network Capacity

[4]

The feasibility can best be explained by focusing on a simple and general power supply problem as shown by Figure 2-1. The power, which can be transmitted to the load, will give the limit of stable supply.

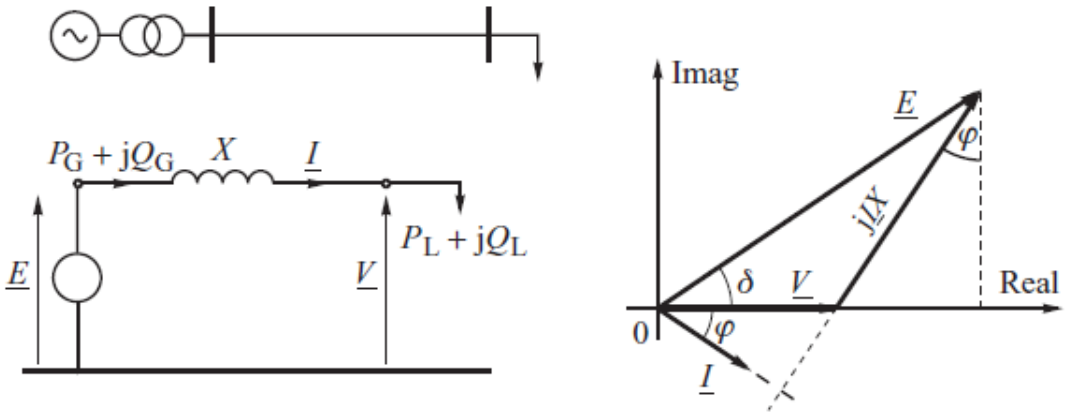

Figure 2-1 [4, p. 300]

As for the network feasibility no load dynamics are taken into account, the network can be represented by an equivalent generator behind an equivalent reactance in steady state operation. Bearing that in mind, the load power can be calculated as shown in 2-1.

$$P_L(V) = VI\cos\varphi = \frac{EV}{X}\sin\delta$$
$$Q_L(V) = VI\sin\varphi = \frac{EV}{X}\cos\delta - \frac{V^2}{X}$$

2-1

Combining the equations for reactive and active power, using the identity $\sin^2 x + \cos^2 x = 1$ a power-voltage equation is achieved that offers the possible solutions for the power supply problem, in case the load characteristics are known.

$$\left(\frac{EV}{X}\right)^2 = [P_L(V)]^2 + \left[Q_L(V) + \frac{V^2}{X}\right]^2$$

2-2

Considering an ideally stiff load the power will be independent from the voltage at its rated value P_n and Q_n. Moreover, the reactive power can be written as a function of the active power.

$$Q_n = P_n tan\varphi \tag{2-3}$$

Substituting this in 2-2 leads to

$$P_n^2 + P_n^2 \tan^2 \varphi + 2P_n \frac{V^2}{X} = \left(\frac{EV}{X}\right)^2 - \left(\frac{V^2}{X}\right)^2 \tag{2-4}$$

Using basic cos/sin-functions the active power can be separated.

$$P_n = -\frac{E^2}{X}\left(\frac{V}{E}\right)^2 sin\varphi cos\varphi + \frac{E^2}{X}\frac{V}{E}\, cos\varphi \sqrt{1 - \left(\frac{V}{E}\right)^2 \cos^2 \varphi} \tag{2-5}$$

By assuming that the equivalent voltage E equals the rated voltage and E^2/X equals the rated power of the system, 2-5 can be expressed with per unit values.

$$p = -v^2 sin\varphi cos\varphi + v\, cos\varphi \sqrt{1 - v^2 \cos^2 \varphi} \tag{2-6}$$

Considering the angle φ as a parameter 2-6 gives a family of curves depending on it.

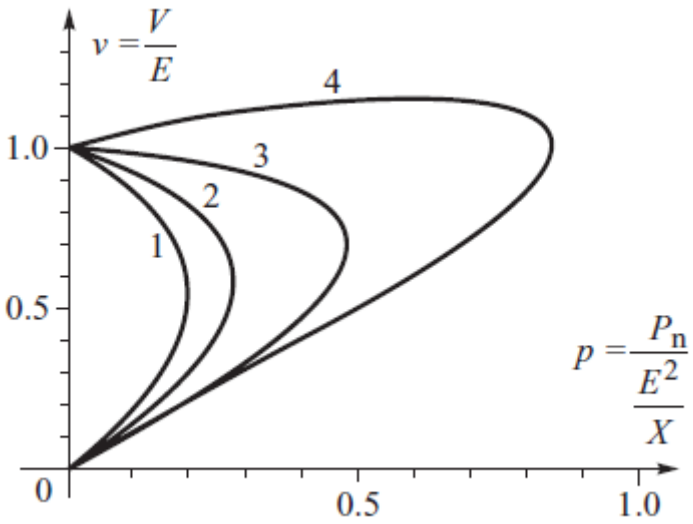

Figure 2-2 [4, p. 302], (1) φ = 45° lag, (2) φ = 30° lag, (3) φ = 0°, (4) φ = 30° lead

These curves describe the voltage behavior according to the active load power. Since 2-6 still includes the power factor as parameter, no singular solution can be obtained. However, a family of curves can be created from 2-2 in the P-Q-plane by assuming Q as a function of P with V as a parameter.

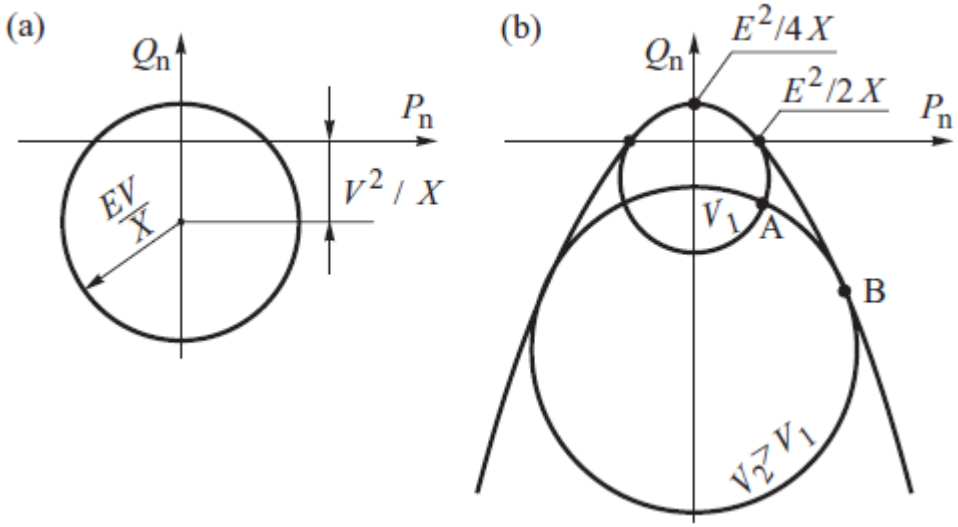

Figure 2-3 [4, p. 302], (a) given voltage V, (b) family of curves and their envelope

The envelope of the family of Q(P)-curves gives an area at the PQ-plane, which includes all possible solutions for the power supply problem. Nevertheless, all points inside the envelope offer two solutions for the parameter V, an example is point A in Figure 2-3. Only the points directly at the envelope have a singular solution for 2-2. The first step to derive an equation, which describes the envelope without the parameter V, is to rearrange 2-2 and assuming (V^2/x) as a variable a quadratic equation is found.

$$\left(\frac{V^2}{X}\right)^2 + \left(2Q_n - \frac{E^2}{X}\right)\left(\frac{V^2}{X}\right) + (P_n^2 + Q_n^2) = 0 \qquad 2\text{-}7$$

Utilizing the full formula for solving quadratic equations results in a singular solution for V, if 2-8 is satisfied

$$\left(2Q_n - \frac{E^2}{X}\right)^2 - 4\,(P_n^2 + Q_n^2) = 0 \qquad 2\text{-}8$$

Now the envelope can be determined by solving 2-8 for Q_n.

$$Q_n = \frac{E^2}{4X} - \frac{P_n^2}{\frac{E^2}{X}} \qquad 2\text{-}9$$

It is notable here, that the crossing points of the P-axes in Figure 2-3 match with the nose point of curve (3) in Figure 2-2.

So far, a stiff load characteristic was considered. This load behavior can be interpreted as a controlled power load, where $P_L(V) = P_n$ and $Q_L(V) = Q_n$. Applying load characteristics for controlled current loads 2-10 and reactive loads 2-11 the shape of the envelope will change as shown in Figure 2-4.

$$P_L(V) = \frac{V}{V_n} P_n$$
$$Q_L(V) = \frac{V}{V_n} Q_n$$

2-10

$$P_L(V) = \left(\frac{V}{V_n}\right)^2 P_n$$
$$Q_L(V) = \left(\frac{V}{V_n}\right)^2 P_n$$

2-11

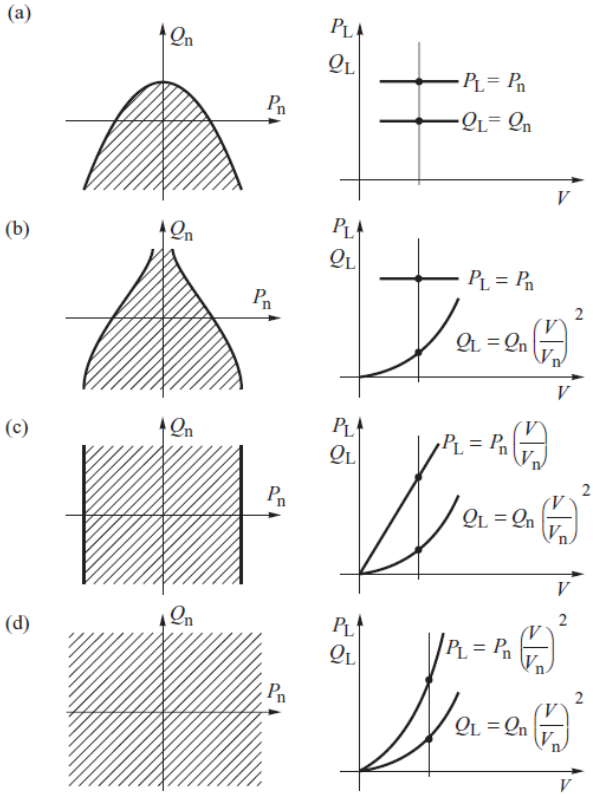

Figure 2-4 [4, p. 304]

As stated before all points in the hatched area provide a solution for two values of V corresponding to P_n and Q_n of the load. The envelope holds only singular solutions for V and outside from it is not possible to transmit power equal to P_n and Q_n to the load.

2.1.2 Static Voltage Stability

[4], [5], [6], [7], [8]

The voltage stability matches with the balance of the reactive power, whereas a lack of reactive power can lead to a voltage collapse. It is necessary to discriminate between static and dynamic stability to describe the mechanism sufficiently. An analysis of the static stability covers undisturbed operation points and their stability. The dynamic stability examines, if the system will reach a stable operation point after a switching or failure in the network. However, before focusing on these parameters one should take a closer look on the general network feasibility and the stability criteria.

Generally it is not possible to determine voltage stability for the whole electrical power network because of the huge amount of elements included in it. Therefore, the system must be divided into detailed modelled parts, which include the point of interest, and more shallow equivalents of superior and minor network areas. The equivalent can be implemented either as sources or sinks, depending on the power flow.

The static voltage stability examines the ability to meet load demands, which are increased slowly and within ordinary operation conditions. A system is stable under the scope of static voltage stability, if the criteria described in 2.1.2.1 are fulfilled.

Besides that, voltage security indices can be found based on the criteria below. Based on the observation of the voltage and the classic dΔQ/dV criterion (see chapter 2.1.2.1), a voltage proximity index can be defined as

$$k_V = \frac{V_S - V_X}{V_S}$$

2-12

Wherein V_X is the voltage, for which $d(Q_S - Q_L)$ reaches its maximum. It can be calculated by meeting following condition

$$\left.\frac{d(Q_S - Q_L)}{dV}\right|_{V=V_X} = 0$$

2-13

[4, p. 320]

According to [5, pp. 189-191] the criterion stated by 2-25 can also be used as a security index for multi node networks.

$$k_Q = \frac{\Delta Q_{Li}}{\sum \Delta Q_{Gf}} = \frac{1}{-\sum S_{fi}}$$

2-14

Note, that S_{fi} is the sensitivity of the generator f in relation to a change of the load demand i. The negative sign results from the active sign convention.

$$S_{fi} = -\frac{\Delta Q_{Li}}{\Delta Q_{Gf}}$$

2-15

2.1.2.1 Stability Criteria

In the previous chapter it was shown, that all operation points inside the envelope in the PQ-plane have two possible solutions for the voltage. This leads to the need to find some criteria to examine, which of the two values of the voltage describes a stable operation point. To distinguish between stable and unstable operation points different criteria can be used, which are based on different variables, but lead to an equivalent result.

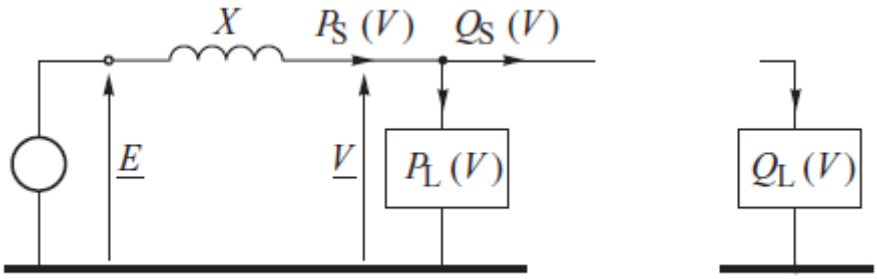

Figure 2-5, equivalent circuit for determining the reactive power characteristic, [4, p. 305]

(1) dΔQ/dV Criterion

This criterion has already been described in [6] and [7] and is named the classic criterion. The main idea is to examine the feasibility of a system to supply reactive power to a load at a certain real power demand. A change of the voltage at the load bus results in an altered power demand of the load and capability to supply it according to their voltage characteristic. Therefore for the load power demand the index L and for the source power supply the index S will be used further on.
Due to the basic behavior of the system the active power is always linked to the transmission line, which means that $P_S(V) = P_L(V)$ for the assumed network shown in Figure 2-1. That is also true for the reactive power at a stable operation point, but to find a way to validate a stability criterion the reactive power supply $Q_S(V)$ will be assumed to be not influenced by the reactive load demand $Q_L(V)$. However the active and reactive powers can be calculated in a similar way as in chapter 2.1.1.

$$P_L(V) = P_S(V) = \frac{EV}{X} sin\delta$$
$$Q_S(V) = \frac{EV}{X} cos\delta - \frac{V^2}{X}$$

2-16

Eliminating of the trigonometric functions and solving for $Q_S(V)$ results in following equation.

$$Q_S(V) = \sqrt{\left[\frac{EV}{X}\right]^2 - [P_L(V)]^2} - \frac{V^2}{X}$$

2-17

If the active load of the system is known, this equation results the curve for the reactive power depending on the voltage. However, the form of the curve is depending on the active load characteristic, which influence is illustrated in Figure 2-4. If a constant load characteristic is assumed, 2-17 describes an inverse parabola, whereat a change in the active power load leads to

a shift down and to the right. For better understanding of the shift caused by the active power assume a vertical line at the value of $P_L(V)$ = constant in Figure 2-3. The resulting curve for $Q_S(V)$ can now be created by point plotting all intersection points of the assumed line with each circle representing a voltage value in a QV-diagram. The resulting curve is shown in Figure 2-6.

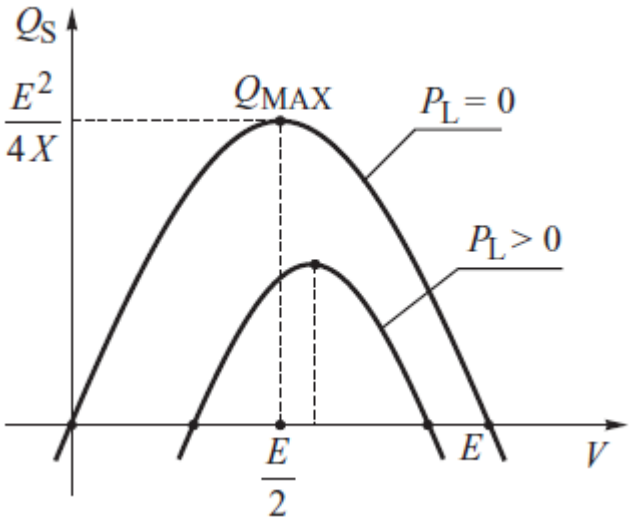

Figure 2-6 [4, p. 306]

So far, just the reactive power supplied by the source at the load terminal was considered. According to the basic rules of an electrical system, the power of the source must be equal to the power demand of the load. Consequently the curve of the voltage characteristic of the reactive load $Q_L(V)$ must have at least one intersection point with $Q_S(V)$. The two curves are illustrated in Figure 2-7.

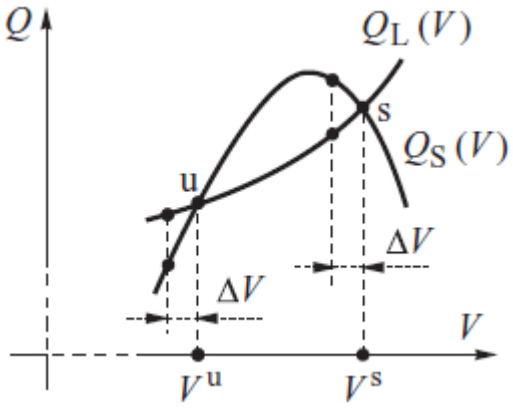

Figure 2-7 [4, p. 306]

The stability of the intersection points can be examined by assuming a small disturbance in the voltage. Starting at point u a negative voltage disturbance will lead to a higher reactive power demand of the load than the source is able to supply under this condition. This lack of reactive power will lead to a further sag of the voltage and an increasing difference in demand and supply. Therefore this point is unstable. Doing the same at point s, the result will be a overshoot of reactive power. This will increase the voltage again till $Q_L(V)$ equals $Q_S(V)$ again at point s. A positive voltage disturbance at point s will result in a lack of reactive power and a return to point s. Consequently s is a stable operation point. The $d\Delta Q/dV$ criterion can now be stated by

$$\frac{d(Q_S - Q_L)}{dV} < 0 \; or \; \frac{dQ_S}{dV} < \frac{dQ_L}{dV}$$

2-18

For simple systems an analytic stability condition can be found using 2-16 and 2-17. The calculations resulting in the stability condition 2-19 can be found in [4, p. 307].

$$\frac{dQ_L}{dV} > \frac{E}{Xcos\delta} - \left(\frac{2V}{X} + \frac{dP_L}{dV} tan\delta\right)$$

2-19

The derivatives are based on the approximated voltage characteristics of the load.
[4, pp. 305-307]

Considering Figure 2-6 and Figure 2-7 and taking the conditions described in chapter 2.1.1 into account it is possible, that $Q_L(V)$ and $Q_S(V)$ have only one equation point. In this case 2-19 is only valid for a positive voltage disturbance. In a family of curves with P_L as a parameter the connection of all singular equation points can be interpreted as the stability border, as it is shown in Figure 2-8.

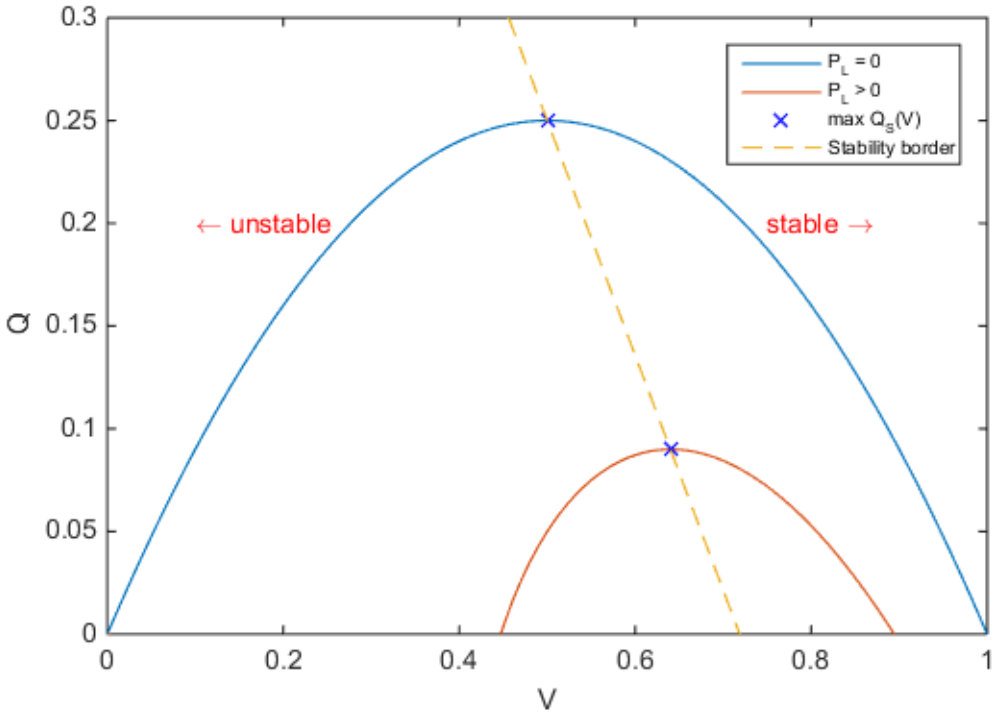

Figure 2-8[1]

The network topology is usually not as simply as assumed above and an analytic solution for the stability criterion cannot always be found. However, a load flow program may be used to estimate the stability border of an arbitrary bus in the network. Therefore, a virtual power plant with unlimited reactive power is added to the examined bus embodied as a PV node. Setting the active power to 0 and changing the voltage of the node results in the Q(V) curve. Note, that the position of the slack node has an influence on the result and should not be set near the examined node [8, p. 57].

[1] E = 1 p.u.; X = 1 p.u.; Load assumed as ideally stiff

(2) dE/dV Criterion

Similar to the dΔQ/dV criterion the system equivalent emf E is calculated from 2-2.

$$E(V) = \sqrt{\left(V + \frac{Q_L(V)X}{V}\right)^2 + \left(\frac{P_L(V)X}{V}\right)^2}$$

2-20

The resulting E(V) characteristic is shown in Figure 2-9. For a constant equivalent emf two solutions are possible. The stability of each intersection point can be tested using a small disturbance in the voltage. For point s a negative voltage disturbance leads to a reduced emf E(V). Because of the higher source emf E the voltage will rise again to the initial point s. When applying a positive voltage disturbance the voltage will also return to s, because the source emf E is smaller than the emf E(V) in this case. If the same voltage disturbances are assumed at point u, the source emf is not able to restore the voltage, since a decrease of the voltage leads to an rising emf E(V).
However, this leads to the criterion stated below.

$$\frac{dE}{dV} > 0$$

2-21

This condition is equivalent to the criterion defined by 2-19, which is shown in [6].

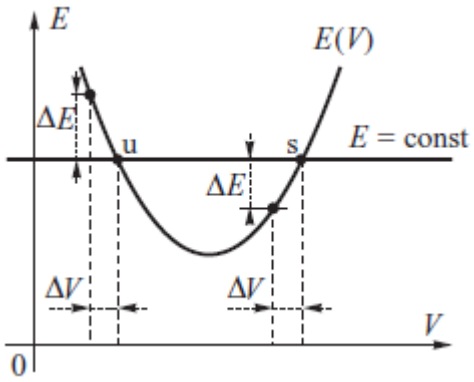

Figure 2-9 [4, p. 308]

The possibility to find a solution for this criterion in a multi node network is described in [4, p. 309].

(3) dQ_G/dQ_L Criterion

This criterion is based upon the respond of the reactive power generation Q_G to changes in the reactive power demand Q_L. The reactive power generation is calculated as following

$$Q_G(V) = \frac{E^2}{X} - \frac{EV}{X}cos\delta$$

2-22

Using 2-1 and 2-2, V and δ can be eliminated, which result in an equation creating a family of curves in the Q_GQ_L-plane with the active load power P_L as parameter.

$$Q_L(V) = -\frac{Q_G^2(V)}{\frac{E^2}{X}} + Q_G^2(V) - \frac{P_L^2(V)}{\frac{E^2}{X}}$$

2-23

Depending on the voltage characteristic of the active power load $P_L(V)$ the basic form of the curves change. It will describe a horizontal parabola for an ideal stiff load $P_L(V) = P_L$ = constant. Varying P_L leads only to a shift in the Q_L-axis, which is shown in Figure 2-10 (a).

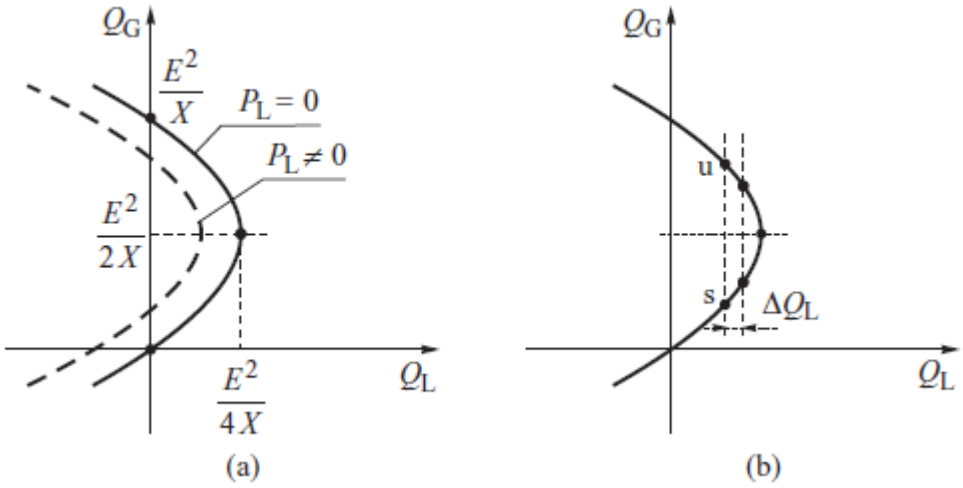

Figure 2-10 [4, p. 310]

The stability can be determined by changing the reactive power demand starting from an initial operation point. If the reactive power generation responds to it with a change in the same direction, the initial point is stable, whereas a respond in the different direction results in an unstable point. When these conditions are turned into an equational form, the criterion is found as

$$\frac{dQ_G}{dQ_L} > 0$$

2-24

In Figure 2-10 (b) an illustration of this criterion is shown, with the stable point s and the unstable point u. However, if $P_L(V)$ has a voltage-dependent characteristic, it is not possible to state an explicit expression for $Q_L(Q_G)$. It must be found by solving the network equations for the given load demand and emf E.

Similar to the two previous criteria, it is only possible to find an analytic expression for in simple network topologies. Multi generator networks must be solved by using a load flow simulation. Thereby the main advantage of the dQ_G/dQ_L criterion is taken into account, since Q_G can be replaced by the sum of reactive power created at all generator nodes in the network and the criterion 2-24 by

$$\frac{\sum \Delta Q_G}{\Delta Q_L} > 0 \qquad 2\text{-}25$$

[4, pp. 309-310]

2.1.3 Dynamic Voltage Stability

[4], [5]

In general, instabilities should be seen as dynamic processes. Therefore, the static voltage stability is a necessary precondition, but it is only able to describe slow variations of composite loads. To describe the real system behavior the dynamics of the load and control units should be covered too. The dynamics can cause differences in the static and dynamic load characteristics and therefore they have a significant influence on the voltage collapse. Because time constants of these factors range from seconds up to minutes, it should be discriminated between short term analysis and long term stability.

The short time analyses focuses on the reaction of the system to fast changes in the network for example failure, which results in a changed topology and network reactance. A higher reactance influences the voltage characteristics, according to the equations in chapters 2.1.1 and 2.1.2, and can lead to a status of unsatisfied load demand.
Due the reaction of the controlled units stability can still be lost, even if the short term reaction leads to a stable operation point. The long-term stability is given, if the system still meets the stability criteria, when all controlled units completed their dynamic reactions.
[5, p. 191]

However, dynamic voltage stability is achieved, if the system reaches a stable operation point after a change or failure in the network or in the load demand. For a better understanding two examples are given below describing dynamic stability loss caused by load behavior and network outtakes.

(1) Load based dynamic voltage instability

Based on a high load demand the voltage in the load area can dip, which starts a cascade of reactions leading to a voltage collapse.

- Controlled loads demand a high reactive and active power despite the voltage dip in load areas.
- If the voltage in distribution and subtransmission networks is controlled by tap-changing transformers, the dependency of the load to the supply voltage is lessened. This can cause a further voltage dip in the transmission network.

- The generators cannot supply enough reactive power to act as a constant voltage source. The armature current and the exciter system are the limiting factors.

Beside these reactions the dynamic voltage characteristics of involved loads and sources influence the actual collapse process. A scenario, where this can cause a stability problem, is stalling induction motors. Due to a voltage dip the torque of them is reduced and may result in stalling. The stalling motor demands high reactive power and decreases therefore the voltage further until the motor protection trips the motor. However after tripping the voltage will rise again and can trigger uncontrolled restore reactions of the load decreasing the voltage again, such as self-restarts of induction motors.

(2) Network Outages

As shown in 2.1.1 and 2.1.2, one of the main factors limiting the maximum power is the equivalent reactance of the network. The reactance will rise, if one parallel transmission line between source and load trips, causing a higher voltage drop and a reduction in the network feasibility. A generator tripping causes similar problems, but additional also the capability to produce power is reduced.

Figure 2-11 shows an example for voltage collapse caused by a line trip. When the dynamics - caused by the tripping - fade away, a short term stability is reached. The reaction of the controlled load units to the voltage dip lead to a reactive power deficit, which is responsible for the increasing voltage drift and final collapse. The actual characteristic is therefore strongly depending on the behavior of the control devices.

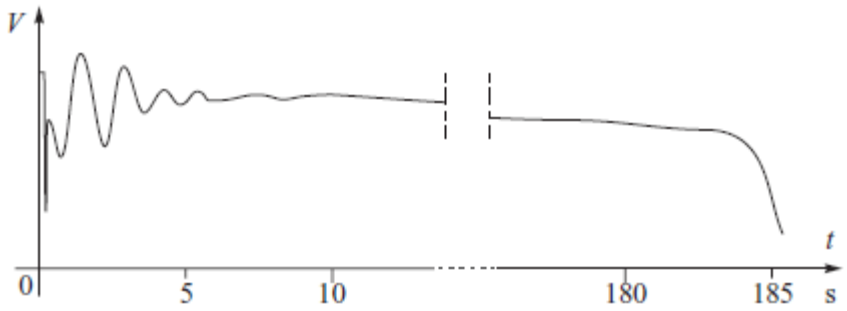

Figure 2-11 [4, p. 322]

2.1.4 Operational Limits of the Synchronous Generator

[4], [9]

Even with the increasing share of power supply linked to the network by inverters, the main part of electric power is still generated with direct linked synchronous generators. Therefore, their operation limits have a huge impact onto the general network behavior.

However, as voltage stability highly depends on the ability to generate reactive power and transmit it to the concerned area in a grid, the capability diagram of synchronous generators gives the most concentrated overview of the concerned limits.

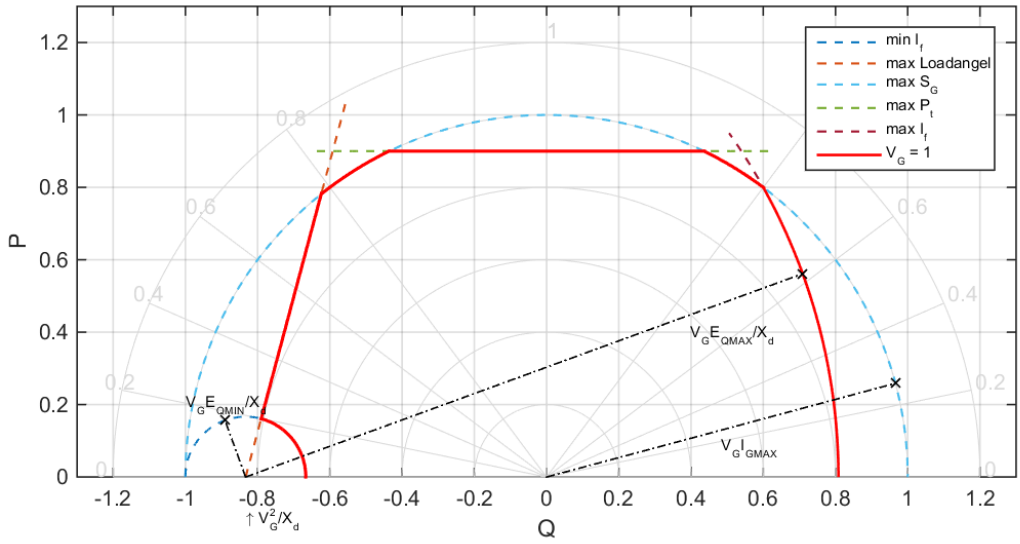

Figure 2-12 Capability diagram[2]

The construction of the capability diagram is shown in [9]. The five dashed lines represent operation limits caused by different factors, which will be explained in the following sections. The general limit is reached by overlaying them.

For reasons of simplification, a generator with cylindrical-rotor is assumed. Figure 2-13 shows the equivalent circuit of the generator.

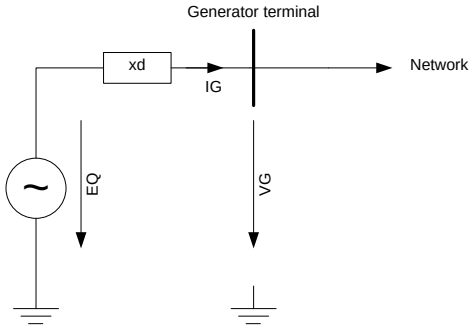

Figure 2-13

[2] Used values for the capability diagram are $S_{G,rated}$ = 1; cos(φ_{rated}) = 0,8; maximum load angle δ_{max} = 75°; maximum turbine power P_t = 0,9, minimum field current I_{fmin} = 0,167; maximum field current I_{fmax} = 1,64 and X_d = 1,2. All values are in p.u. and in the generator arrow reference systemactive sign convention.

(1) Rated apparent power

In long-term operation this limit is given by the apparent power - respectively the maximum stator current - causing armature heating.
In the PQ-plane it is described as a half circle with the center in the origin and radius S_{max}.

$$P^2 + Q^2 = \left(V_G \cdot I_{G,max}\right)^2$$

2-26

Separation into active and reactive power results in

$$P = V_G \cdot I_{G,max} \cdot cos\varphi$$
$$Q = V_G \cdot I_{G,max} \cdot sin\varphi$$

2-27

(2) Maximum turbine power

Usually the maximum mechanical power of the turbine is smaller than the maximum apparent power of the generator, leading to limitation in the maximum active power.

(3) Maximum field current

This limit is set by the heating of the field winding. In [4, pp. 76-104] it is shown, how to represent the field current as the internal emf E_Q and the direct synchronous reactance X_d. Using that and the power equations, this limit can be introduced in the PQ-plane.

$$P = \frac{E_{Qmax} \cdot V_G}{x_d} sin\delta_g$$

2-28

$$Q = \frac{E_{Qmax} \cdot V_G}{x_d} cos\delta_g - \frac{V_G^2}{x_d}$$

2-29

$$x_d = X_d + X_{ref}$$

2-30

Hereby X_{ref} is the reactance between the generator terminals and the stiff bus with the voltage V.

(4) Minimal field current

The minimal field current ensures a minimal overturning torque. The equations for the PQ-plane can be stated as for the maximum field current by replacing the field current by the internal emf and the synchronous reactance.

(5) Maximal load angle

The maximum load angle matches with the static active power stability border of the synchronous generator which is reached at

$$\frac{dP}{d\delta} = 0$$

2-31

Dividing 2-28 by 2-29 and setting $\delta_g = \delta_{max}$ results in 2-32. This limit corresponds to a straight line, which crosses the Q-axis at $V_G^2/x_d \cdot \tan(\delta_{max})$.

$$P = \left(Q + \frac{V_G^2}{x_d}\right) tan\delta_{\max}$$

2-32

The theoretical limit is given by $\delta_{max,theoretical} = 90°$ but should be reduced to scope with load fluctuation to e.g. $\delta_{max} = 75°$ [9, p. 327].

2.1.5 Generator Frame and System Frame

[10], [11]

According to the Park transformation, the complex 3-phasor geometry of a synchronous generator can be simplified by transforming the stator based phase variables into new variables, which are referred to a generator frame moving with the rotor (dq0-system). The new variables are calculated by the projection of the phase variables onto the three axes of the generator frame. These axes are the direct axis (d-axis), which position is set by the rotor field winding, the quadrature axis (q-axis) and a stationary axis (0-axis). The q-axis lags 90° to the d-axis.

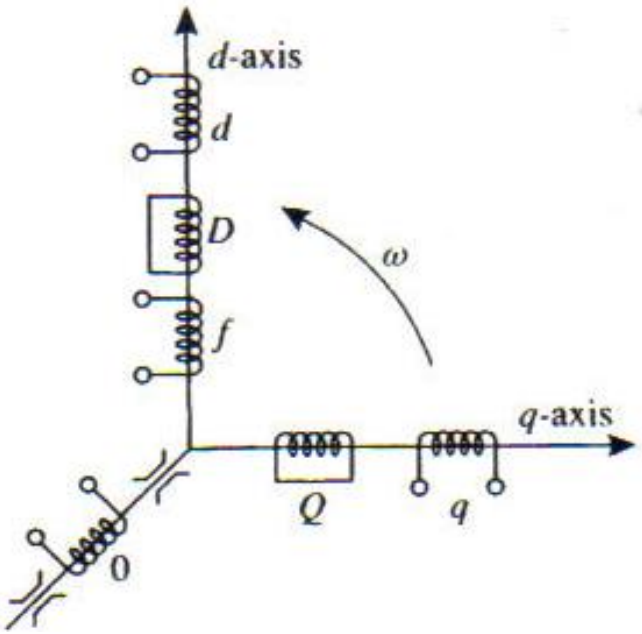

Figure 2-14 [10, p. 14]

The transformed variables display the same effects as the origin variables. Therefore the transformation can be described by the Park transformation matrix P.

$$P = \sqrt{2/3}\begin{bmatrix} 1/\sqrt{2} & 1/\sqrt{2} & 1/\sqrt{2} \\ \cos\theta & \cos(\theta - \frac{2\pi}{3}) & \cos(\theta + \frac{2\pi}{3}) \\ \sin\theta & \sin(\theta - \frac{2\pi}{3}) & \sin(\theta + \frac{2\pi}{3}) \end{bmatrix}$$

2-33

$$\theta = \omega t$$

2-34

As the matrix is orthogonal, the invers can easily calculated as the its transposed matrix.

$$P^{-1} = P^{T} = \sqrt{2/3}\begin{bmatrix} 1/\sqrt{2} & \cos\theta & \sin\theta \\ 1/\sqrt{2} & \cos(\theta - \frac{2\pi}{3}) & \sin(\theta - \frac{2\pi}{3}) \\ 1/\sqrt{2} & \cos(\theta + \frac{2\pi}{3}) & \sin(\theta + \frac{2\pi}{3}) \end{bmatrix}$$

2-35

The transformation between stator based and rotor based variables can now be described as following.

$$x_{0,d,q} = P\, x_{a,b,c}$$

2-36

$$x_{a,b,c} = P^{-1}\, x_{0,d,q}$$

2-37

[11, p. 321]

This transformation can be even more simplified, if symmetrical cases are considered exclusively. The stator variables are solely described by their positive system vector in a complex plane. The complex plane and the dq-plane stand still in relation to themselves. If the real axis is fixed at the generator terminal voltage, the angle between both coordinate systems is the load angle δ_g.

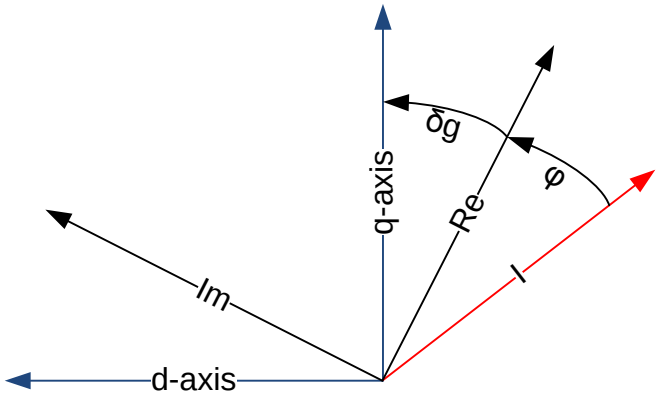

Figure 2-15, Relation between dq-plane, complex plane and as example the generator current

By calculating the projection from the complex-plane into the dq-plane and backwards the simplified transformation matrix T and its inverse can be found.

$$T = \begin{bmatrix} -\sin\vartheta_g & \cos\delta_g \\ \cos\delta_g & \sin\delta_g \end{bmatrix}$$

2-38

$$T^{-1} = \begin{bmatrix} -\sin\delta_g & \cos\delta_g \\ \cos\delta_g & \sin\delta_g \end{bmatrix}$$

2-39

Having these matrices, the transform can be calculated as shown below.

$$x_{d,q} = T\, x_{Re,Im}$$

2-40

$$x_{Re,Im} = T^{-1}\, x_{d,q}$$

2-41

However, all variables are referred to the frame of one single generator. Usually there are more generators involved in a network simulation and therefore a system frame must be defined. One opportunity for a system frame is, to set the q-axis of the reference generator as real axis of the system. Figure 2-16 shows the resulting angles between the system frame, dq-axis and the current of generator k[3].

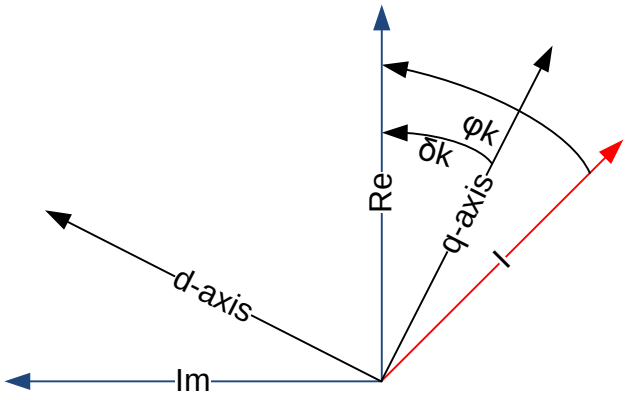

Figure 2-16

For the simulation these relations can be implemented by the following equations.

$$\begin{bmatrix} Re(E'') \\ Im(E'') \end{bmatrix} = \begin{bmatrix} -\sin\vartheta_k & \cos\delta_k \\ \cos\delta_k & \sin\delta_k \end{bmatrix} \begin{bmatrix} E_d'' \\ E_q'' \end{bmatrix}$$

2-42

$$\begin{bmatrix} I_d \\ I_q \end{bmatrix} = \begin{bmatrix} -\sin\vartheta_k & \cos\delta_k \\ \cos\delta_k & \sin\delta_k \end{bmatrix} \begin{bmatrix} Re(I_G) \\ Im(I_G) \end{bmatrix}$$

2-43

2-43 can be simplified to 2-44 by using sin/cos-relations.

$$\begin{bmatrix} I_d \\ I_q \end{bmatrix} = |I_G| \begin{bmatrix} \sin(\varphi_k - \delta_k) \\ \cos(\varphi_k - \delta_k) \end{bmatrix}$$

2-44

[3] Note that the angle δ_k is the angle between q-axis of the slack generator and generator k and not the load angle of generator k

2.1.6 Thevenin Impedance for Stability Calculations

[3]

It is shown in [3], that the Thevenin impedance Z_{Th} can be used to establish an online stability monitoring. The algorithm requires the topology of the scoped part of the network and PMU measurements on the concerned load buses. Thereby the generators are assumed without any limits and can be treated as ideal voltage sources with $V_G = V_{ref}$.

According to the Thevenin theorem, all load and source impedances, except the one at the concerned bus, are integrated in the topology and Z_{Th} is the resulting equivalent impedance of the electrical circuit representing this topology.

When Z_{Th} is known, the equivalent electric circuit of any network is reduced to Figure 2-17.

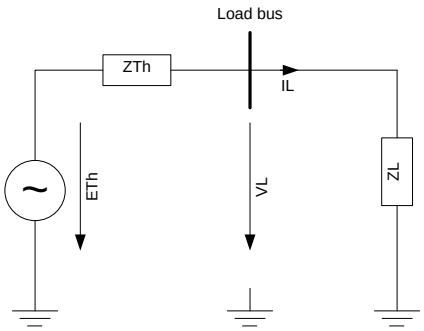

Figure 2-17

In this circuit the maximum loadability will be reached at the condition stated in 2-45 and will have the value according to 2-46[4].

$$|Z_{Th}| = |Z_L| \qquad 2\text{-}45$$

$$S_{max} = \frac{\left|E_{Th}^2\right|[|Z_{TH}| - (imag(Z_{Th})sin\delta + real(Z_{Th})cos\delta)]}{2[imag(Z_{Th})cos\delta - real(Z_{Th})sin\delta]^2} \qquad 2\text{-}46$$

The equivalent Thevenin voltage E_{Th} equals in this case the rated voltage at the generator terminal.

Depending on the load composition, a higher power demand as the maximum loadability can lead to a voltage collapse. Constant power and constant current loads state the worst case scenario.

[4] δ is the load power angle in this case.

2.1.7 Calculation of Thevenin Impedance for Active Power Limitation

[3], [12]

However, in 2.1.6 the implemented generators were assumed with infinite active and reactive power and therefore treated as ideal voltage sources connected to the generator terminal for the calculation of the Thevenin impedance. This leads to correct results as long none of the limits discussed in 2.1.4 is reached, whereby the AVR keeps the terminal voltage at the rated value. A generator operated on its limit can be described as a source with an internal impedance. The magnitude of this impedance is depending on the limit and the general generator parameters.

However, in [3] a method is proposed, which adjusts the Thevenin impedance to scope with an active power dispatch[5].
The basic idea can be explained by assuming the equivalent circuit shown in Figure 2-17 consisting only of resistances R_{Th} and R_L. According to the Thevenin theory the maximum active load power will occur, if R_{Th} equals R_L.

$$P_{L,max} = \frac{E_{Th}^2}{4R_{Th}}$$

2-47

Conversely, the maximum active power of the source is the same and the Thevenin resistance can be calculated as a function of source voltage and maximum active source power.

$$R_{Th} = \frac{E_{Th}^2}{4P_{Source,max}}$$

2-48

Since 2-48 is also valid for a reactance [12, p. 29], the impedance between the limited generator and the load bus can be replaced by a reactance, which depends on the generators rated voltage and active power. Hereby, the maximum active power is not the rated one, since the governor can restrict the active power according to its control parameters.

$$X_{Gen\ to\ Load} = \frac{V_{G,rated}^2}{4P_{G,max}}$$

2-49

This reactance includes the former connection impedance and the additional internal impedance of the voltage source representing the generator.

[5] As this method only takes the limitations in active power into account, the result is only matching for increasing active power leading to a voltage collapse.

2.1.8 Calculation of Thevenin Impedance for Armature Current Limiters

So far, the only considered limit was a dispatch of active power through limited mechanical power of the turbine. As shown in 2.1.4 also the armature current is limited to avoid overheating of the stator windings. This limit makes it inevitable to adjust the actual impedance between the generator bus and the concerned load bus for the calculation of the Thevenin impedance similar to 2.1.7.

However, in case of reaching this limit the generator can be assumed as a constant current source with a Norton impedance. Similar to 2.1.7 the equivalent circuit Figure 2-18 is assumed only containing resistors to simplify the explanation.

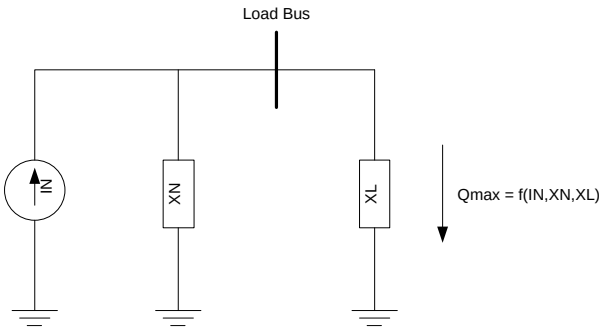

Figure 2-18

The power at the load can be derivated as a function of a Norton impedance X_N, the source current I_N and the load impedance X_L.

$$Q_L = \left(I_N \cdot \frac{X_N}{X_N + X_L}\right)^2 \cdot X_L$$

2-50

Assuming that only the value of the load resistor is not fixed, the maximum loadability will occur when 2-52 is fullfilled.

$$\frac{dQ_L}{dX_L} = I_N^2 \cdot Q_N^2 \frac{(Q_N + Q_L)^2 - 2 \cdot Q_L \cdot (Q_N + Q_L)}{(Q_N + Q_L)^4}$$

2-51

$$\frac{dQ_L}{dX_L} = 0, if\ Q_N = Q_L$$

2-52

By using the conditions for the maximum loadability and 2-50 the Norton resistor can be calculated as function of the source current and maximum load.

$$Q_N = \frac{4 \cdot Q_{L,max}}{I_N^2}$$

2-53

The actual implemented impedance can be calculated as 2-54.

$$X_{Gen\ to\ load} = \frac{4 \cdot S_{G,rated}}{I_{G,rated}^2} = \frac{4 \cdot V_{G,rated}}{I_{G,rated}} \qquad 2\text{-}54$$

According to basic network theory the Norton impedance of a current source equals the Thevenin impedance of an equivalent voltage source. That offers the opportunity to include the adjusted impedance into the network admittance matrix as the impedance between the generator bus and the concerned load bus and the Thevenin impedance of the adjusted network can be calculated.

In contrast to the solution shown in 2.1.7, this adjustment leads to a correct estimation of the voltage collapsing point independently from the rising amount of active or reactive power.

2.1.9 Calculation of Thevenin Impedance for Excitation Limiters

Aside from the limits that have already been discussed, also the maximum field current must be taken into account. Figure 2-12 shows, that the actual apparent power is reduced compared to its maximum value after reaching the maximum field current. Following the same way of adjustment as in 2.1.8 the generator and the connection to the load bus can be displayed as a current source parallel to its Norton impedance. Yet, the injected currents value is not a constant. Instead its value equals the actual stator current. That leads to the following connection impedance between generator bus and load bus.

$$X_{Gen\ to\ load} = \frac{4 \cdot S_{G,rated}}{I_G^2} = \frac{4 \cdot V_{G,rated}}{I_G} \qquad 2\text{-}55$$

However, since operational borders are changing with the actual voltage at the generator bus this limit must not necessarily be reached. The dependency of the generators capability to the voltage at the generator bus is shown in Figure 2-19.

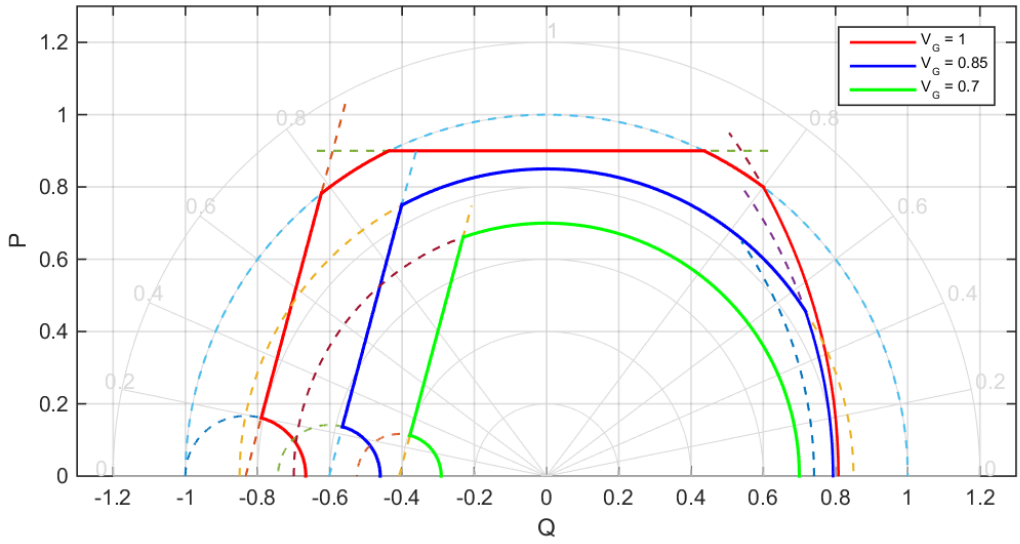

Figure 2-19[6]

[6] Values of the displayed generator in per unit: $I_{G,rated} = 1$; $\cos(\varphi_{rated}) = 0{,}8$; $X_d = 1{,}2$; $P_t = 0{,}9$; $E_{Qmin} = 0{,}2$; $\delta_{max} = 75°$

2.2 Model Description

[4], [8], [10], [11]

The idea behind the used model is to design a dynamic simulation model, which can be used to simulate different problems. Therefore flexibility in the model parameter is needed, which is achieved by dividing the overall model into several sub models.

The synchronous generators are represented by their 5th order model and are introduced into the network as a current injection on their bus [7]. As the network is represented with its admittance matrix the load can be integrated as an additional admittance at the load bus.
The flow chart describes the basic simulation steps [10].

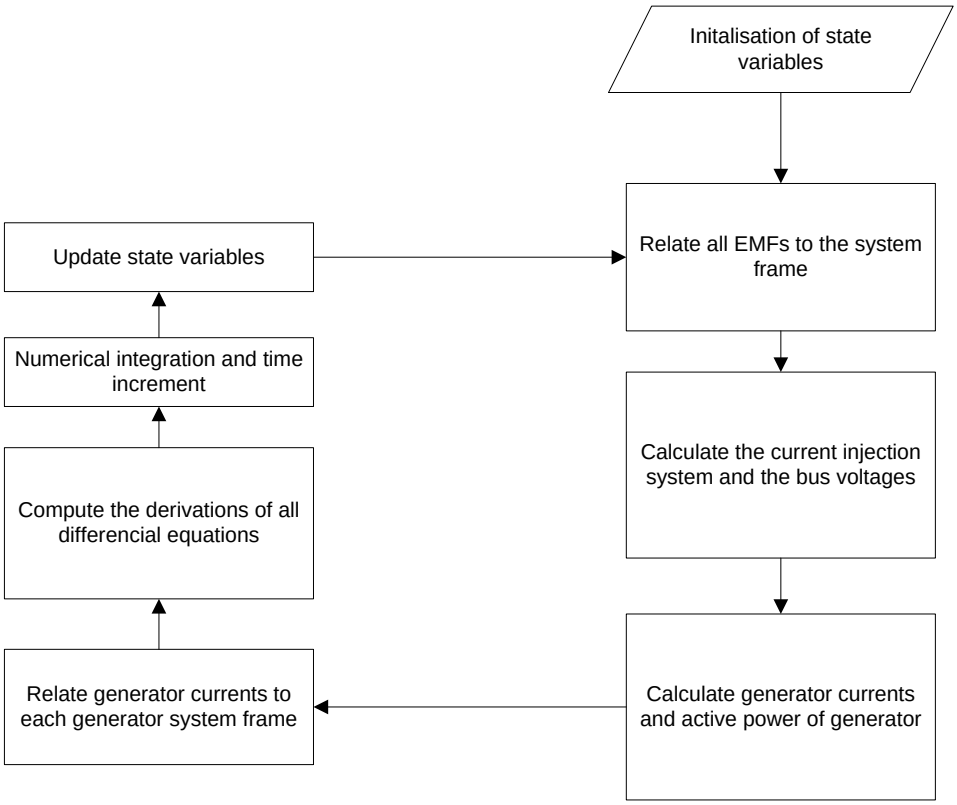

Figure 2-20

The main use of this model for this thesis is to provide a simulation of a small grid including saturation effects of the used generators to examine their influence on the estimation of the Thevenin impedance seen from a concerned load bus. The implementation, described on the following pages, offers the needed easy access to all system parameters and opportunity to change them.

However, the function of all model parts have to be validated, especial because the whole model is built from the scratch. As the function of the AVR and controlled load are crucial for this work, their tests and results are described briefly in the associated theory chapter. The actual implementation and more tests ran for the validation of them and the other parts can be found in the chapters appendix 6.1 to 6.5.

[7] These currents have to be related to the system frame, which is set by the slack generator. The calculation of the network gives the generator currents, which are used as input for the electric model and must therefore be referred to the system frame of each generator.

2.2.1 Model Synchronous Generator

[4], [8], [10], [11]

The Simulink model is divided into the three subsystems “electric model”, “governor and mechanical system” and “AVR”. This division is necessary to ease the implementation of additional controllers, e.g. the limitation of the exciter output without deterioration in the overview.

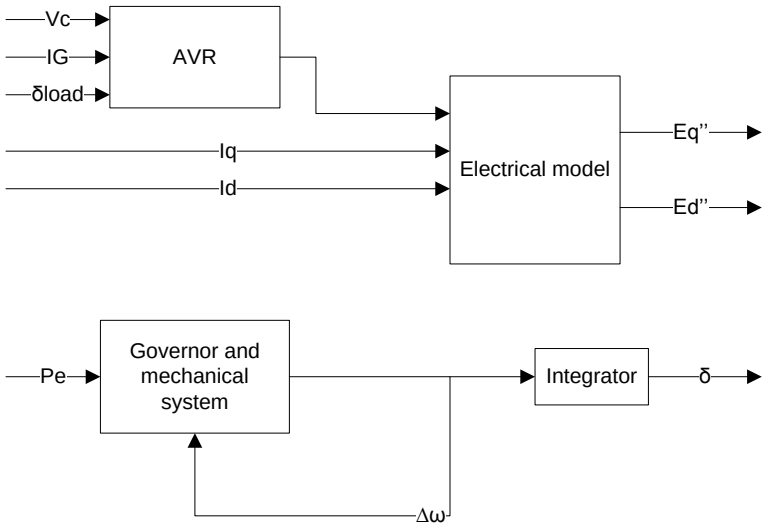

Figure 2-21

Since the model should be able to simulate the influence of changing loads in combination with a limited power output of the generators on the voltage stability, the 5th order model was chosen. This model contains the equations of motion and the electrical differential equations describing the dynamic emfs. One simplification made from the complete (6th order) model is neglecting the screening effect of eddy currents in the rotor body. That results in $E_d' = 0$ and $X_q' = X_q$ However, it is described by the set of the following equations (2-56).

[4, p. 455]

$$M\,\Delta\dot{\omega}_m = P_m - P_e \qquad \text{Mechanical system}$$

$$\dot{\delta} = \Delta\omega \qquad \text{Mechanical system}$$

$$T'_{d0}\,\dot{E}'_q = E_f - E'_q + I_d(X_d - X'_d) \qquad \text{Electrical system}$$

$$T''_{d0}\,\dot{E}''_q = E'_q - E''_q + I_d(X'_d - X''_d) \qquad \text{Electrical system}$$

$$T''_{q0}\,\dot{E}''_d = -E''_d - I_q(X'_q - X''_q) \qquad \text{Electrical system}$$

2-56

2.2.1.1 Electric Model

The electric model implements the electrical differential equations using state models. The state variables E_q', E_q'' and E_d'' must be initialized.

To get the implemented system, the electrical equations in 2-56 have to be transformed using Laplace. The results are the following transfer functions

$$E_q' = \frac{1}{T_{d0}' \cdot s + 1}(E_f + I_d(X_d - X_d'))$$

$$E''_q = \frac{1}{T''_{d0} \cdot s + 1}(E_q' + I_d(X'_d - X''_d))$$

$$E_d'' = -\frac{1}{T''_{q0} \cdot s + 1} I_q\left(X'_q - X''_q\right)$$

2-57

The actual implementation in Simulink and the results of a short circuit test are shown in 6.1.

Thus the generator can be seen as an controlled voltage source behind an impedance. Consequently the voltage on the generator bus is depending on the emf and the generator current. To connect the above described model to the grid, represented by the admittance matrix, the subtransient voltages E_d'' and E_q'', provided by 2-57 are converted into an equivalent current source.[8].

Hereby, the subtransient internal emf E_Q'' is given by its d- and q-axis components related to the system frame with the angle δ. E_Q'' can be calculated with the equation 2-42.

$$E_Q'' = E_q'' \cdot cos\delta_k - E_d'' \cdot sin\delta_k + j(E_q'' \cdot sin\delta_k + E_d'' \cdot cos\delta_k)$$

2-58

The generator reactance Z_G contains the subtransient d- and q-axis reactance, but it can be simplified by only using the d-axis reactance.

$$I_{inj} = \frac{E_Q''}{Z_G + Z_T}$$

2-59

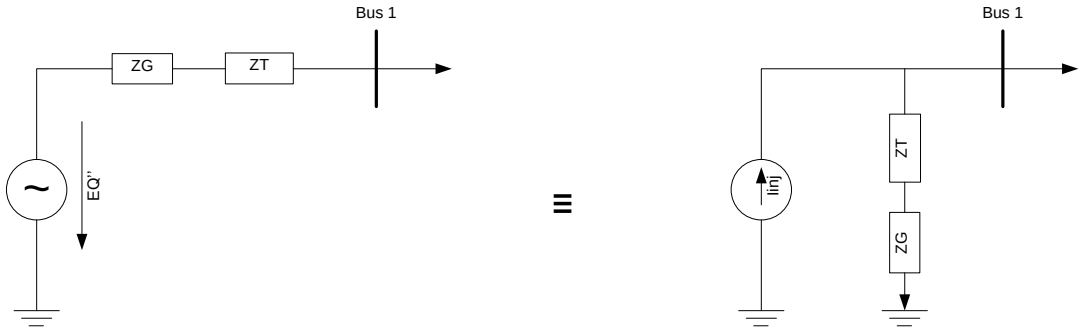

Figure 2-22

[8] The generator impedance Z_T disappears, if the generator is linked to the bus without a block transformer

After transforming all generators into current sources described by the injected current, the bus voltages of the system and later on the generator currents can be calculated.[9]

$$V_G = Y^{-1} I_{inj}$$

2-60

$$I_G = \frac{E_Q'' - V_G}{Z_G + Z_T}$$

2-61

2.2.1.2 Governor and Mechanical Model

This subsystem contains, apart from the differential motion equations of the synchronous generator and the primary power control, also a turbine model and the secondary control. To get more flexibility in the model, the secondary control and the turbine model can be deactivated (by the switch and by setting $T_H = 0$).

The primary controller has the task to stabilize the frequency of the system after a change in the active load. The frequency difference depends on the power plant droop σ.

$$\sigma = -\frac{\Delta f / f_n}{\Delta P / P_n}$$

2-62 [8, p. 69]

The used primary control is a standard governor with static droop and additional transient droop. The controller is reacting like proportional control with a gain of 1/σ.

The result is an inclined control characteristic as shown in Figure 2-23, where σ is representing the inclination. In a network with more power plants, a change in the active power load will be dispatched to these according to their control characteristic.

[9] The bus voltage of one single generator can also be calculated by applying the injected current to the parallel circuit of the Thevenin impedance seen from the generator bus and the generator impedance

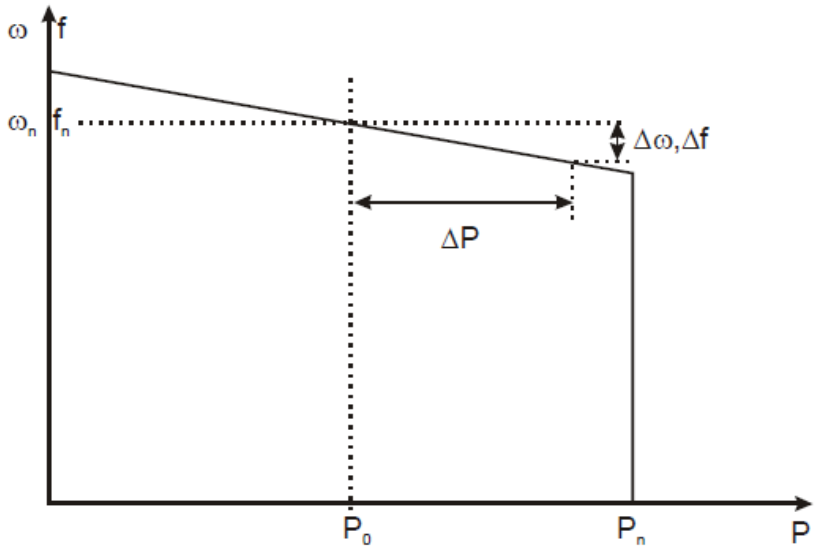

Figure 2-23 [8, p. 69]

However, as a change in the opening of the valves in water power plants results in a change of turbine power, which first reaction is in opposite direction as indented, there is a need of an additional control element to secure stability. That element has the function to ensure a small amplification in the moment of a fast load change but not to influence the control characteristic for steady state or slow changing loads. Therefore, a serial PD block is implemented, the so called transient droop.

The secondary control reacts slower than the primary control and is necessary to eliminate the frequency deviation. It is modelled as a PI-controller parallel to the primary controller.

The mechanical model is based on the first equation in 2-56. By the introduction of the moment of inertia J and conversion from the mechanical frequency ω_m to the electric frequency ω, following equations can be obtained.

$$J \cdot \omega_n \frac{\Delta\omega(\dot{t})}{p} = p \cdot \Delta P(t)$$

2-63[10]

$$\omega = p \cdot \omega_m$$

2-64

$$J\Delta\omega(\dot{t}) = M_{m(t)} - M_{e(t)}$$

2-65

$$M = \frac{P}{\omega}$$

2-66

[10] The mechanical damping is neglected, because of its relatively small values compared to the damping through the damper winding implemented in the electrical model

In the next step the introduction of the inertia constant H and scaling ΔP to the rated power S_n and ω to the rated frequency ω_n leads to

$$2H\Delta\omega(\dot{t}) = \Delta P(t) \tag{2-67}$$

$$H = \frac{1}{2}\frac{J\,\omega_n^2}{S_n\,p^2} \tag{2-68}$$

This equation must now be transformed using Laplace to calculate the implementable transfer functions of the system.

$$\Delta\omega(\dot{s}) = \frac{1}{2H\cdot s}\Delta P(s) \tag{2-69}$$

$$\delta(s) = \frac{\omega_n}{s}\Delta\omega(s) \tag{2-70}$$

The Simulink model and its reaction of a load change are shown in appendix 6.2.

2.2.1.3 AVR and Exciter

The automatic voltage regulator (AVR) is used to keep the voltage at the generator terminal or a given point in the network on the reference value. The basic block diagram of the AVR subsystem is shown in Figure 2-24.

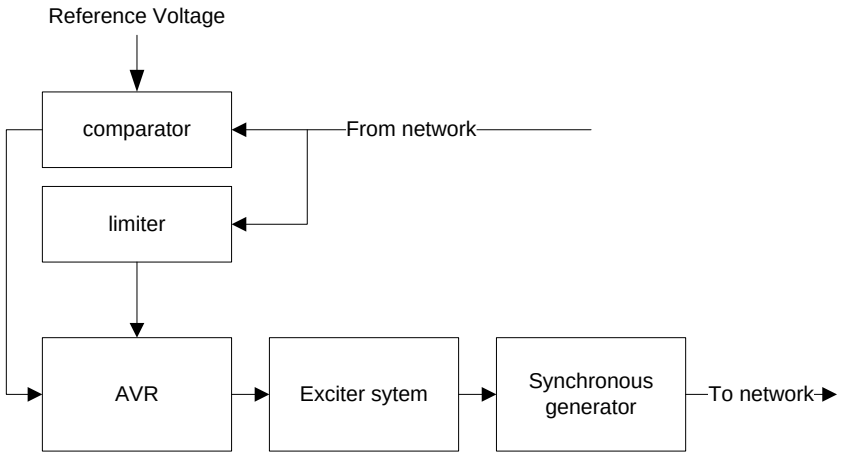

Figure 2-24

The load compensation element provides an offset depending on the generator current, which is added to the reference voltage. Through the value of the compensation impedance it is possible to shift position of the voltage regulation point [4, p. 95].

$$V_C = \left|\underline{V_G} + \underline{Z_C} \cdot \underline{I_G}\right| \qquad 2\text{-}71$$

For a generator with block transformers the compensation impedance is used to shift the virtual regulation point into the transformer. If only the reactive part of the compensation impedance is taken into account, the compensation reactance can be calculated as

$$\underline{Z_C} = -jX_C = -(1-\kappa) \cdot X_T \qquad 2\text{-}72$$

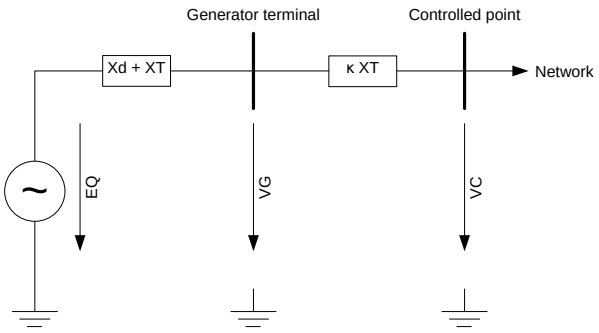

Figure 2-25, overview voltages

The output of the AVR is limited by the operation limits of the exciter system and the generator. These limits are maximal exciter current, maximal stator current and maximal power angle. That leads to four operation states of the AVR.

Each of these operation states can be described with its specific V(Q) characteristic. The combination of them will give the overall V(Q) characteristic of the generator unit.

I. Unlimited operational point

In this case, the generator is able to control the voltage at a given point in the network, resulting in $V_C = V_{ref}$ and the reactive power can be calculated from

$$P^2 + \left(Q + \frac{V_G^2}{\kappa \cdot X_T}\right)^2 = \left(\frac{V_{ref} V_G}{\kappa \cdot X_T}\right)^2$$

2-73

as

$$Q = \sqrt{\left(\frac{V_{ref} V_G}{\kappa \cdot X_T}\right)^2 - P^2} - \frac{V_G^2}{\kappa \cdot X_T}$$

2-74

II. Maximum field current

In this case the exciter unit is working on its upper limit, which means that the emf of the generator is at the maximum level E_{Qmax}. The generator is now acting as a constant voltage source behind an impedance.

$$Q = \sqrt{\left(\frac{E_{Qmax} V_G}{X_d + X_T}\right)^2 - P^2} - \frac{V_G^2}{X_d + X_T}$$

2-75

III. Maximum Power angle

Starting with the equations for transported power over a reactance, shown in 2-77 and 2-77,

$$P = \frac{V_1 V_2}{X_{12}} \sin \delta$$

2-76

$$Q + \frac{V_2^2}{X_{12}} = \frac{V_1 V_2}{X_{12}} \cos \delta$$

2-77

it is possible to get an equation for the reactive power as a function of active power, load angle and terminal voltage.

$$Q = P \cot \delta_{max} - \frac{V_G^2}{X_d + X_T}$$

2-78

IV. Maximum stator current

Equation 2-79 can be used. With V = V_G and I = $I_{G,rated}$ it can be transformed to equation 2-80.

$$\sqrt{P^2 + Q^2} = V \cdot I \qquad 2\text{-}79$$

$$Q = \sqrt{\left(V_G \cdot I_{G,rated}\right)^2 - P^2} \qquad 2\text{-}80$$

The combination of the Q(V)-characteristics of the four states is shown in Figure 2-26. In (a) P = 0 and in (b) P > 0.

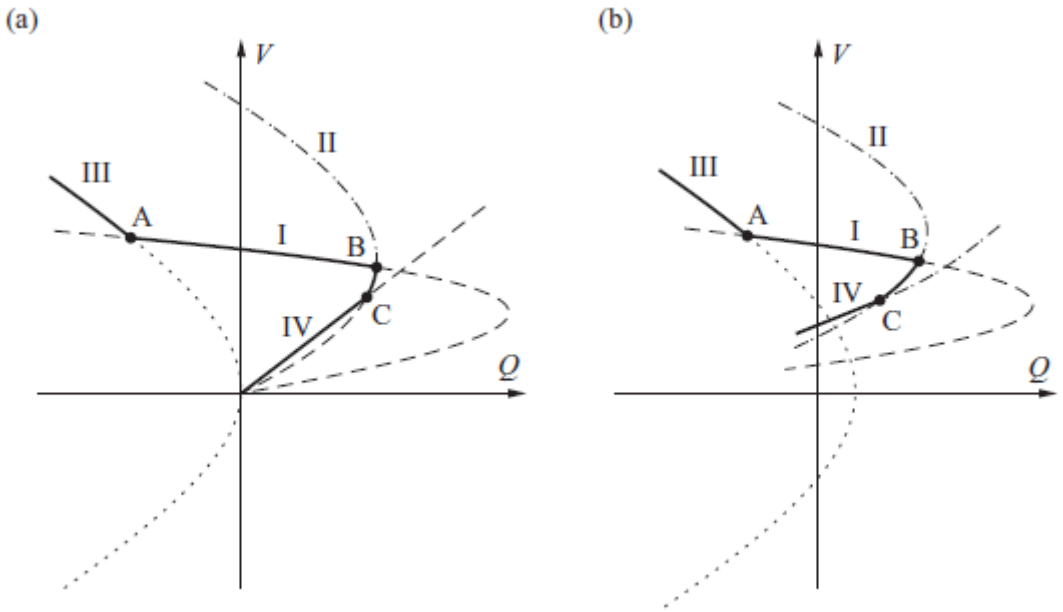

Figure 2-26 [4, p. 96]

The implementation of these limits in Simulink is accomplished with a dynamic saturation function. The upper limit is the minimum of the maximum exciter voltage (limit II) and the output of a PI-controller added to the maximum exciter voltage (limit IV). The input signal for that PI-controller is the difference between maximum stator current and the actual stator current. The integration part is limited to a range between the negative maximum exciter voltage and 0. That ensures a fast respond to an exceeding current.

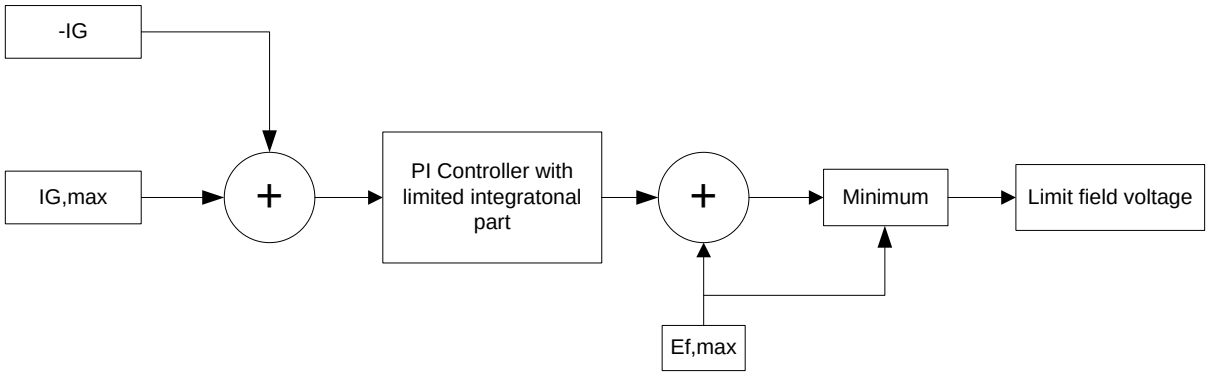

Figure 2-27, basic block diagram for upper limit

The lower limiter is based on the same idea. Its output is the maximum of minimal exciter voltage and the PI-controller output added to it (limit III). The input of the PI-controller is the difference between maximum load angle and actual load angle. As for the upper limiter the integration part is limited between 0 and maximum exciter voltage.

However, the dynamic saturation blocks at the limiters are used to get the minimum and maximum and to avoid simulation failures though exceeding the lower limit above the upper limit.

Following the validation and testing of the AVR functions are briefly described. The detailed Simulink model of the AVR can be found in appendix 6.3.

Figure 2-28 shows the test topology for the main function of the AVR. After running the simulation for 5 sec with a reference voltage of 1 p.u., the reference voltage is changed to 1,1 p.u., with the time response of the terminal voltage at bus 1 shown in Figure 2-29.

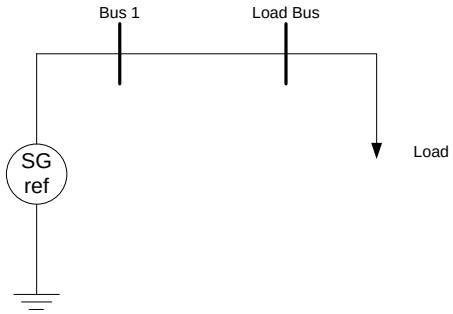

Figure 2-28

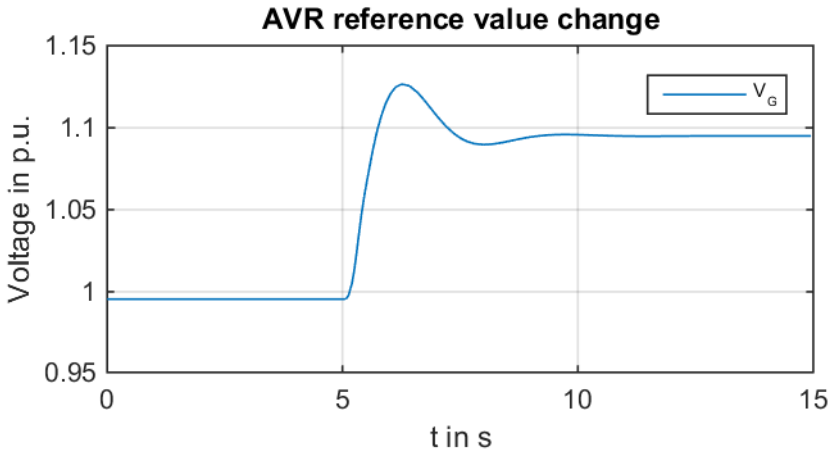

Figure 2-29

The in the AVR implemented limiter does not have to be tested separately as its correct function can be seen in the main results of this work.

2.2.2 Load Model

In reality the load seen from the network is a mix of different load behaviors, e. g. constant power or simple constant impedance loads. To get a simple load model, which is able to scope the reality and offering an adjustable division into constant power and constant impedance load, a parallel structure was chosen.

With the division parameter given as the percentage of resistive load, the resistive load amount can be modelled by multiplying this parameter with the rated power. The modelling of the constant power load is done by adding a PI-controller with the amount of controlled power as reference into the second branch. However, it is necessary to split the load calculation in the network model into controlled and resistive load power to get the correct actual values for the PI-controller.

The integration into the network can be accomplished by calculating the load impedance for both, controlled and resistive load, at the rated voltage[11].

$$Z_{L,controlled} = \frac{1}{conj(P_{controlled} + j \cdot Q_{controlled})} \quad 2\text{-}81$$

$$Z_{L,resistive} = \frac{1}{conj(P_{resistive} + j \cdot Q_{resistive})} \quad 2\text{-}82$$

[11] As the whole model is working with p.u. values, the rated voltage is 1

As the overall load impedance seen from the load bus is

$$Z_L = Z_{L,controlled} || Z_{L,resistive} = \frac{Z_{L,controlled} \cdot Z_{L,resistive}}{Z_{L,controlled} + Z_{L,resistive}}$$

2-83

or with using 2-81 and 2-82

$$Z_L = \frac{1}{conj(P_{L,controlled} + P_{L,resistive} + j \cdot (Q_{L,controlled} + Q_{L,resistive}))}$$

2-84

The actual load power can now be calculated, as shown bellow

$$S_L = V_L * conj\left(\frac{V_L}{Z_L}\right)$$

2-85

In appendix 6.4 the Simulink model and its load recovery behavior is shown for different divisions between resistive and controlled load.

The function test for the load model is done by assuming it connected to two generators with parallel lines, see Figure 2-30. After 50 sec a tripping of one parallel line is assumed, which leads to a voltage drop at the load bus. As the load is integrated into the network as an impedance, the voltage drop causes the load power to decrease. The controlled part of the load recovers with a rate depending on the time constant of its controller.

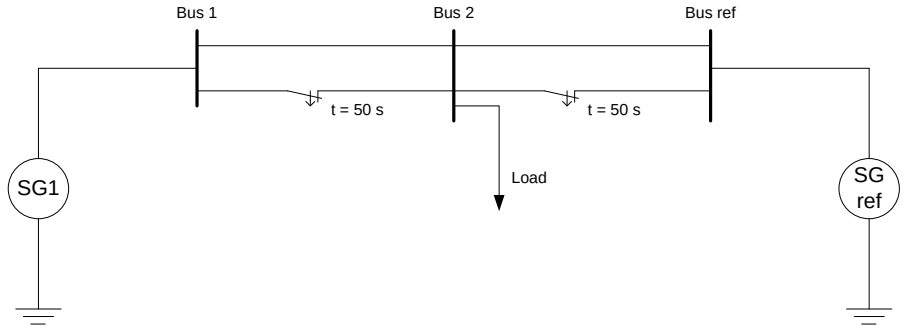

Figure 2-30[12]

[12] The topology was chosen with to generators, because it offers the meanings to test the load behaviour with only a small necessary change in the network admittance from the main model.

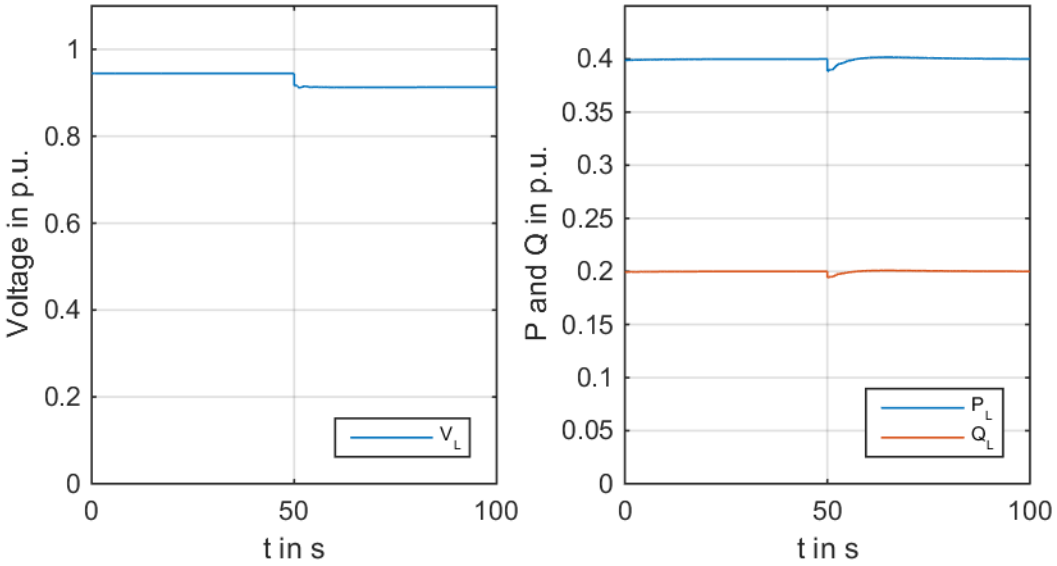

Figure 2-31, 100% controlled load

2.2.3 Network

Due to the simple estimation of the admittance matrix the network is represented by it.

$$Y = \begin{bmatrix} Y_{11} & \cdots & Y_{1n} \\ \vdots & \ddots & \vdots \\ Y_{n1} & \cdots & Y_{nn} \end{bmatrix}$$

$$= \begin{bmatrix} \sum of\ all\ Y\ connected\ to\ 1 & \cdots & -\sum of\ all\ conneting\ Y\ between\ 1\ and\ n \\ \vdots & \ddots & \vdots \\ -\sum of\ all\ conneting\ Y\ between\ 1\ and\ n & \cdots & \sum of\ all\ Y\ connected\ to\ n \end{bmatrix}$$

2-86

3 Results

The accuracy of the proposals to estimate the Thevenin impedance for saturated generators was tested by running a simulation of a simple subtransmission network, which is shown in Figure 3-1. The generator SG_{ref} represents the transmission network and is therefore assumed without any limits. To show the influence of each discussed operation limit, the limiting parameters of generator SG_1 are set depending on the goal for each simulation.

The complete list of the generator parameters is found in 6.6 for all simulations.

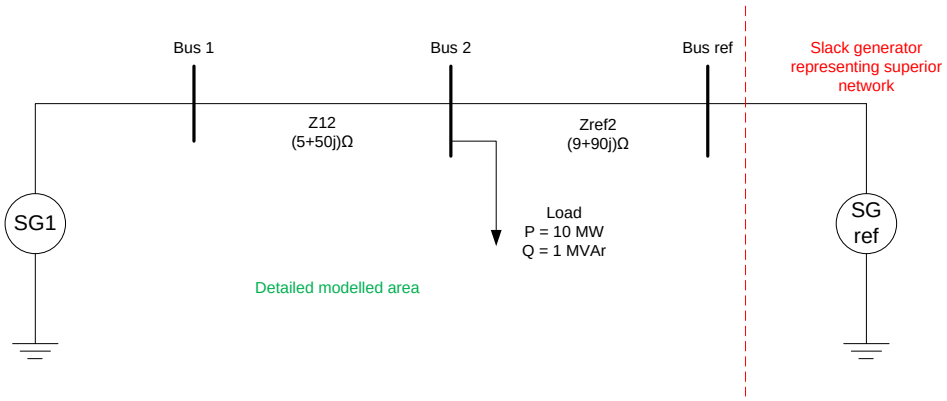

Figure 3-1

The original Thevenin impedance seen from the load is calculated as

$$Z_{Th} = jZ_{12} || jZ_{ref2} = j\,\frac{Z_{12} \cdot Z_{ref2}}{Z_{12} + Z_{ref2}}$$

3-1

The adjusted Thevenin impedance, which considers all limits of SG_1, is depending on the adjustments for Z_{12}.

$$Z_{12,adjusted} = \begin{cases} Z_{12} & no\ limits\ reached \\ \dfrac{j}{4P_{G,max}} & active\ power\ dispatch \\ \dfrac{4j}{I_G} & field\ current\ limit \\ \dfrac{4j}{I_{G,rated}} & stator\ current\ limit \end{cases}$$

3-2

$$Z_{Th,adjusted} = jZ_{12,adjusted} || jZ_{ref2} = j\,\frac{Z_{12,adjusted} \cdot Z_{ref2}}{Z_{12,adjusted} + Z_{ref2}}$$

3-3

As an accuracy index the deviation in the apparent load power is used and calculated as following

$$Deviation = \frac{S_{max} - S(|Z_{Th,adjusted}| = |Z_{load}|)}{S_{max}} \quad 3\text{-}4$$

The implemented algorithm replaces the original connection impedance with the adjusted, if the concerned limiting parameter (active power, field current, armature current) falls below a 5 % margin based on its rated maximum value. In case more than one parameter is inside this margin, the one with a smaller percent reserve is chosen. However, for operating a generator with constant active power, the margin definition for active power dispatch must be changed. Instead of the maximum rated active power, the set active power plus 1% defines the reference value. The additional 1 % added is necessary, because the actual active power will always equal the set active power. Otherwise, even reaching the other limits would not change the impedance.

To evaluate the influence of operation parameters several different configuration of the load and SG_1 were used. An overview is shown in Table 1. Additional the influence of the restricting parameters of the generator were evaluated. Therefor only the examined parameter was limited and the simulation run with different values for it.

	P_{SG1}	Q_{SG1}	P_{SG_ref}	Q_{SG_ref}	P_L	Q_L
Influence active power demand	controlled	controlled	controlled	controlled	constant	+ 0,002 p.u./s
controlled load						
resistive load						
Influence active power SG1 1	constant	controlled	controlled	controlled	+ 0,002 p.u./s	constant
controlled load						
resistive load						
Influence active power SG1 2	constant	controlled	controlled	controlled	+ 0,002 p.u./s	+ 0,002 p.u./s
controlled load						
resistive load						
Influence armature current limit	constant	controlled	controlled	controlled	+ 0,002 p.u./s	+ 0,002 p.u./s
controlled load						
resistive load						
Influence exciter current limit	constant	controlled	controlled	controlled	+ 0,2 MW/s	+ 0,002 p.u./s
controlled load						
resistive load						

Table 1

For a correct interpretation of the results, it must be noticed, that the operation status marked in the criteria diagrams are correlated to the time at which load impedance and Thevenin impedance equal each other. However, the marked status for the unadjusted Thevenin impedance is not conform with the theoretical maximum loadability without saturation effects of the generators.

3.1 Constant P_L, increasing Q_L

The following diagrams show the influence of the active power load on the accuracy of the estimated Thevenin impedance. The reactive power was increased with a rate of 0,002 p.u./s starting at the time t = 50 s. The simulation was done for controlled and impedance load. Because this resulted into a huge amount of diagrams, only one time graph is shown here as an example. The others can be found in appendix 6.7.

Figure 3-2 shows the time course of the exciter voltage E_f and the armature current I_G for the generator SG_1. After constantly increasing load, starting at t = 50s, the field current reaches its maximum value approximately at t = 160 s. The adjusted Thevenin impedance $Z_{Th,adjusted}$ increases due the change of the impedance Z_{12} approximately at t = 145 s, since the 5 % margin is already reached at that time. Henceforth, $Z_{Th,adjusted}$ decreases steadily with increasing armature current until the maximum armature current is reached. Reaching the maximum armature current the implemented armature current limiter forces the AVR to reduce the exciter current. The impedance Z_{12} take on a constant value again according to 3-2. However, no jump in the value of the impedance will occur at that time, since the actual armature current, defining the adjusted impedance for the excitation limit, is equal to the rated (maximum) armature current, defining the adjusted impedance for the armature current limit. The detailed transition of $Z_{Th,adjusted}$ between reaching the two limits is shown in Figure 3-3.

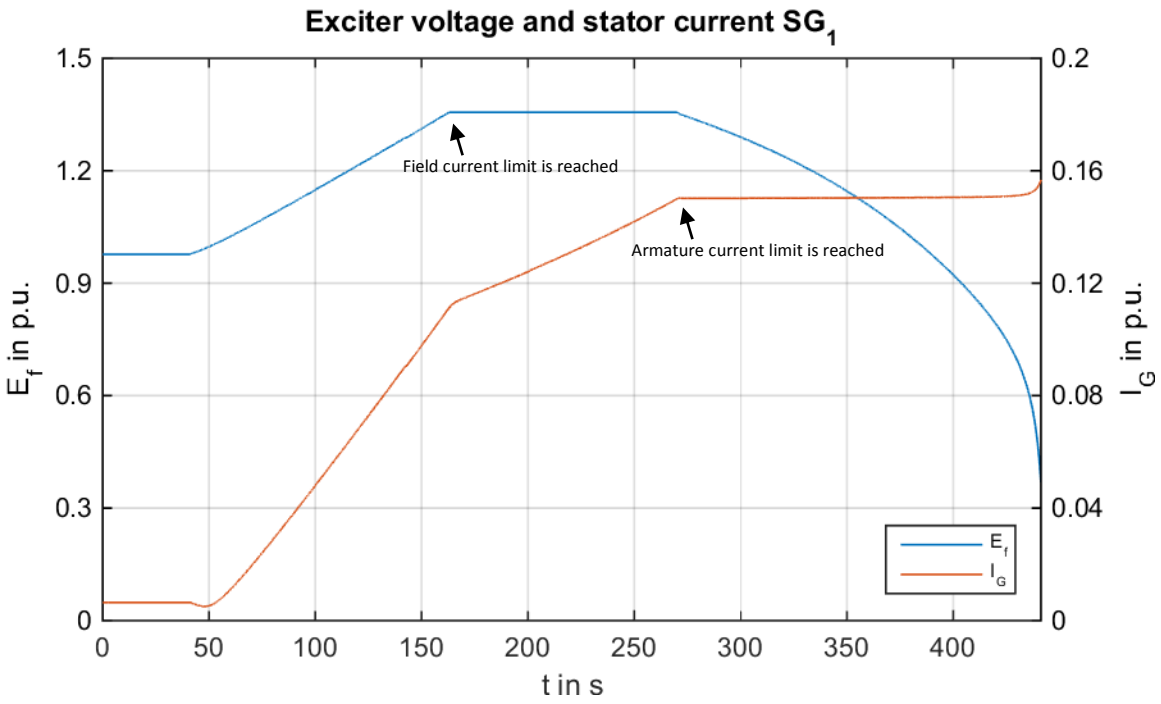

Figure 3-2, P_L = 0,01 p.u., 100% controlled load

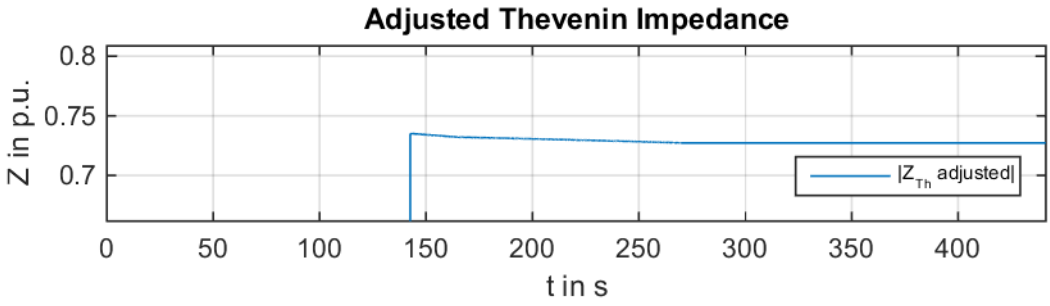

Figure 3-3, P_L = 0,01 p.u., 100% controlled load

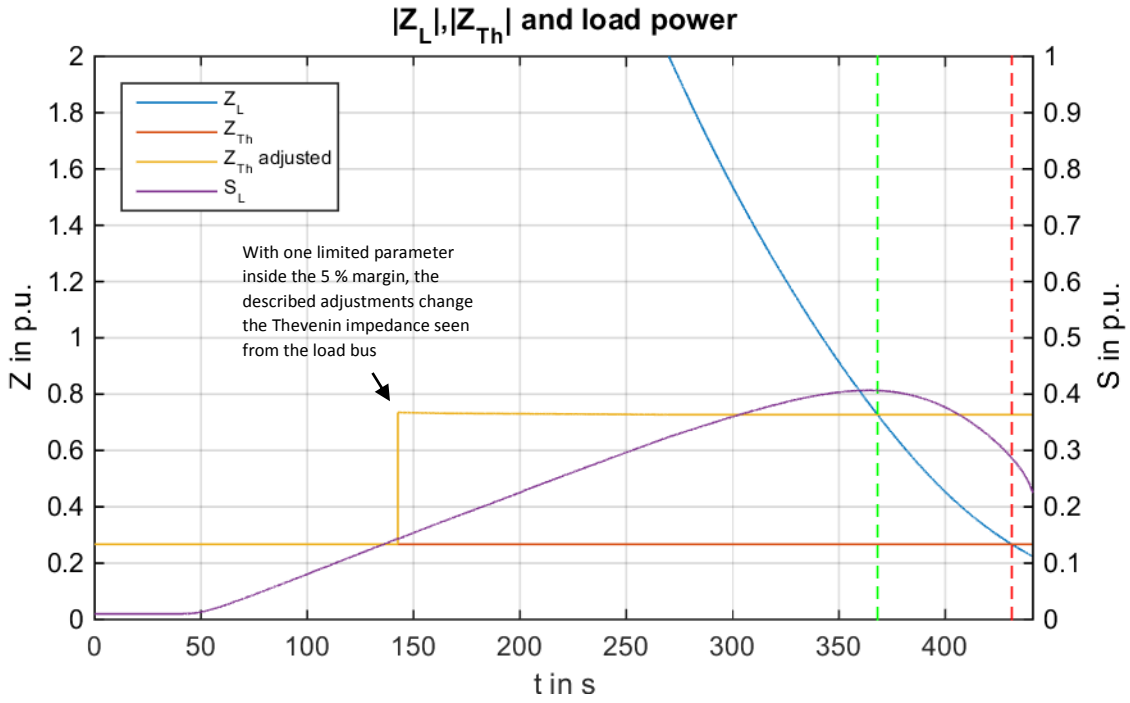

Figure 3-4, P_L = 0,01 p.u., 100% controlled load

In Figure 3-4 the time course of the apparent load power S_L and the considered impedances is shown. Before any of the limiting parameters falls below the 5 % margin, the adjusted and original Thevenin impedance are equal. The dotted lines indicate the time at which the Thevenin condition for maximum load power is met, green for the adjusted impedance and red for the original one.

The evaluation of the voltage stability, based on the criteria described above, is done by tagging the operational conditions at the moment fulfilling the Thevenin condition. Figure 3-5 and Figure 3-6 show the results for different amounts of active load power.

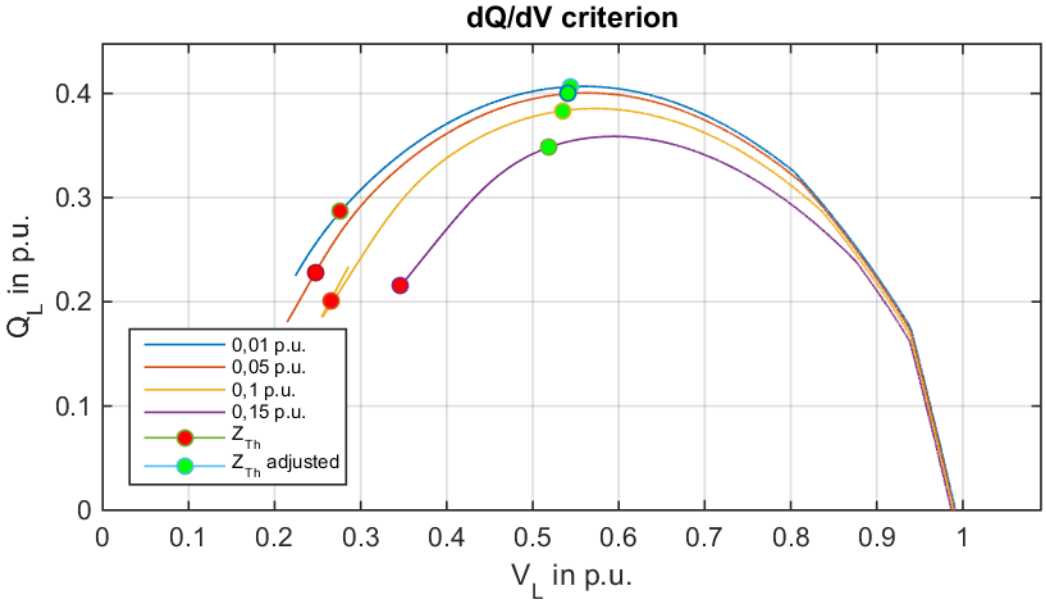

Figure 3-5, 100% controlled load

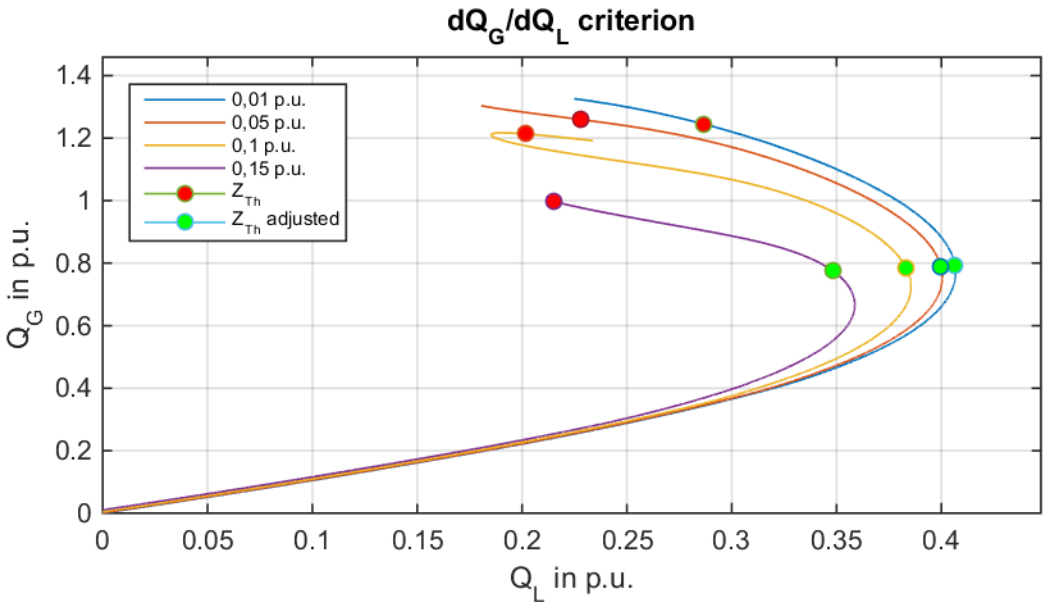

Figure 3-6, 100% controlled load

The accuracy of the described method is exploited by calculating the deviation in the apparent load power as stated in 3-4.

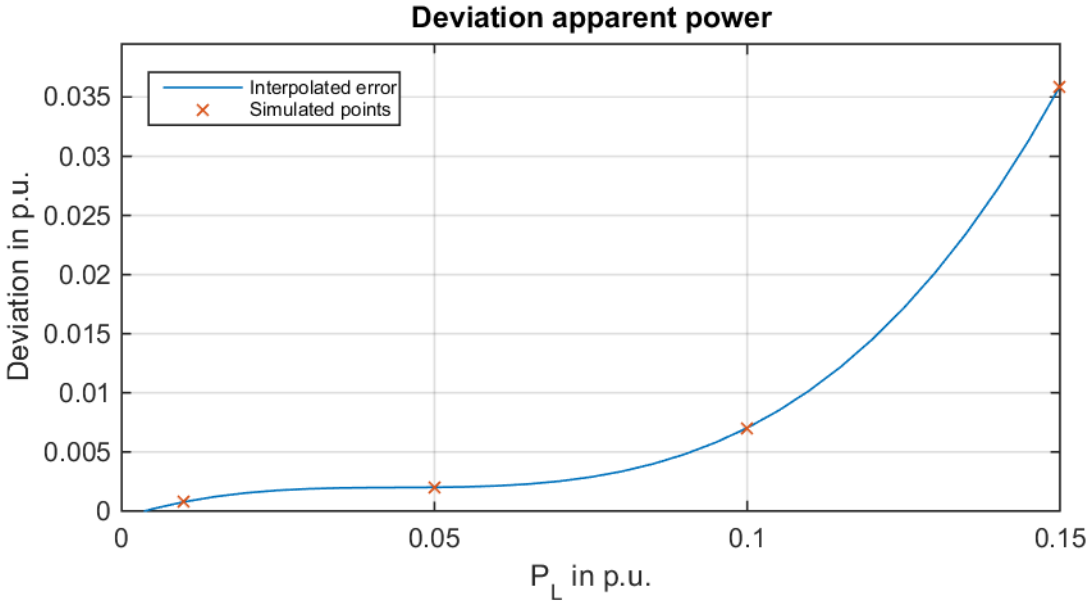

Figure 3-7, 100% controlled load

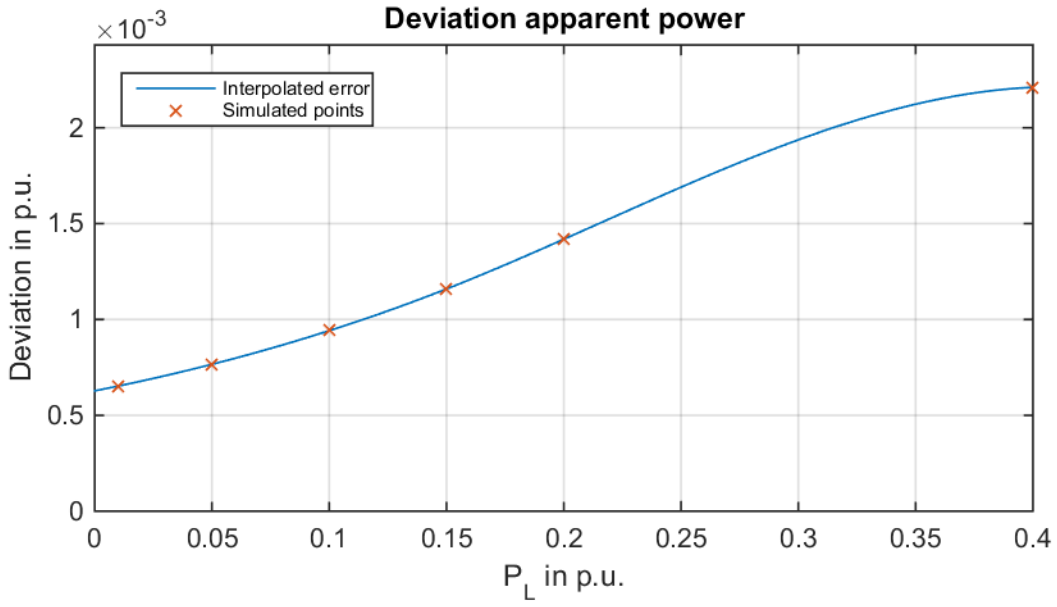

Figure 3-8, 100% impedance load

3.2 Constant active power of small generator, increasing load demand

In this case the governor of the smaller generator SG1 was deactivated. Its active power was seen as a parameter influencing the estimation of the Thevenin impedance. The simulation was done with controlled and impedance load. Moreover for both only the active load and active and reactive load were increased. The following diagrams only show an example, where P_L and Q_L were increased with a rate of 0,002 p.u./s. The whole simulation results can be found in 6.7.

Figure 3-9 shows the time course of the exciter voltage E_f and the armature current I_G for the generator SG_1. After constantly increasing load power the field current reaches its maximum value approximately at t = 110 s. The adjusted Thevenin impedance $Z_{Th,adjusted}$ changes its value approximately at t = 90 s, since the margin of the field current falls below the margin of the active power limit at this time. As described above the active power margin is set to 1 % for constant active power operation. Henceforth, $Z_{Th,adjusted}$ decreases steadily with increasing armature current until the maximum armature current is reached. Reaching the maximum armature current the implemented armature current limiter forces the AVR to reduce the exciter current. The impedance Z_{12} takes a constant value again according to 3-2. However, no jump in the value of the impedance will occur at that time, since the actual armature current, defining the adjusted impedance for the excitation limit, is equal to the rated (maximum) armature current, defining the adjusted impedance for the armature current limit. The detailed transition of $Z_{Th,adjusted}$ is shown in Figure 3-10.

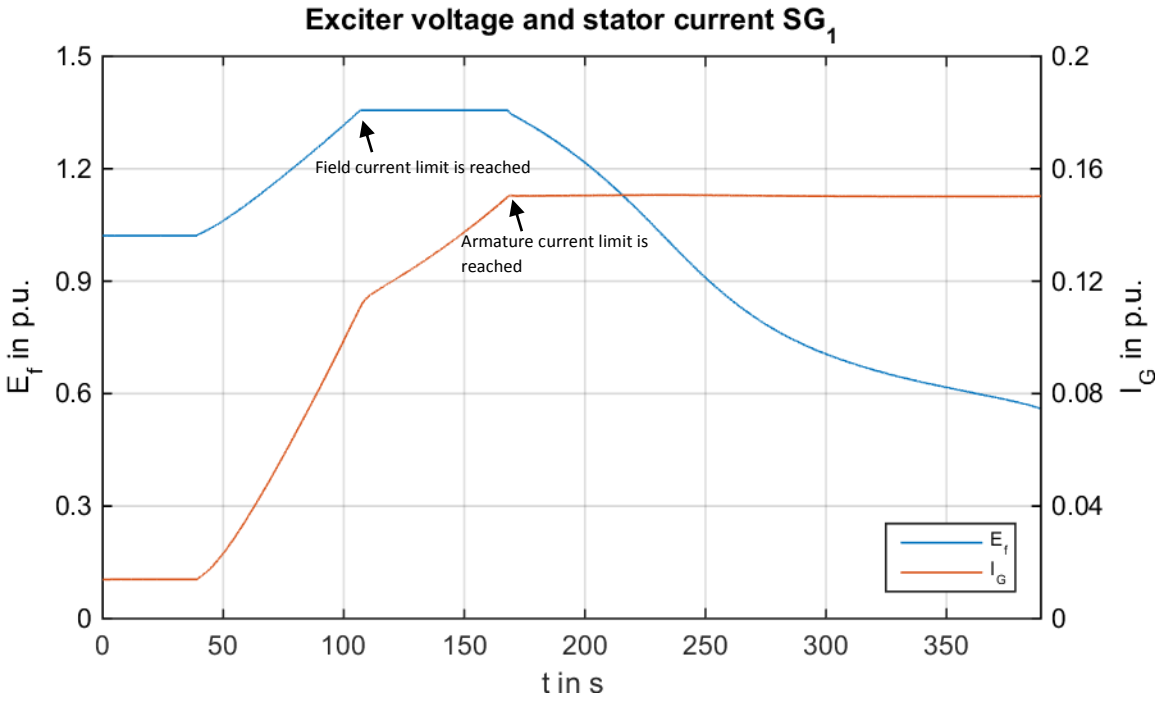

Figure 3-9, P_1 = 0,01 p.u., P_L and Q_L increasing, 100% controlled load

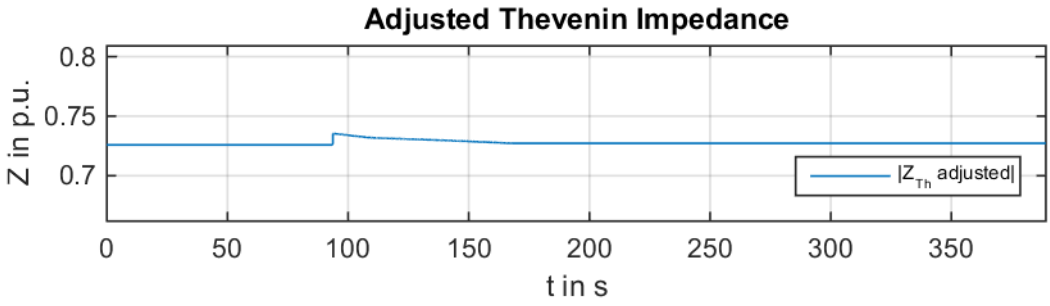

Figure 3-10, P_1 = 0,01 p.u., P_L and Q_L increasing, 100% controlled load

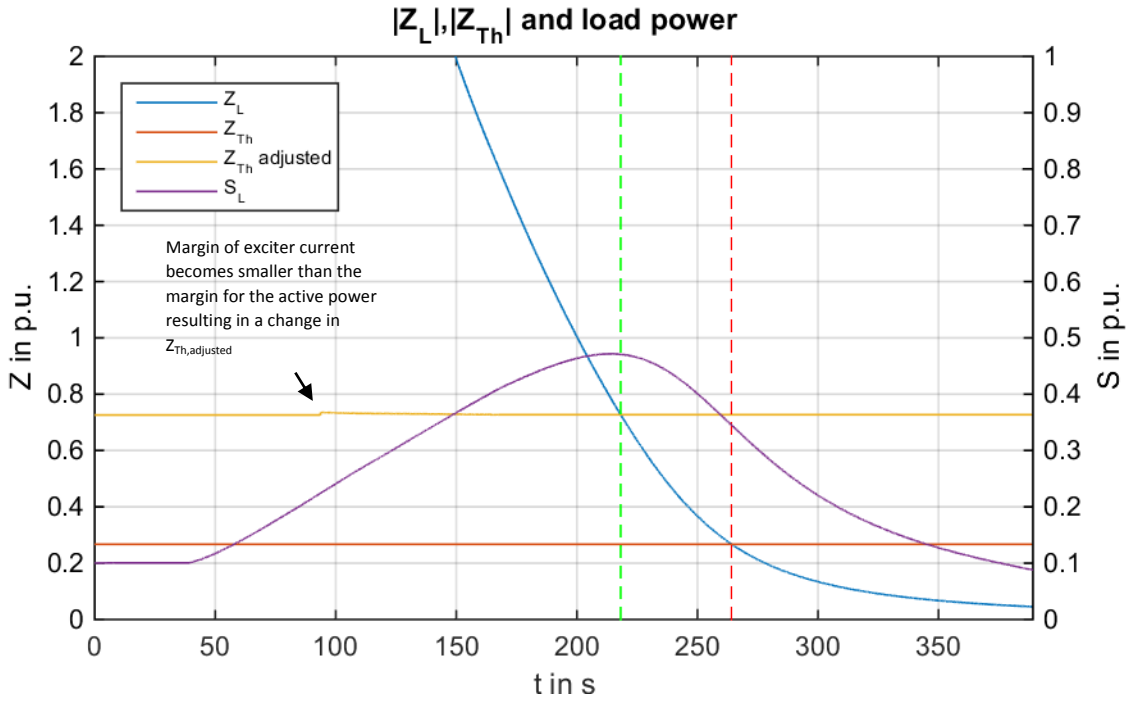

Figure 3-11, P_1 = 0,01 p.u., P_L and Q_L increasing, 100% controlled load

In Figure 3-11 the time course of the apparent load power S_L and the considered impedances is shown. The adjusted and original Thevenin impedance are different from the beginning on, since the constant active power of the generator SG_1 must be treated as its active power limit. The dotted lines indicate the time at which the Thevenin condition for maximum load power is met, green for the adjusted and red for the original one.

The evaluation of the voltage stability based on the criteria described above is done by tagging the operational conditions at the moment fulfilling the Thevenin condition. Figure 3-12 and Figure 3-13 show the results for different amounts of active power.

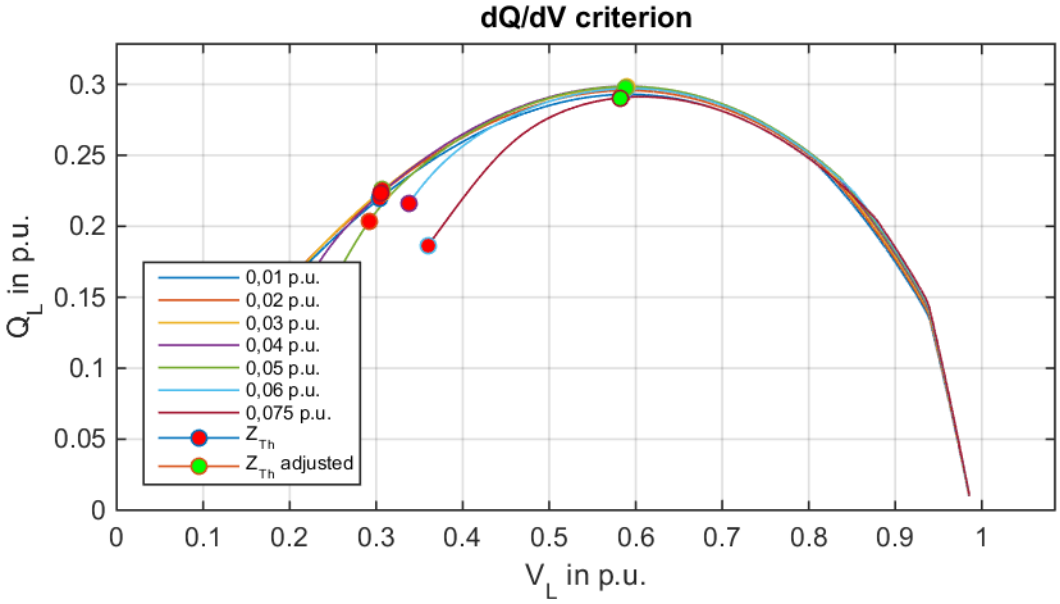

Figure 3-12, P_1 = 0,01 p.u., P_L and Q_L increasing, 100% controlled load

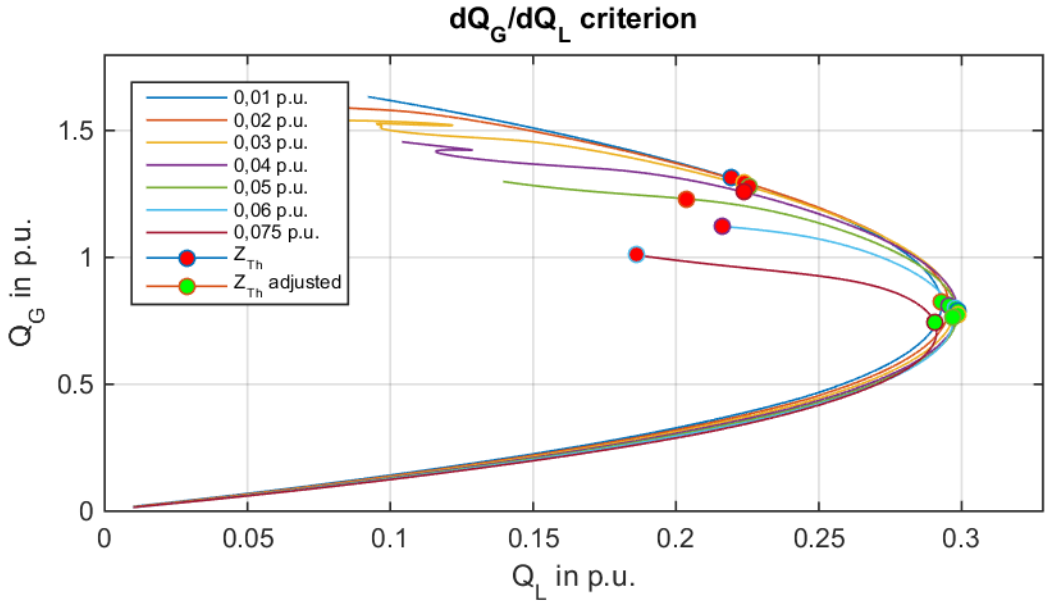

Figure 3-13, P_1 = 0,01 p.u., P_L and Q_L increasing, 100% controlled load

The accuracy of the described method is exploited by calculating the deviation in the apparent load power as stated in 3-4.

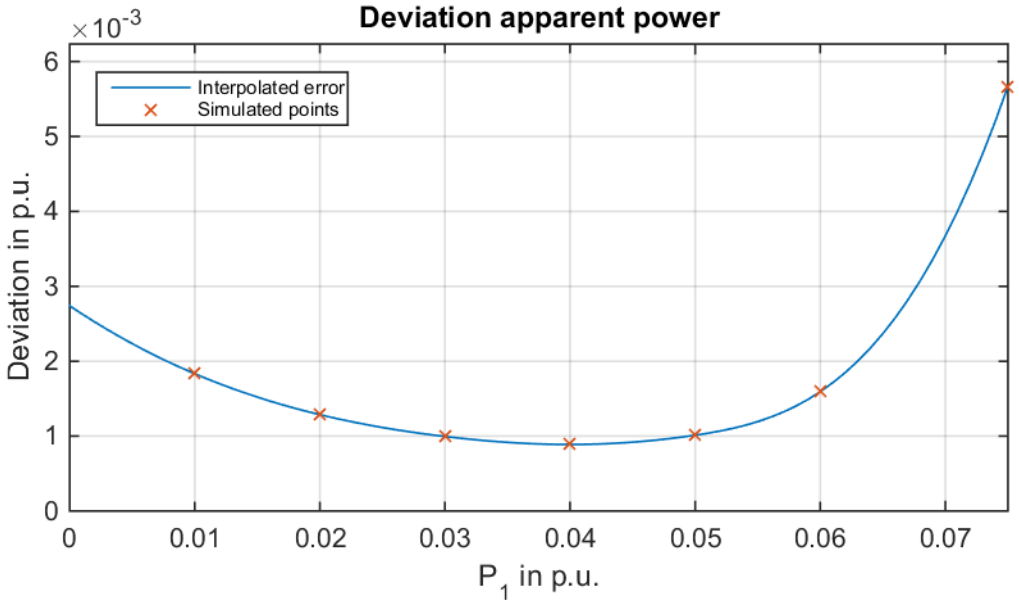

Figure 3-14, P_L and Q_L increasing, 100% controlled load

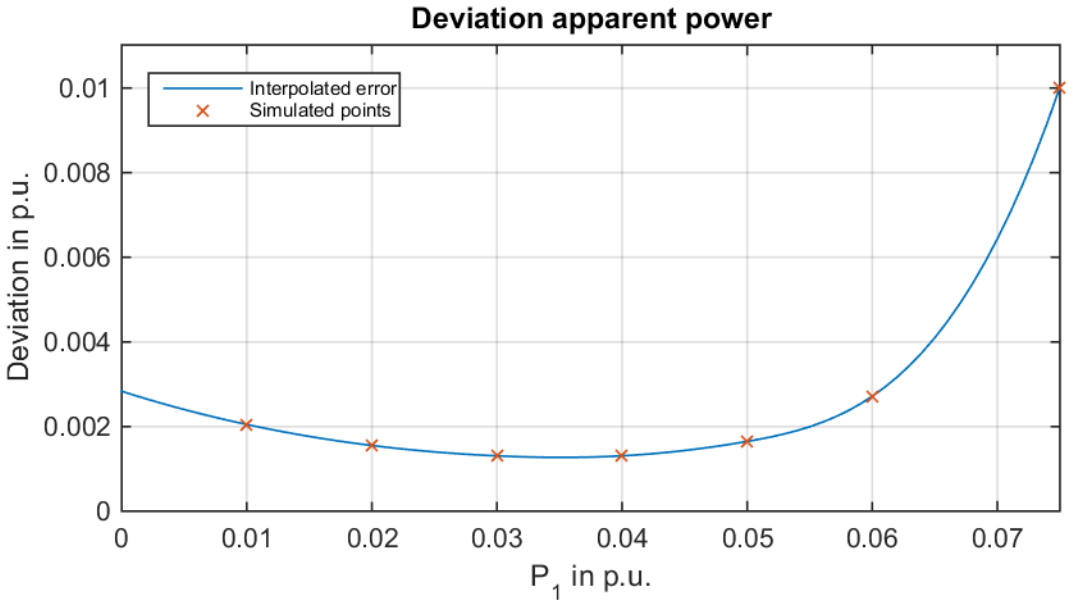

Figure 3-15, P_L and Q_L increasing, 100% impedance load

3.3 Limited Exciter

To test the influence the limitation of the exciter current the maximum apparent power of generator SG_1 was set to a value, which was not reached before the voltage collapse. The active power of SG_1 was set to 0,05 p.u. and the governor deactivated.
The load was simulated to be 100% controlled and started to increase with a rate of 0,002 p.u./s at the time t = 50 s.

In Figure 3-16 it can be seen, that reaching the excitation limit causes the armature current to rise slower. The armature current can be seen as unlimited, since the set limit with 10 p.u. is not reached before the system collapses. Focusing on the adjusted Thevenin impedance, Figure 3-15, that leads to a steadily decreasing value. The jump at approximately t = 100 s is caused by changing form the adjustment for the active power limit to the excitation limit.

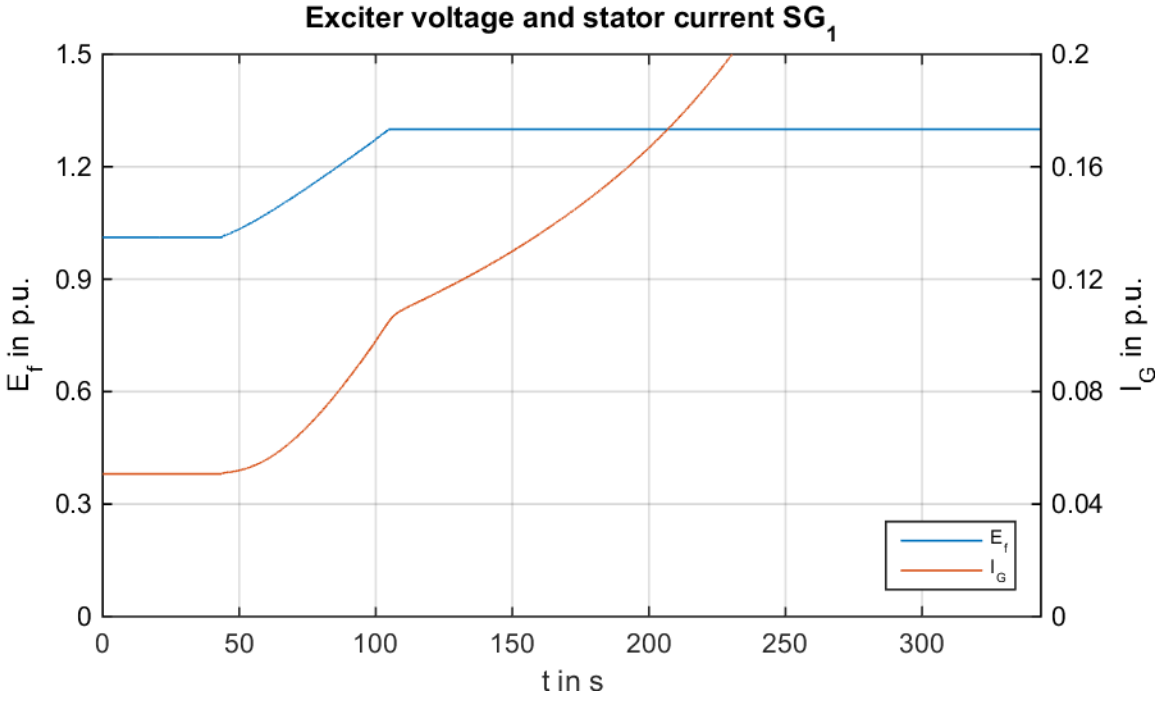

Figure 3-16, E_f = 1,3 p.u. $I_{G1,max}$ = 10 p.u., P_1 = 0,05 p.u.

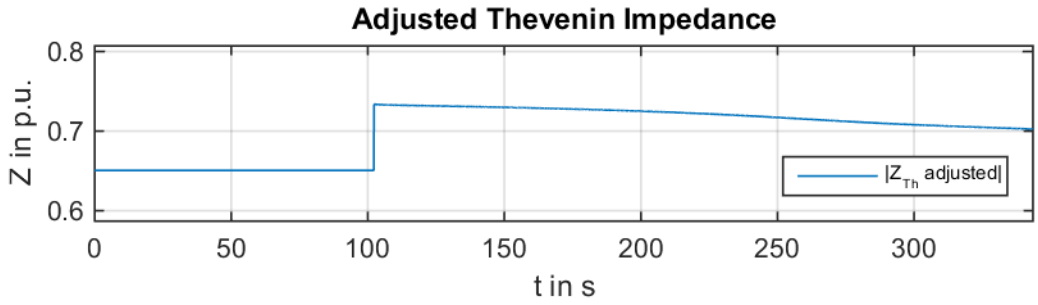

Figure 3-17, E_f = 1,3 p.u. $I_{G1,max}$ = 10 p.u., P_1 = 0,05 p.u

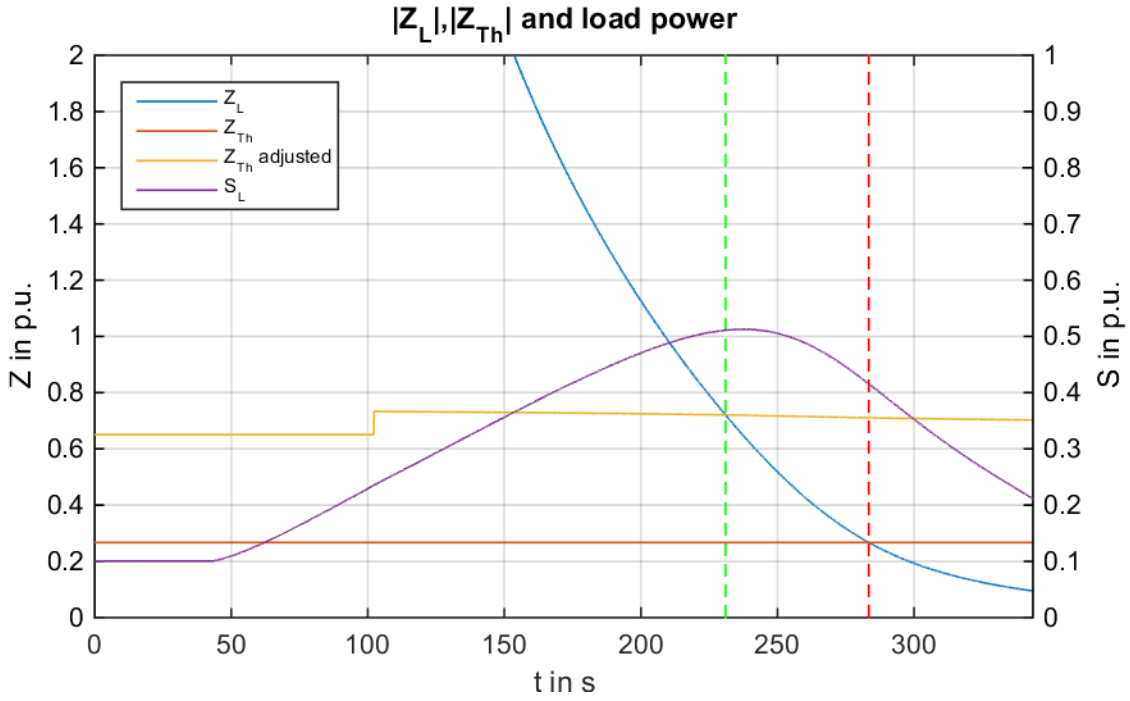

Figure 3-18, E_f = 1,3 p.u. $I_{G1,max}$ = 10 p.u., P_1 = 0,05 p.u

In Figure 3-18 the time course of the apparent load power S_L and the considered impedances is shown. The adjusted and original Thevenin impedance are different from the start, since a constant active power is set for generator SG_1. The dotted lines indicate the time at which the Thevenin condition for maximum load power is met, green for the adjusted and red for the original one.

The evaluation of the voltage stability based on the criteria described above is done by tagging the operational conditions at the moment fulfilling the Thevenin condition. Figure 3-19 and Figure 3-20 show the results for different excitation limits.

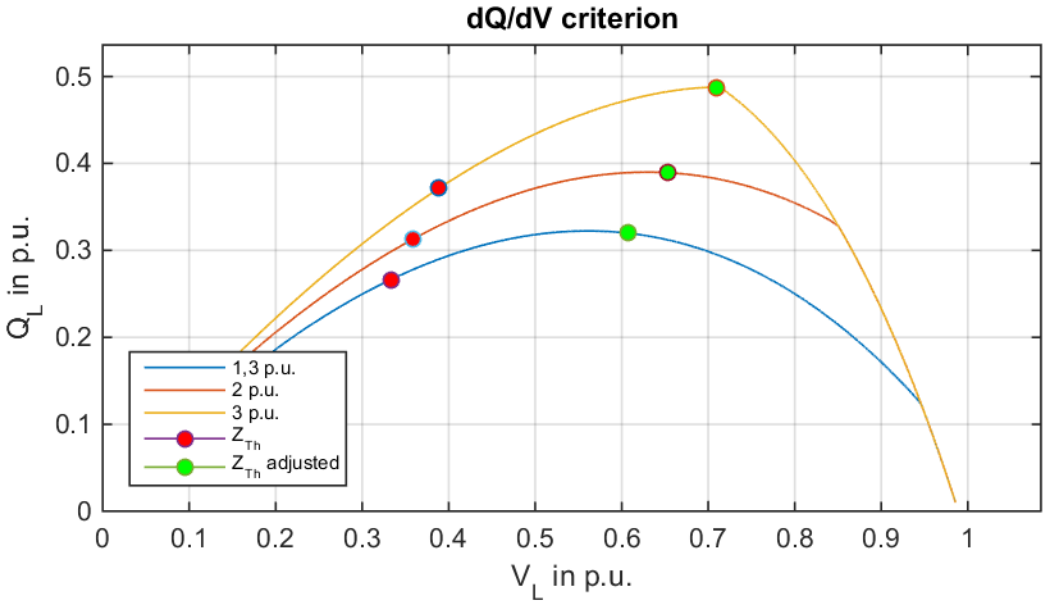

Figure 3-19, $I_{G1,max}$ = 10 p.u., P_1 = 0,05 p.u.

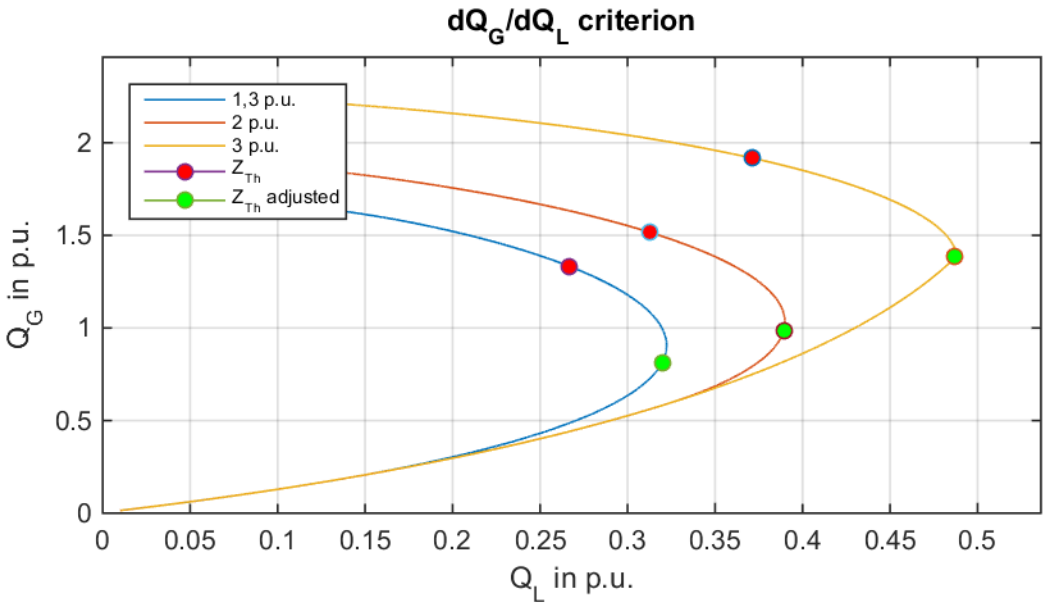

Figure 3-20, $I_{G1,max}$ = 10 p.u., P_1 = 0,05 p.u.

The accuracy of the described method is exploited by calculating the deviation in the apparent load power as stated in 3-4.

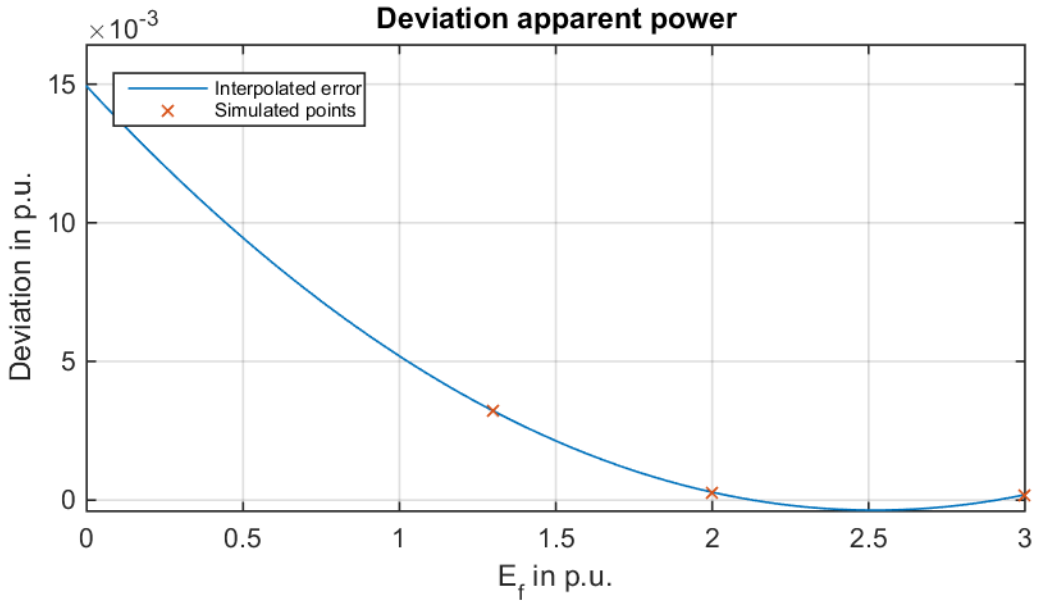

Figure 3-21, $I_{G1,max}$ = 10 p.u., P_1 = 0,05 p.u.

3.4 Limited Armature Current

The maximum exciter output was set to a none reached level to test the influence of the limitation of the armature current. To achieve comparable results, the active power of SG_1 was set to 0,05 p.u. and the governor was deactivated.
The load was simulated to be 100% controlled and started to increase with a rate of 0,002 p.u./s at the time t = 50 s.

In the time course of the exciter voltage and armature current, Figure 3-22, the behavior of the controller imitating the armature current can be seen. Since the excitation limit is assumed as infinite, the excitation is reduced nearly immediately after the armature current reaches its maximum value. The overshoot and its time constant are depending on the controller parameters and can be interpreted as the overload capability of the generator. In this simulation the parameters were set to keep the overshoot small, since the influence of the maximum armature current was examined.

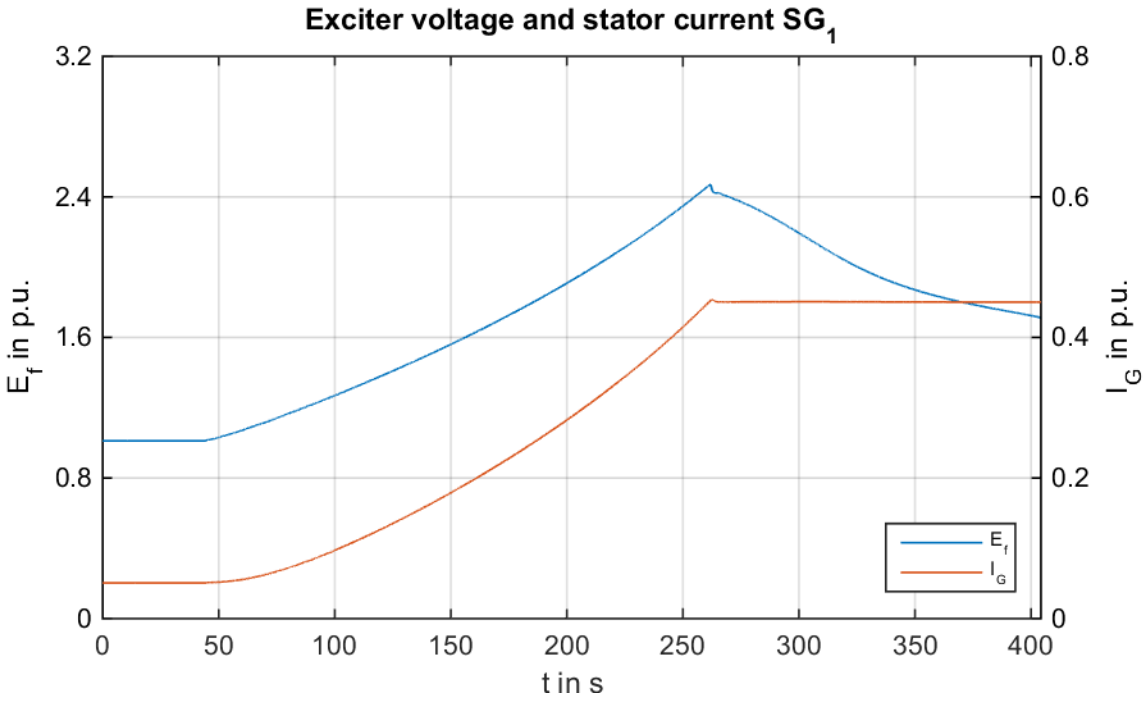

Figure 3-22, $I_{stator,max,SG1}$ = 0,45 p.u., $E_{f,max,SG1}$ = 2,5 p.u., P_{SG1} = 0,05 p.u.

Due the constant active power of the generator SG_1 the adjusted Thevenin impedance has a higher value than the original one from the beginning on. Approximately at t = 260 s the adjusted value jumps from the assigned to the active power limit to the one for the armature current limit. This behavior can be observed in the time course of the impedances and the load power shown in Figure 3-23. The dotted lines there indicate the time at which the Thevenin condition for maximum load power is met, green for the adjusted and red for the original one.

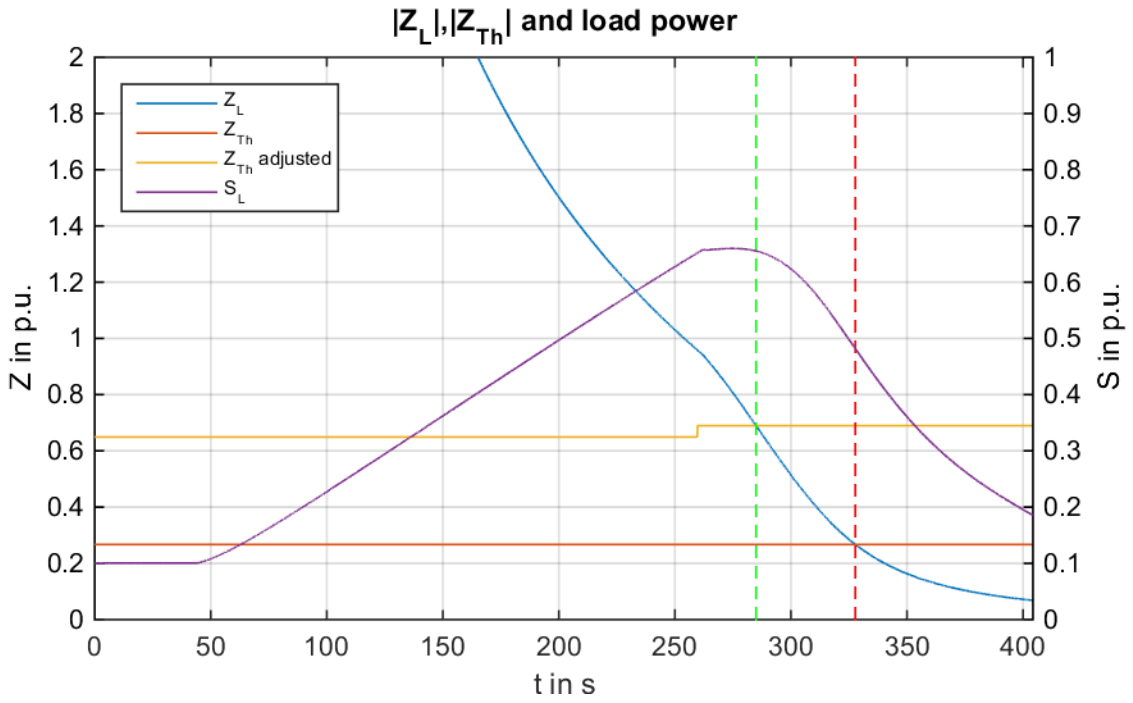

Figure 3-23, $I_{stator,max,SG1}$ = 0,45 p.u., $E_{f,max,SG1}$ = 2,5 p.u., P_{SG1} = 0,05 p.u.

Figure 3-24 shows the reactive power distribution between the infinite reference generator and the limited generator SG_1. After reaching the armature current limit the reactive power of SG_1 decreases immediately, but the voltage breakdown is delayed by the increasing reactive power of the reference generator.

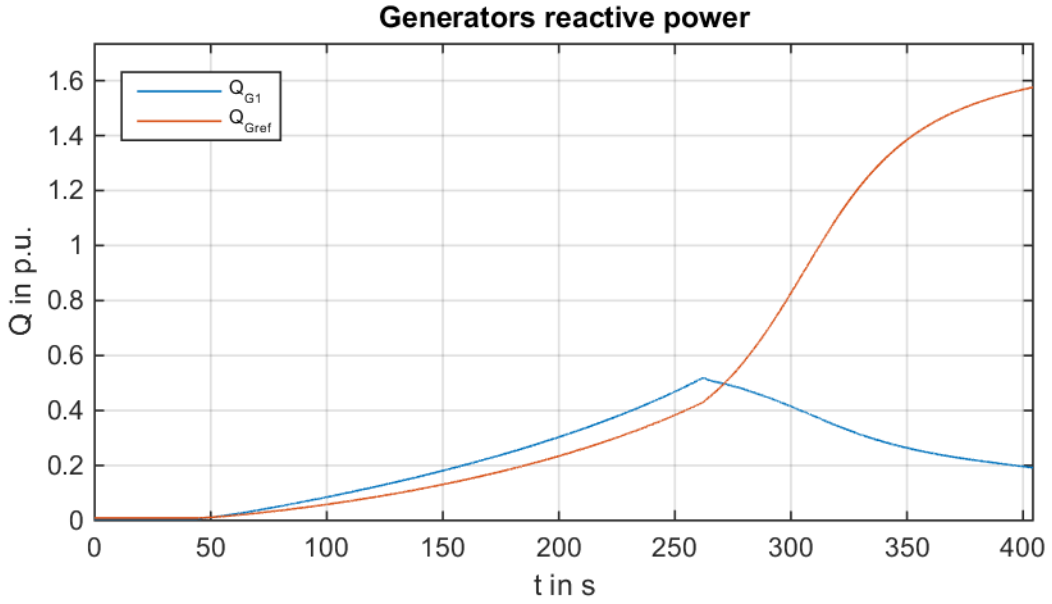

Figure 3-24, $I_{stator,max,SG1}$ = 0,45 p.u., $E_{f,max,SG1}$ = 2,5 p.u., P_{SG1} = 0,05 p.u.

The evaluation of the voltage stability based on the criteria described above is done by tagging the operational conditions at the moment fulfilling the Thevenin condition. Figure 3-25 and Figure 3-26 show the results for different armature current limits.

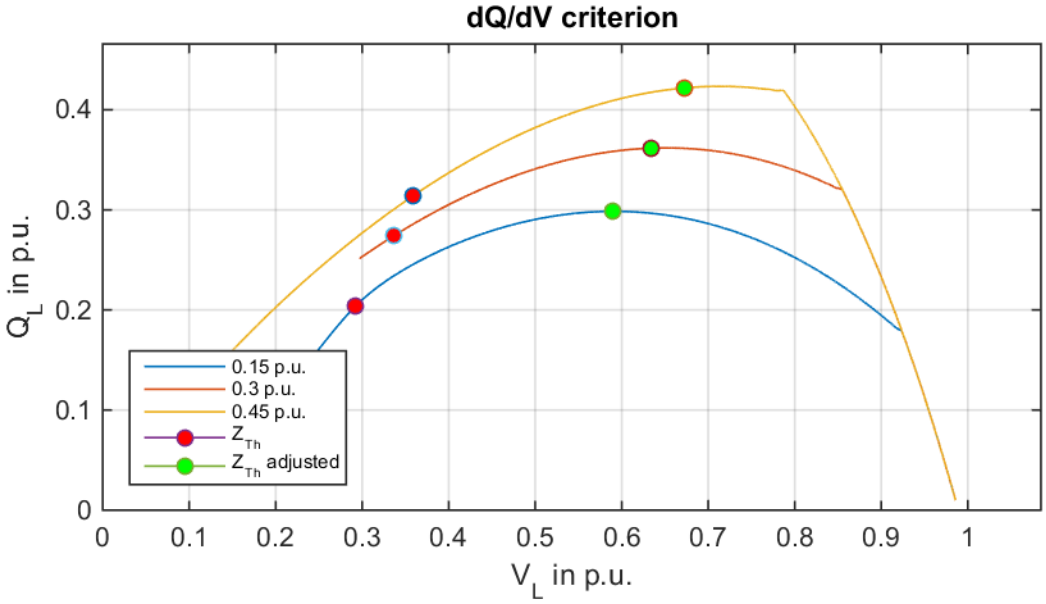

Figure 3-25, P_{SG1} = 0,05 p.u.

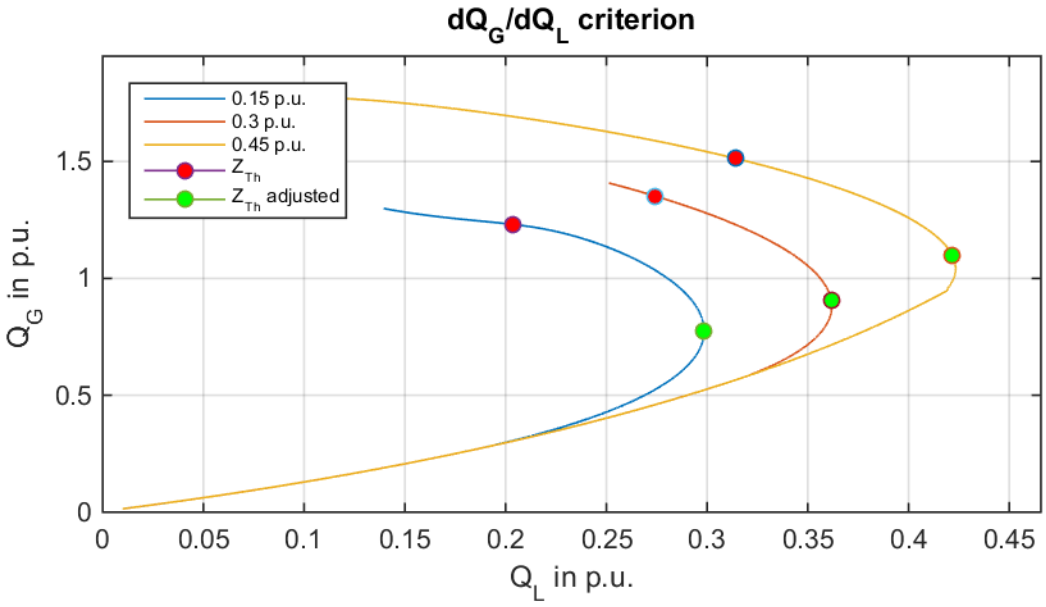

Figure 3-26, P_{SG1} = 0,05 p.u.

The accuracy of the described method is exploited by calculating the deviation in the apparent load power as stated in 3-4.

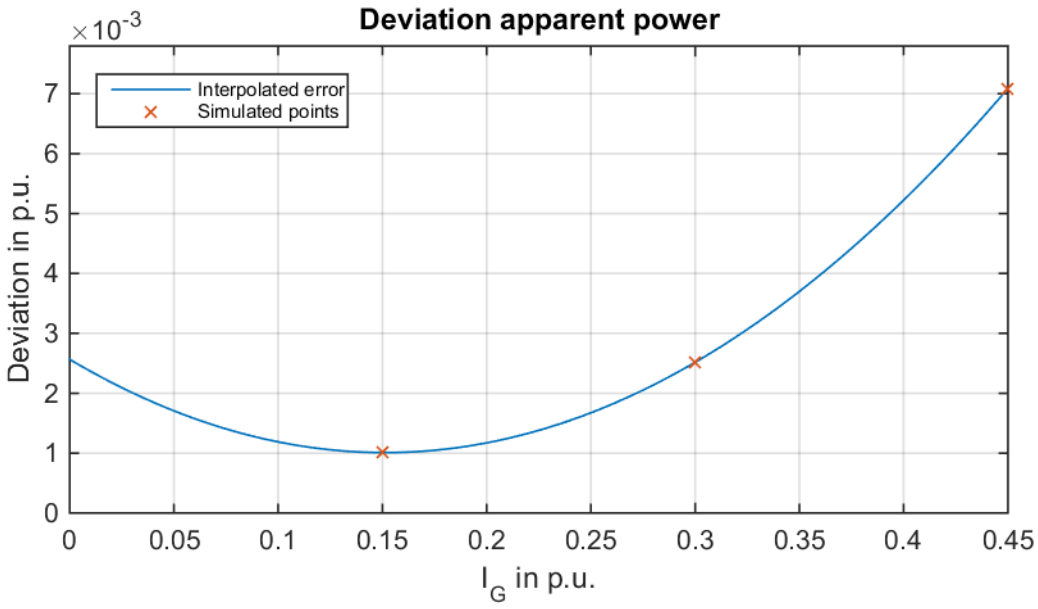

Figure 3-27, P_{SG1} = 0,05 p.u.

4 Discussion and Outlook

The results of the simulations show an improvement in the estimation of the actual system Thevenin impedance compared to the original one. The accuracy of the estimation is slightly influenced by the operation condition of the network and the capability borders of the generator. However, it should be emphasized, that, so far, only a simple network was simulated. If a multi generator network with no direct connections between load and saturated generator is examined, the adjustments discussed in this work are harder to implement. An idea how to improve the method when utilizing it for general networks is described briefly in 4.3.

4.1 Influence of the Operation Conditions

Both a constant active power demand and a constant active power production of the smaller generator lead to an increasing gap between the occurring apparent power at the estimated time of maximum power transmission and the in fact maximum apparent load power.

However, only if the load is considered as controlled and with constant active power, the difference is not in a range of 1%, see Figure 3-7. In contrast to this, the simulation with impedance load shows a nearly linear increase and a significantly reduced dependency on the active load power. This leads to the conclusion, that for controlled loads not only the amount of active power but also the interaction of time constants of the control load units and generators have an influence of the actual Thevenin impedance seen from the load bus.

4.2 Influence of the Generator Parameters

The simulations with different exciter limits show a decrease in error between the estimated and actual value. The reason for it can be found in the distribution of the produced reactive power between the two generators. Before the excitation limit is reached the distribution of reactive power is mainly defined by the network topology. If one generator is operated with its maximum field current, the reactive power transmitted from this generator to the load rises with a lesser slope leading to a change in the distribution. The smaller the difference between unsaturated distribution and actual distribution is, the more accurate is the estimation of the Thevenin impedance.

Unfortunately, this is not applicable for a limitation of the armature current. After the maximum stator current is reached, the control unit reduces the field current to avoid an further increase of the stator current. This leads to a decreasing terminal voltage and less reactive power is transmitted to the load. Due to this reaction the second generator is forced to transmit more reactive power to the load. The resulting misbalance in reactive power transmission causes the increasing mismatch between estimated and actual values for maximum power transmission.

4.3 Idea for Implementation into General Network Topologies

The mentioned methods for replacing the impedance between generator terminal and load terminal are only applicable for simple network topologies. To cope with the situation in more general topologies the method should be developed in a way to avoid the so far necessary direct connections between load and generator terminal. The first step to achieve that is to assume the generators as ideal voltage sources with a constant terminal voltage, which is not affected by the load of the generator.
However, the terminal voltage will decrease after the exciter or armature current limiter is reached. In contrast to the discussed solution, it should also be possible to adjust the impedance by introducing a virtual terminal, which is connected to the actual by an impedance. If the voltage is still assumed to equal the uninfluenced generator terminal voltage, the impedance between virtual and actual terminal can be calculated as following, therefore providing a possibility to solve the problem.

$$X_{virtual} = \frac{V_{G,rated} - V_G}{I_G} \qquad 4\text{-}1$$

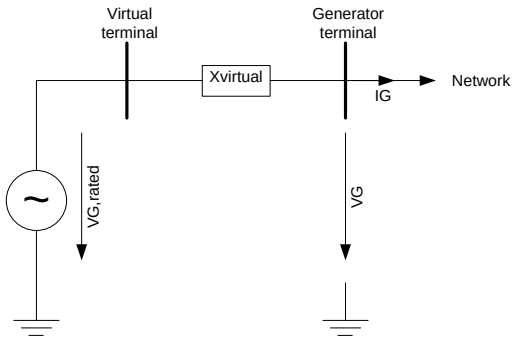

Figure 4-1

5 Bibliography

[1] V. Ajjarapu and C. Christy, “The continuation power flow: a tool for steady state voltage stability analysis,” *IEEE Trans. Power Syst., vol. 7,* pp. 416-423, February 1992.

[2] B. Gao, G. K. Morison and P. Kundur, "Voltage stability evaluation using modal analysis," *IEEE Trans. Power Syst., vol 7,* pp. 1529-1542, November 1992.

[3] D. T. Duong, K. Uhlen and S. Løvlund, "A Method for Real Time Voltage Stability Monitoring in Sub-transmission Networks," IEEE, Trondheim, 2013.

[4] J. Machowski, J. W. Bialek and J. R. Bumby, Power System Dynamics: Stability and Control, vol. 2, Chichester: John Wiley & Sons, 2008.

[5] V. Crastan, Elektrische Energieversorgung 3, 3. bearbeitete Auflage, Evilard: Springer-Verlag Berlin Heidelberg, 2011.

[6] V. A. Venikov, Transient Processes in Electrical Power Systems, Moscow: Mir, 1978.

[7] B. M. Weedy, Electric Power Systems, 3rd rev. edn, Chichester: John Wiley & Sons, Ltd, 1987.

[8] H. Renner, Regelung und Stabilität Elektrischer Energiesysteme, Graz: Institut für Elektrische Anlagen, TU Graz, 2013.

[9] R. Fischer, Elektrische Maschinen, 16. aktualisierte Auflage, Esslingen: Hanser, 2013.

[10] O. B. Fosso and K. Uhlen, Advanced modelling, Lectures to TET4180, Trondheim: Dept. of Electric Engineering NTNU, 2015.

[11] H. Saadat, Power System Analysis, Milwaukee: Kevin Kane, 1999.

[12] C. W. Taylor, Power System Voltage Stability, Portland, Oregon: McGraw-Hill, Inc., 1992.

6 Appendix

6.1 Implementation and Test of Electric System

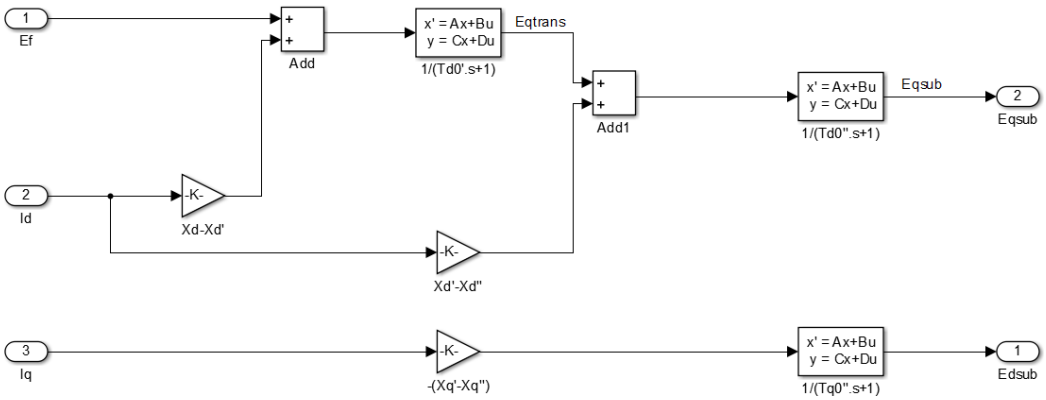

Figure 6-1

To verify the electrical system of the synchronous generator a short circuit was simulated and the generator current was scoped. However, as that test should be scoped only on the electrical system and kept simple, the AVR was replaced by a constant exciter voltage. The short circuit was simulated by reducing the load impedance to 1% of its former value after 2 s. The used topology is shown in Figure 6-2.

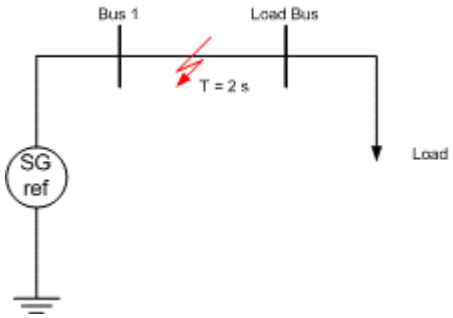

Figure 6-2

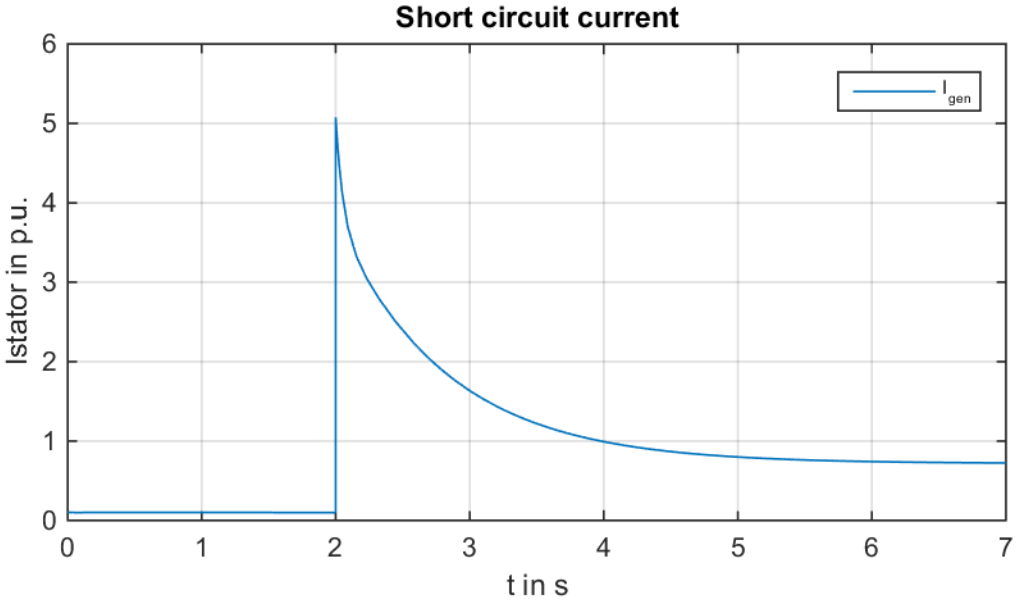

Figure 6-3, short circuit current

6.2 Implemented Mechanical System and Test

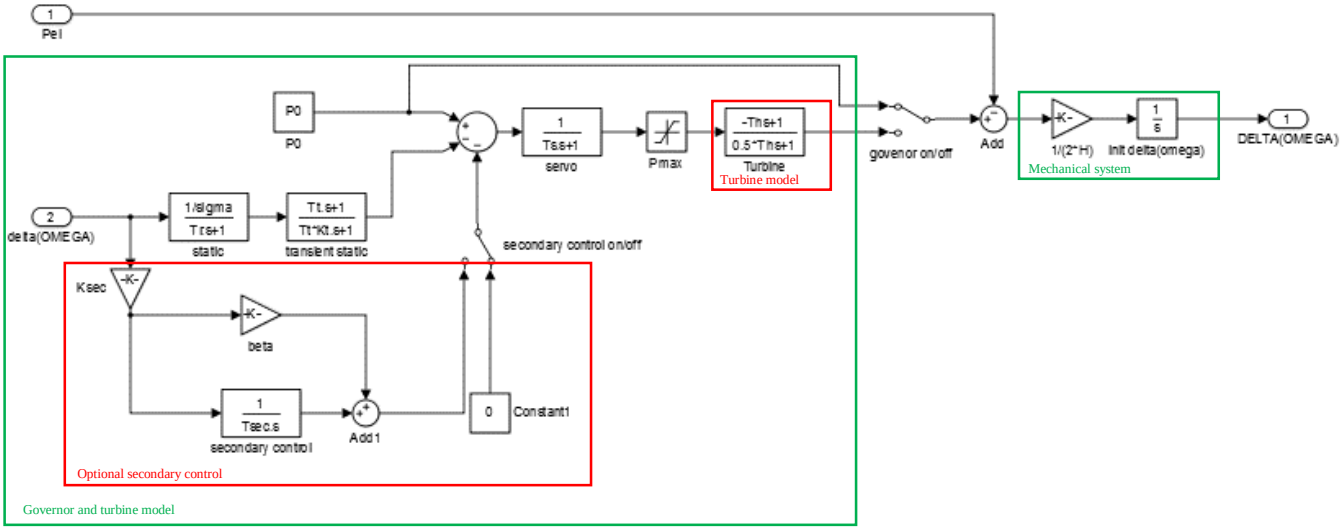

Figure 6-4

The response of the mechanical system to an abrupt load change was simulated by doubling the load after the system achieved a stable state before. The used topology is shown in Figure 6-5.
The test was done for activated and deactivated secondary control.

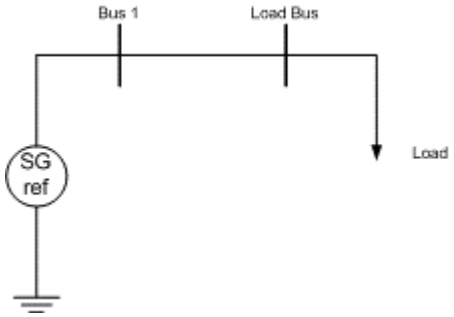

Figure 6-5

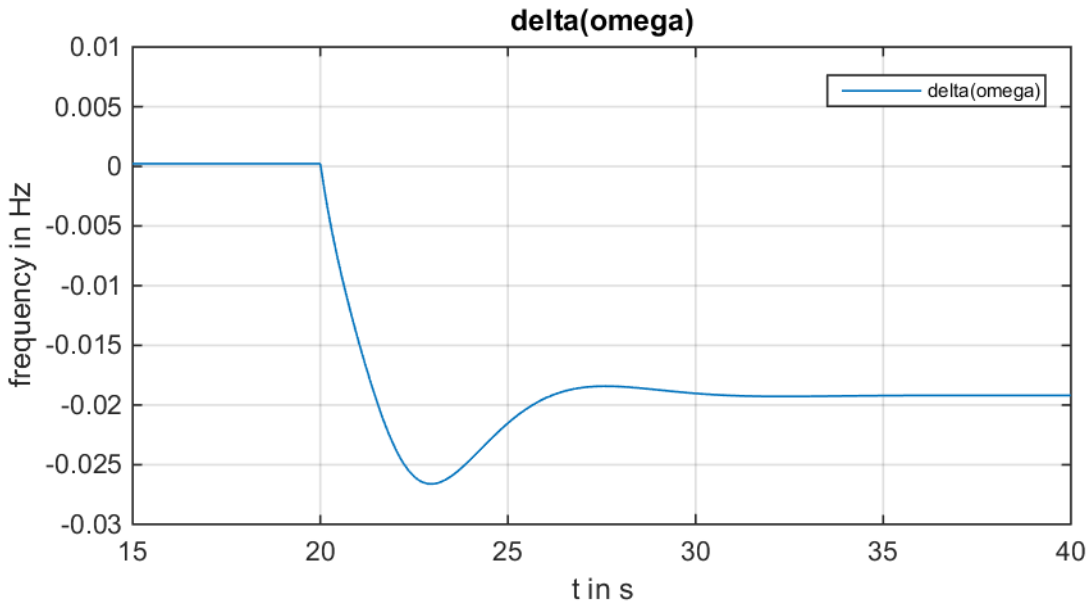

Figure 6-6, Δω without secondary control

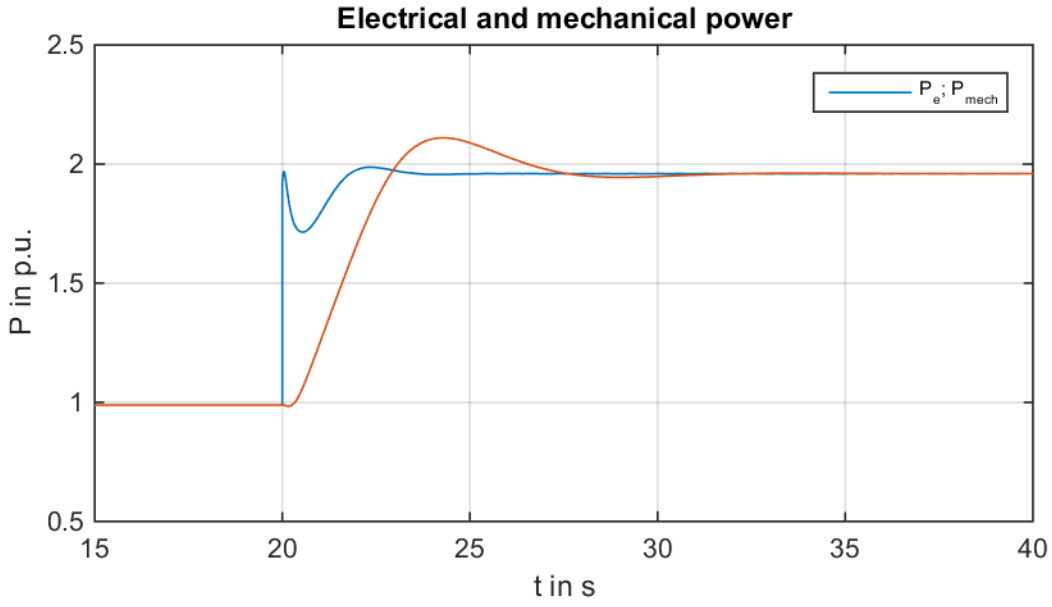

Figure 6-7, P without secondary control

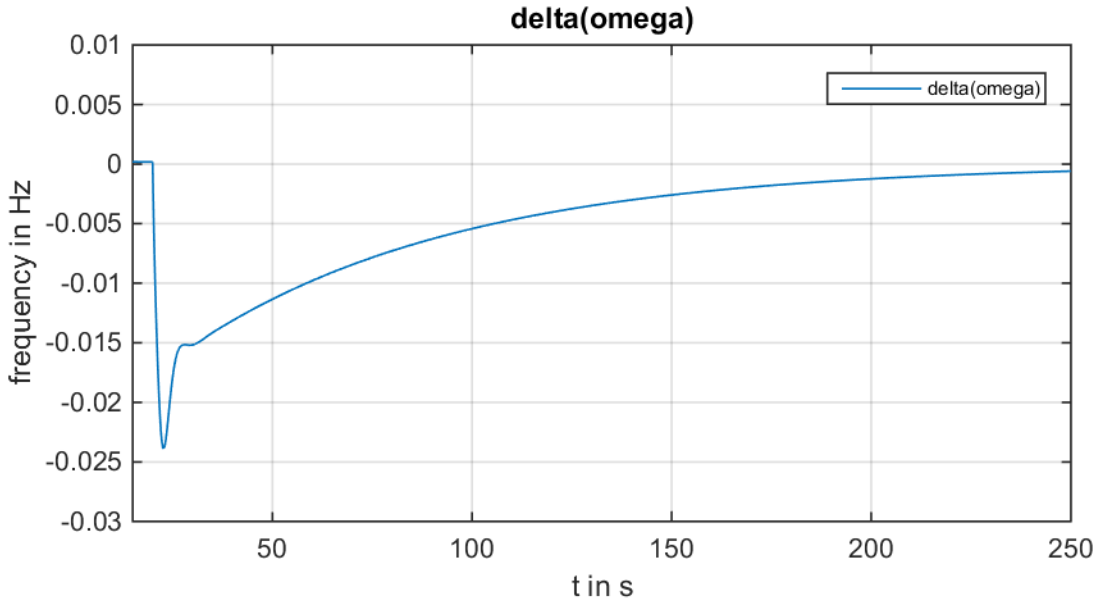

Figure 6-8, Δω with secondary control

6.3 AVR Modell Implementation

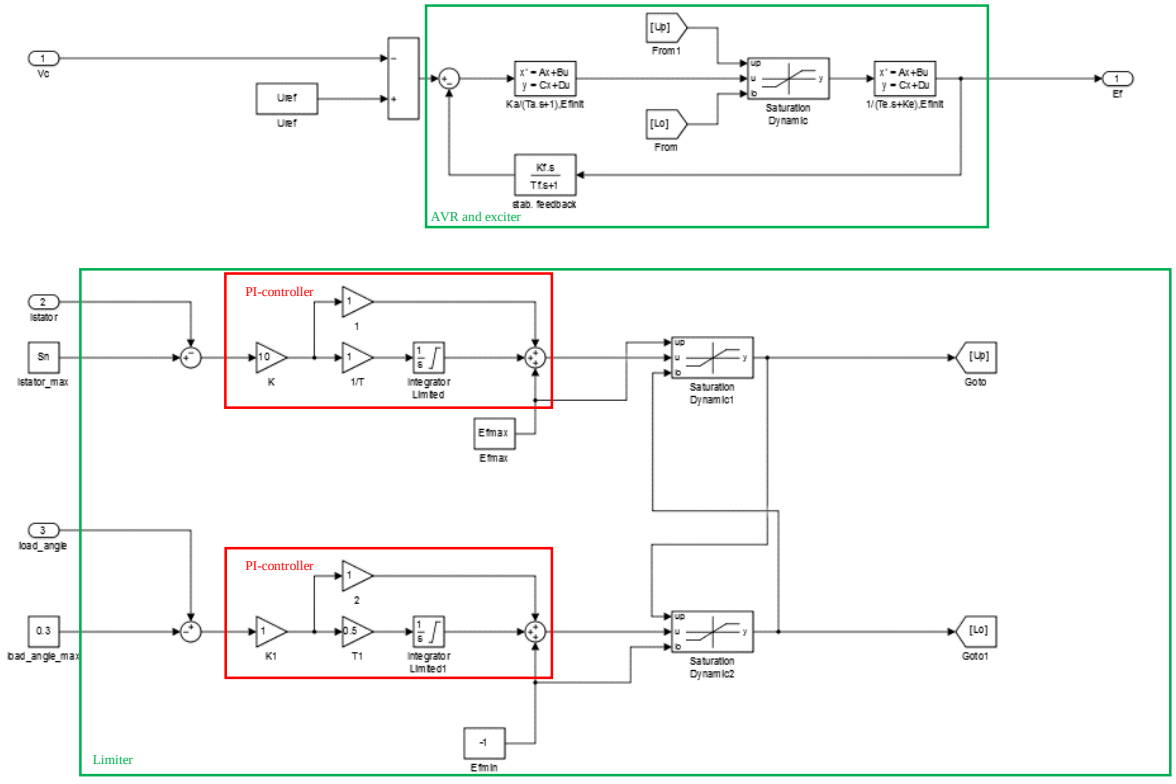

Figure 6-9

6.4 Load recovery tests

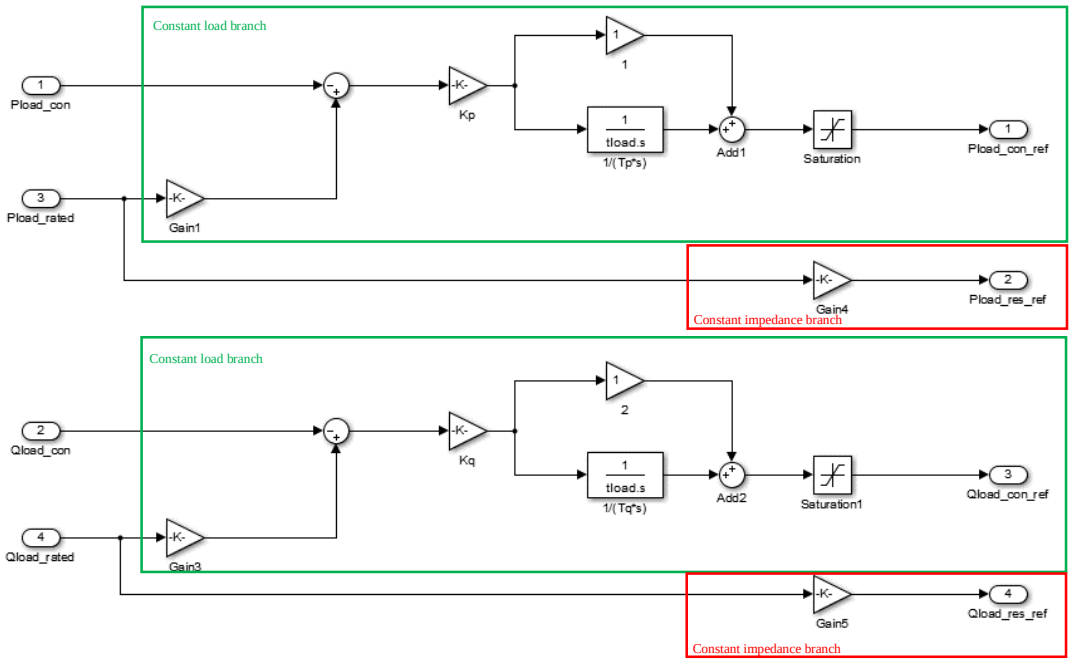

Figure 6-10

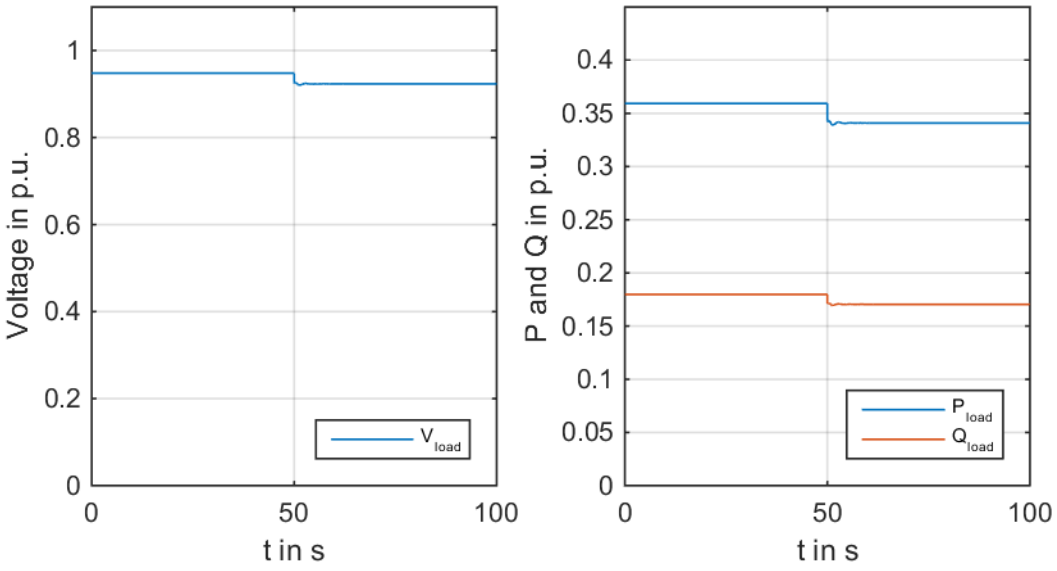

Figure 6-11, 100% resistive load

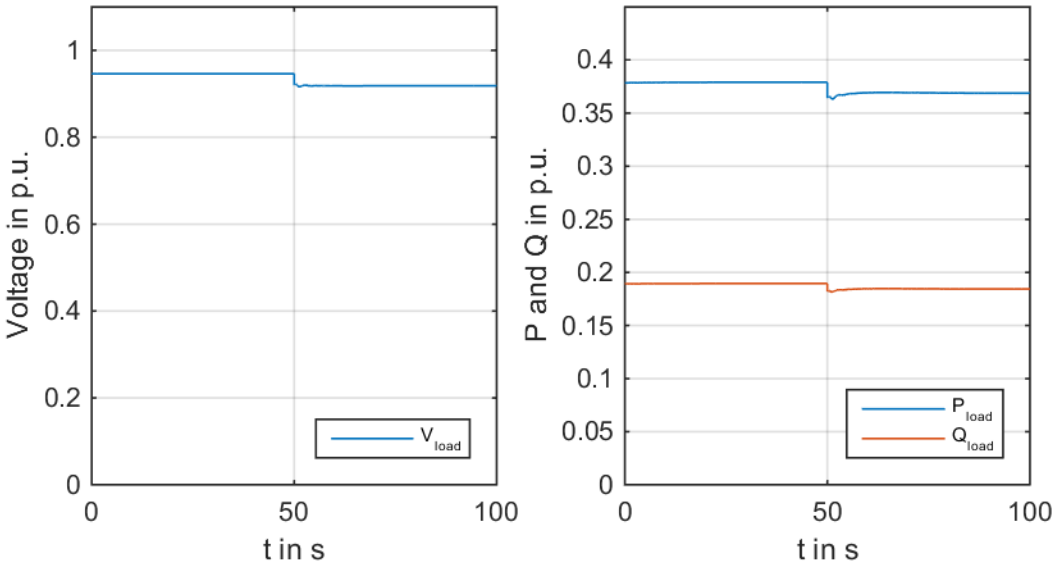

Figure 6-12, 50% resistive 50% controlled load

6.5 Implemented MATLAB code

```
function [Id_ref, Iq_ref, Pe_ref, Vc_ref, Istator_ref, load_angle_ref,
Uterm_ref, Q_ref, Id1, Iq1, Pe1, Vc1, Istator1, load_angle1, Uterm1, Q1,
Uterm2, Pload, Qload, Pload_con, Qload_con, Iline12_abs, Pline12, Qline12,
Iline2ref_abs, Pline2ref, Qline2ref, Z_load, Zth, Zth_adjusted, Zth_thuc,
current_margin1, power_margin1, exciter_margin1, threshhold1] =
network(Edsub_ref, Eqsub_ref, Edsub1, Eqsub1, Delta1, Ef1, Pload_con_ref,
Pload_res_ref, Qload_con_ref, Qload_res_ref, lock_saturation1)


% Definition of Systemparameters

Xt_ref = 0;
Xdsub_ref = 0.28;
Zc_ref = 0.0i;              % Zc here positiv, because voltage is measured
on the highvoltage side of the block transformer. Positive Zc will bring
the reference point into transformator

Xt1 = 0.0;
Xdsub1 = 0.389;
Zc1 = 0.00i;
Istator1_max = 0.15;         % equals Srated in Simulink model, Urated = 1!
Pe1_max =0.05*1.02;              % max. turbine power, or initial Pt*1.02
if governor is deactivated
Ef1_max = 1.3561;

Z12 = (5+50i)/121;
Z2ref = (9+90i)/121;
```

```
Zload =
1/conj(Pload_con_ref+Pload_res_ref+1i*Qload_con_ref+1i*Qload_res_ref);
% Un = 1

% System matrix

Zgen = [1i*(Xt1+Xdsub1); 100000; 1i*(Xt_ref+Xdsub_ref)];            % For
buses without use a high value of Zgen
Zc = [Zc1; 0; Zc_ref];                                              % For
buses without AVR or without load compensation fill in 0
Y = [(1/Zgen(1)+1/(Z12)) -1/(Z12) 0; -1/(Z12) (1/Zload+1/(Z12)+1/(Z2ref)) -
1/(Z2ref); 0 -1/(Z2ref) (1/Zgen(3)+1/(Z2ref))];

Eqsub = [Eqsub1; 0; Eqsub_ref];                                     % For
buses without genarator use 0
Edsub = [Edsub1; 0; Edsub_ref];                                     % For
buses without genarator use 0
Delta = [Delta1; 0; 0];                                             % For
buses without genarator and for slack bus use 0

% Injection model

Ug = Eqsub.*(cos(Delta)+1i*sin(Delta))+Edsub.*(-sin(Delta)+1i*cos(Delta));

Iinj = Ug./Zgen;

% Terminal voltages, generator currents and electrical power

Uterm = Y\Iinj;

Igen = (Ug-Uterm)./Zgen;
Vc = abs(Uterm + Igen.*Zc);

Iq = abs(Igen).*cos(Delta-angle(Igen));
Id = -abs(Igen).*sin(Delta-angle(Igen));

Pe = Edsub.*Id+Eqsub.*Iq;
Qgen = Edsub.*Iq-Eqsub.*Id;
load_angle = asin(Pe.*abs(Zgen)./(abs(Ug).*abs(Uterm)));

% Output generator

Id1 = Id(1);
Iq1 = Iq(1);
Pe1 = Pe(1);
Uterm1 = abs(Uterm(1));
Vc1 = Vc(1);
Istator1 = abs(Igen(1));
load_angle1 = load_angle(1);
Q1 = Qgen(1);

Uterm2 = abs(Uterm(2));

Id_ref = Id(3);
Iq_ref = Iq(3);
Pe_ref = Pe(3);
Uterm_ref = abs(Uterm(3));
Vc_ref = Vc(3);
Istator_ref = abs(Igen(3));
```

```
load_angle_ref = load_angle(3);
Q_ref = Qgen(3);

% Powerflow over line and to load
Iline12 = (Uterm(1)-Uterm(2))/(Z12*1i);
Sline12 = Uterm(2)*conj(Iline12);
Pline12 = real(Sline12);
Qline12 = imag(Sline12);
Iline12_abs = abs(Iline12);


Iline2ref = (Uterm(3)-Uterm(2))/(Z2ref*1i);
Sline2ref = Uterm(2)*conj(Iline2ref);
Pline2ref= real(Sline2ref);
Qline2ref = imag(Sline2ref);
Iline2ref_abs = abs(Iline2ref);

Sload = Uterm(2)*conj(Uterm(2)/Zload);
Pload = real(Sload);
Qload = imag(Sload);

% For mixed load the controlled part of Sload must be calculated
if Pload_con_ref ~= 0 || Qload_con_ref ~= 0
    Zload_con = 1/conj(Pload_con_ref + 1i*Qload_con_ref);
    Sload_con = Uterm(2)*conj(Uterm(2)/Zload_con);
    Pload_con = real(Sload_con);
    Qload_con = imag(Sload_con);
else
    Pload_con = 0;
    Qload_con = 0;
end

% adjusting thevenin impedance to limits
current_margin1 = (Istator1_max - Istator1)/Istator1_max;
power_margin1 = (Pe1_max - Pe1)/Pe1_max;
exciter_margin1 = (Ef1_max - Ef1)/(Ef1_max);

if (0.05 + lock_saturation1) < min(current_margin1, min(power_margin1,
exciter_margin1))
    Z12_adjusted = Z12;                                                  %
operation inside the borders of the capability of the generator
    threshhold1 = 0;
else
    threshhold1 = 0.1;
    if current_margin1 <= min(power_margin1, exciter_margin1)
        Z12_adjusted = 4i/Istator1_max;                                  %
acording to x_new = 4/Istator_rated, Urated = 1, max. stator current is
reached
    else
        if power_margin1 <= min(current_margin1, exciter_margin1)
            Z12_adjusted = 1i/(4*Pe1_max);                               %
acording to x_adjusted = 1/(4*Pmax), Urated = 1, max. active power is
reached
        else
            Z12_adjusted = 4i/Istator1;                                  %
acording to x_new = 4/Istator, Urated = 1, max. stator excitation is
reached
        end
    end
end
```

```
Zth_thuc = (1i/(4*Pe1_max)*Z2ref)/(1i/(4*Pe1_max)+Z2ref);
Zth_adjusted =  (Z12_adjusted*Z2ref)/(Z12_adjusted+Z2ref);
Zth = (Z12*Z2ref)/(Z12+Z2ref);

Z_load = Zload;
end
```

6.6 Simulation Parameters

	SG1	SG_ref	SG1	SG_ref	SG1	SG_ref	SG1	SG_ref
Xd	3,3	1,28	3,3	1,28	3,3	1,28	3,3	1,28
Xd1	0,662	0,37	0,662	0,37	0,662	0,37	0,662	0,37
Xd2	0,389	0,28	0,389	0,28	0,389	0,28	0,389	0,28
Xq1	0,662	0,37	0,662	0,37	0,662	0,37	0,662	0,37
Xq2	0,389	0,28	0,389	0,28	0,389	0,28	0,389	0,28
Td01	4,85	9,7	4,85	9,7	4,85	9,7	4,85	9,7
Td02	0,018	0,05	0,018	0,05	0,018	0,05	0,018	0,05
Tq02	0,32	0,25	0,32	0,15	0,32	0,25	0,32	0,25
Sn	0,15	3,2	variable	3,2	variable	3,2	3	3,2
H	5,5	10,8	5,5	10,8	5,5	10,8	5,5	10,8
Ptmax	0,14	3,1	0,14	3,1	0,14	3,1	0,14	3,1
P0	0,14	3,1	---	3,1	---	3,1	---	3,1
sigma	0,02	0,02	---	0,02	---	0,02	---	0,02
Tr	0,2	0,2	---	0,2	---	0,2	---	0,2
Kt	2	2	---	2	---	2	---	2
Tt	1	1	---	1	---	1	---	1
Ts	0	0	---	0	---	0	---	0
Th	0	0	---	0	---	0	---	0
Ksec	---	---	---	---	---	---	---	---
Tsec	---	---	---	---	---	---	---	---
beta	---	---	---	---	---	---	---	---
Uref	1	1	1	1	1	1	1	1
Efmax	1,3561	5	1,3561	5	variable	5	variable	5
Ka	100	200	100	200	100	200	100	200
Ta	0,1	0,125	0,1	0,125	0,1	0,125	0,1	0,125
Ke	1	1	1	1	1	1	1	1
Te	0,1	0,5	0,1	0,5	0,1	0,5	0,1	0,5
Kf	0,01	0,05	0,01	0,05	0,01	0,05	0,01	0,05
Tf	0,7	0,5	0,7	0,5	0,7	0,5	0,7	0,5
	Influence active power demand		**Influence active power SG1**		**Influence armature current limiter**		**Influence exciter current limiter**	

Table 2

6.7 Further Results

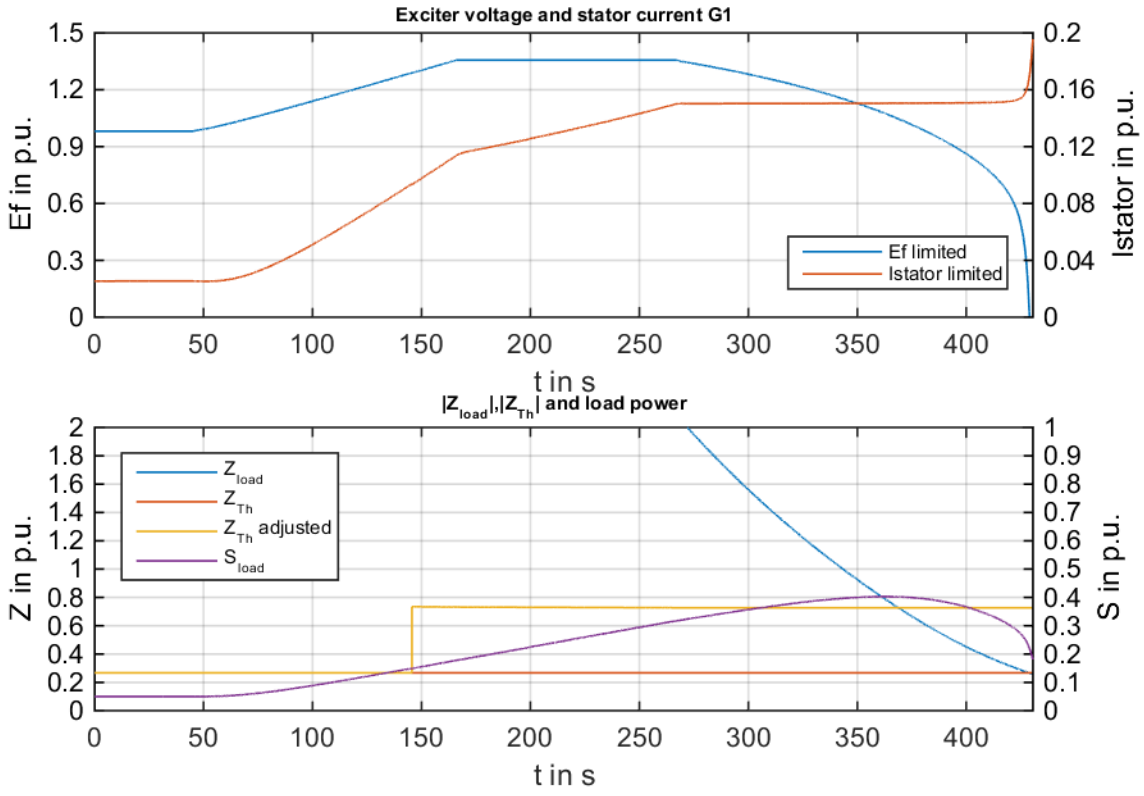

Figure 6-13, P_{load} = 0,05 p.u., 100% controlled load, Q_{Load} increasing

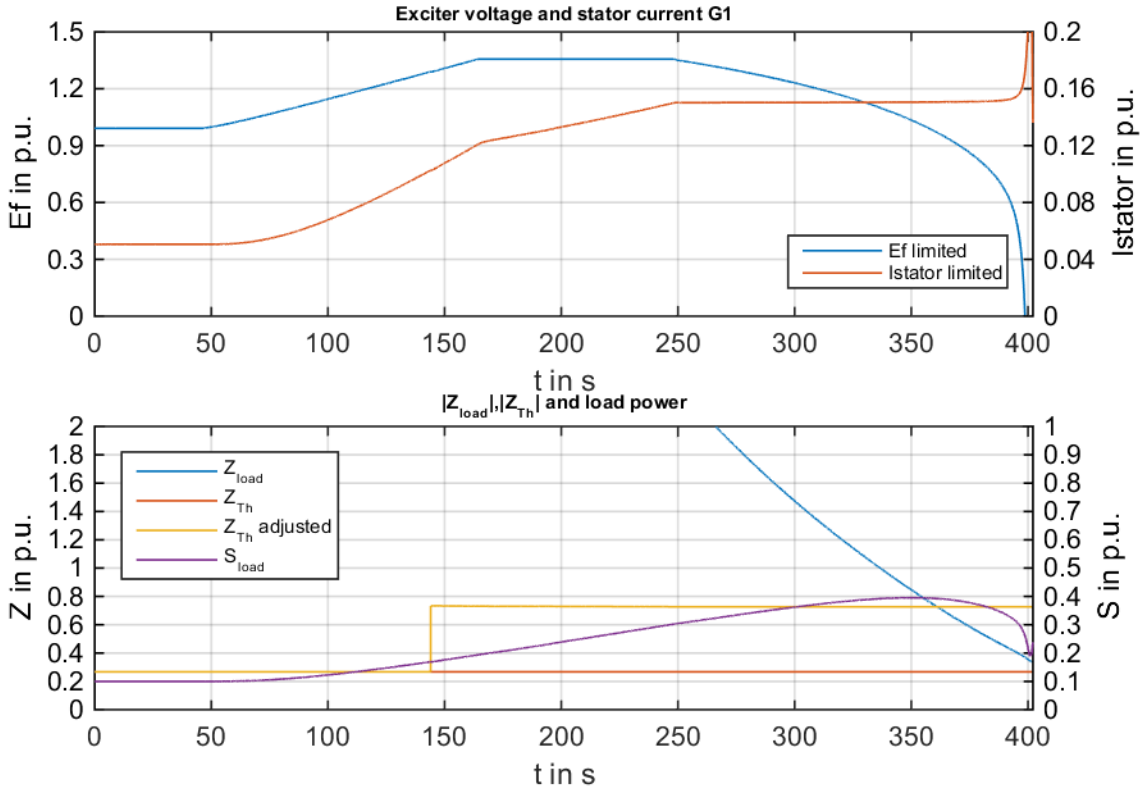

Figure 6-14, P_{load} = 0,1 p.u., 100% controlled load, Q_{Load} increasing

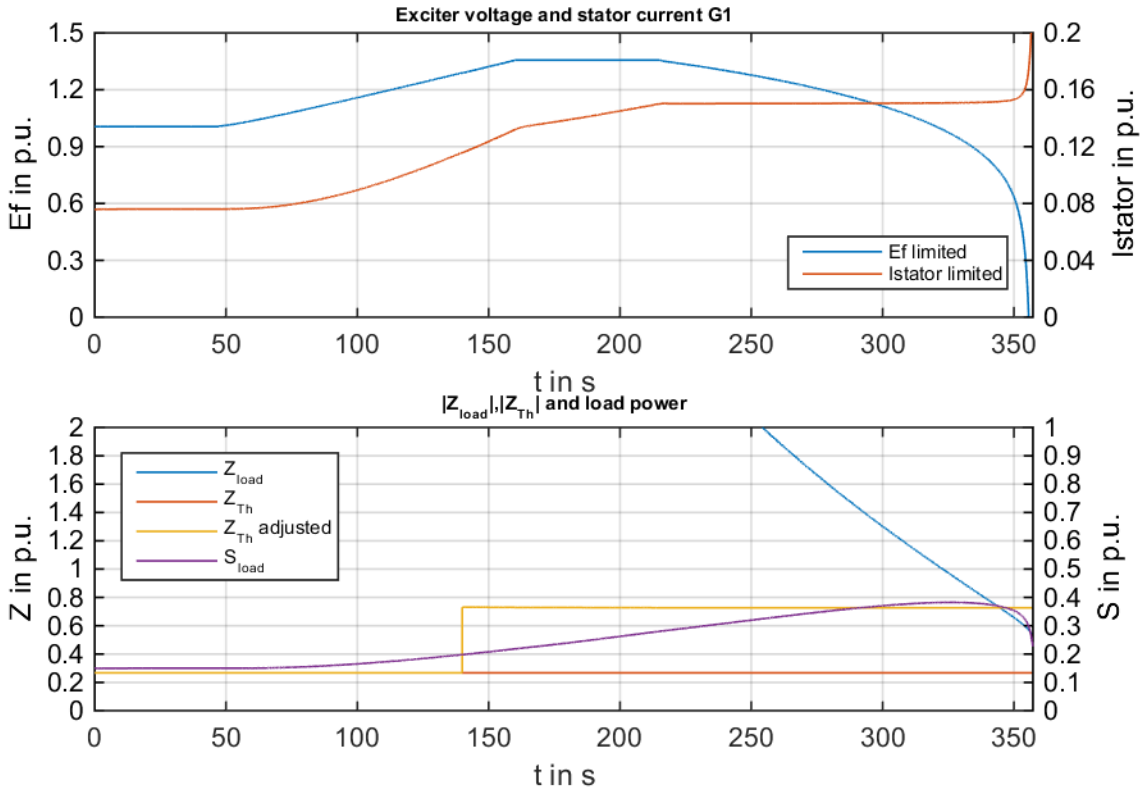

Figure 6-15, P_{load} = 0,15 p.u., 100% controlled load, Q_{Load} increasing

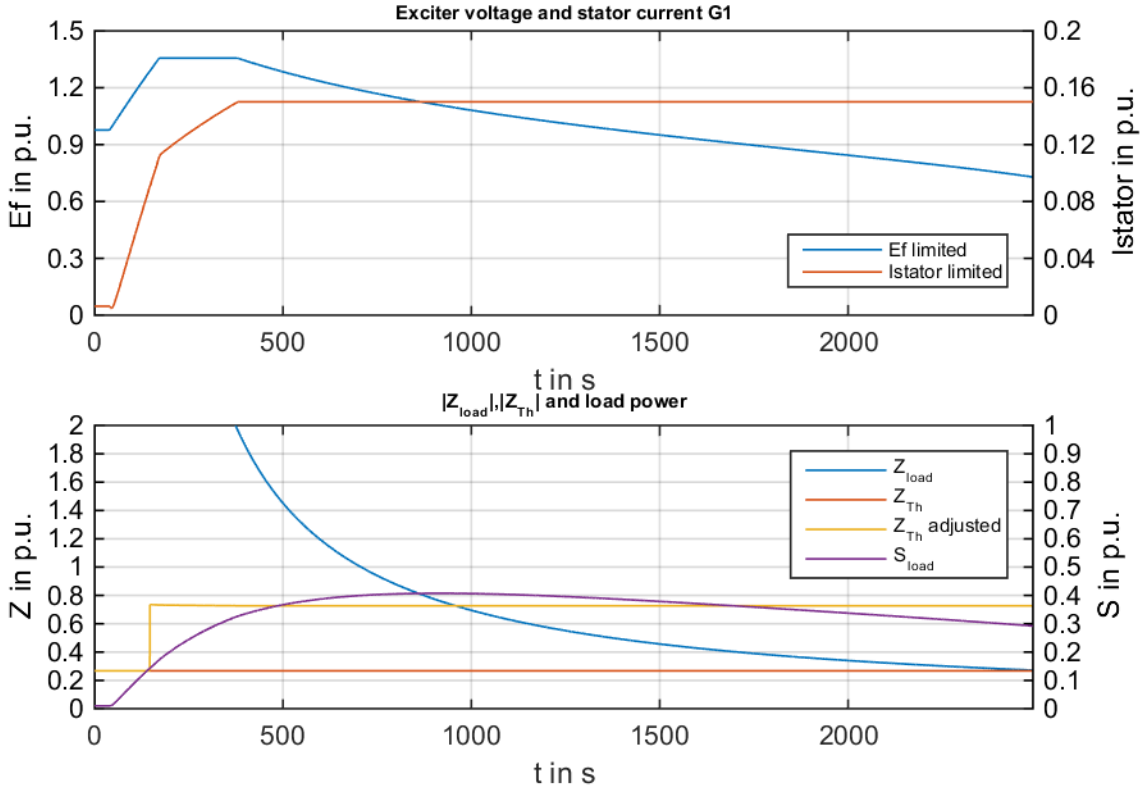

Figure 6-16, P_{load} = 0,01 p.u., 100% resistive load, Q_{Load} increasing

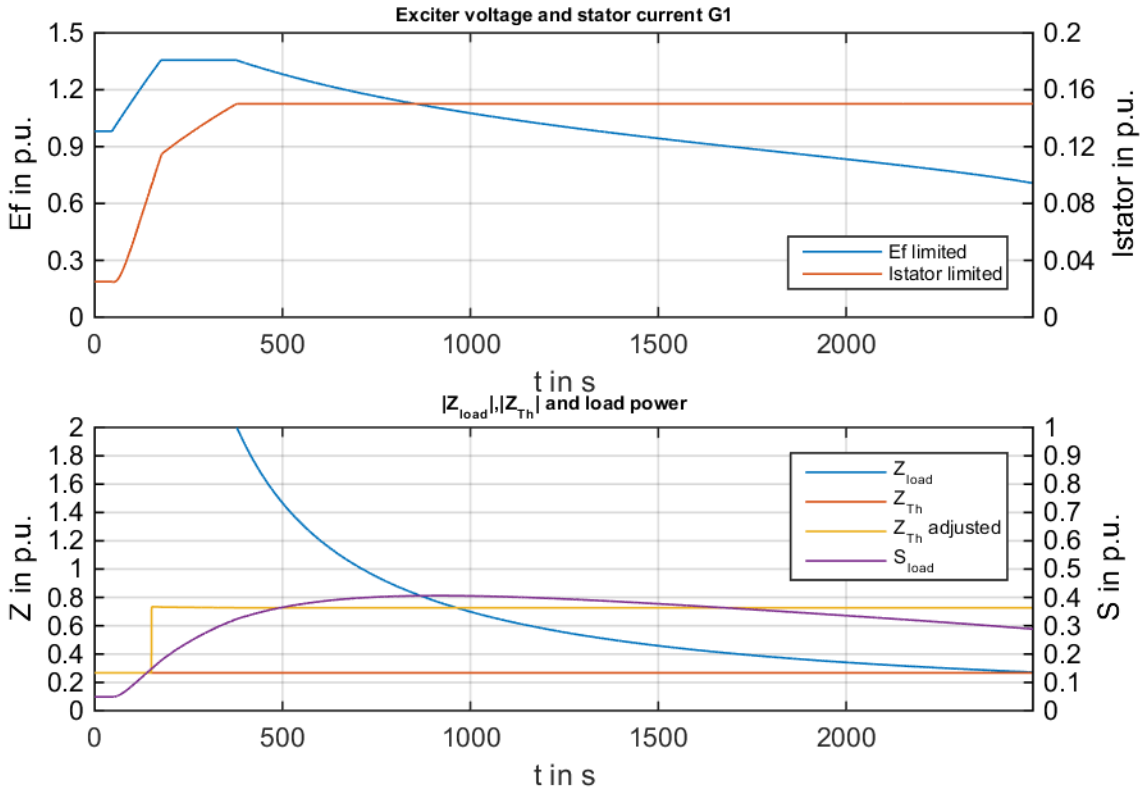

Figure 6-17, P_{load} = 0,05 p.u., 100% resistive load, Q_{Load} increasing

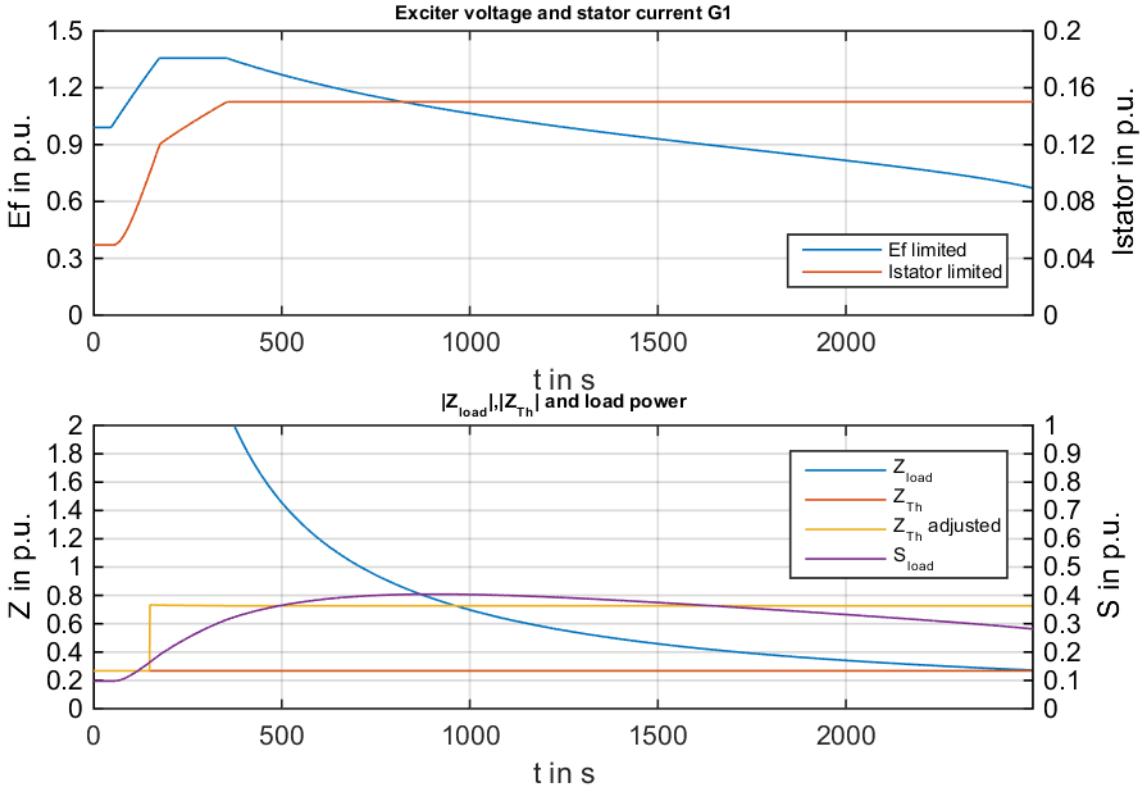

Figure 6-18, P_{load} = 0,1 p.u., 100% resistive load, Q_{Load} increasing

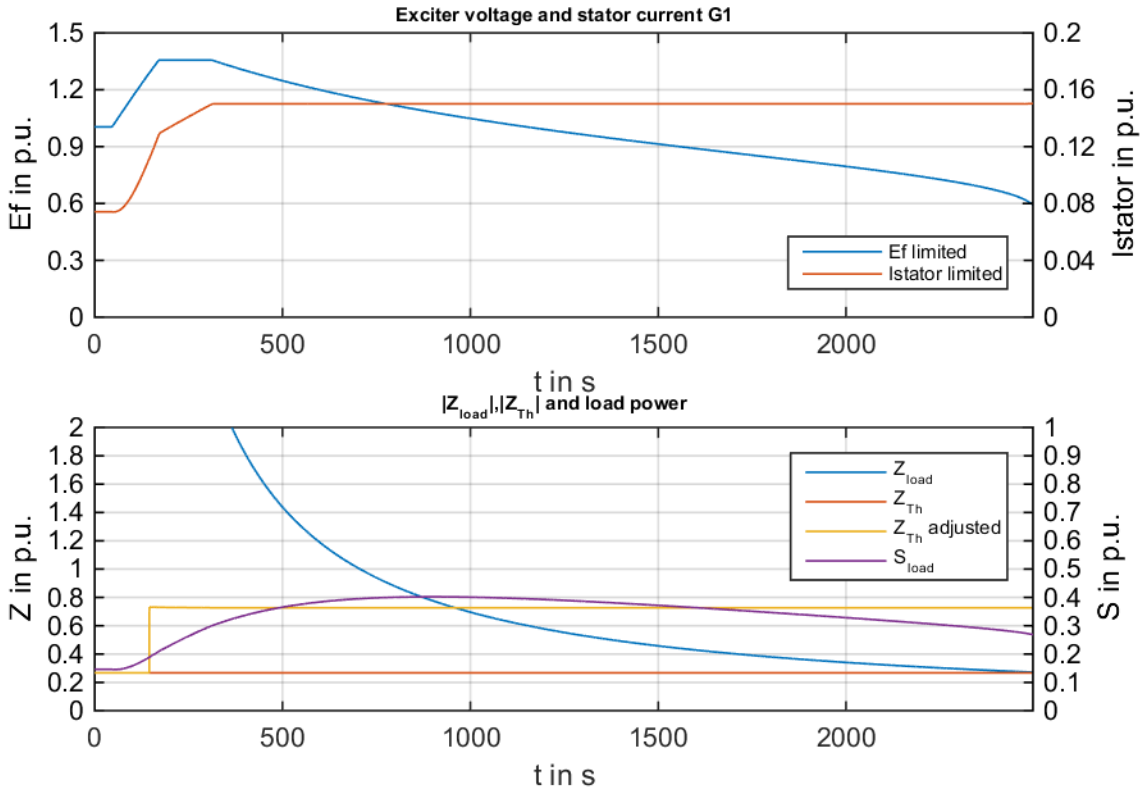

Figure 6-19, P_{load} = 0,15 p.u., 100% resistive load, Q_{Load} increasing

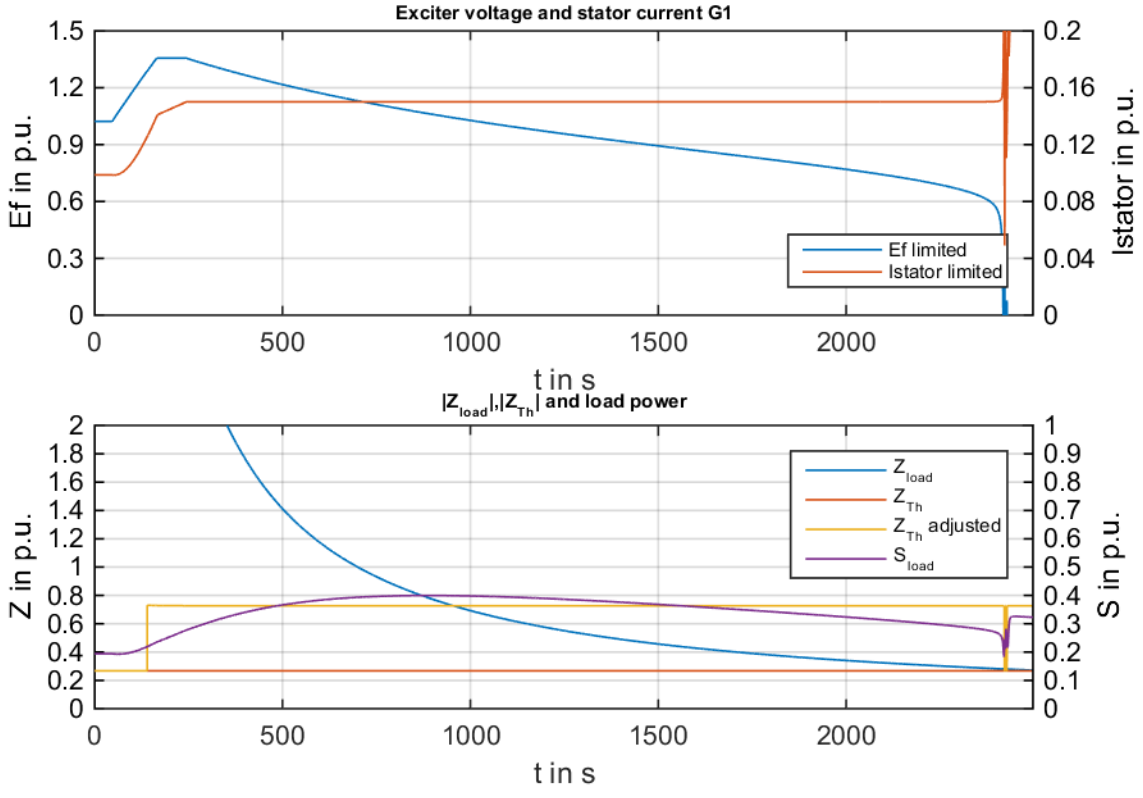

Figure 6-20, P_{load} = 0,2 p.u., 100% resistive load, Q_{Load} increasing

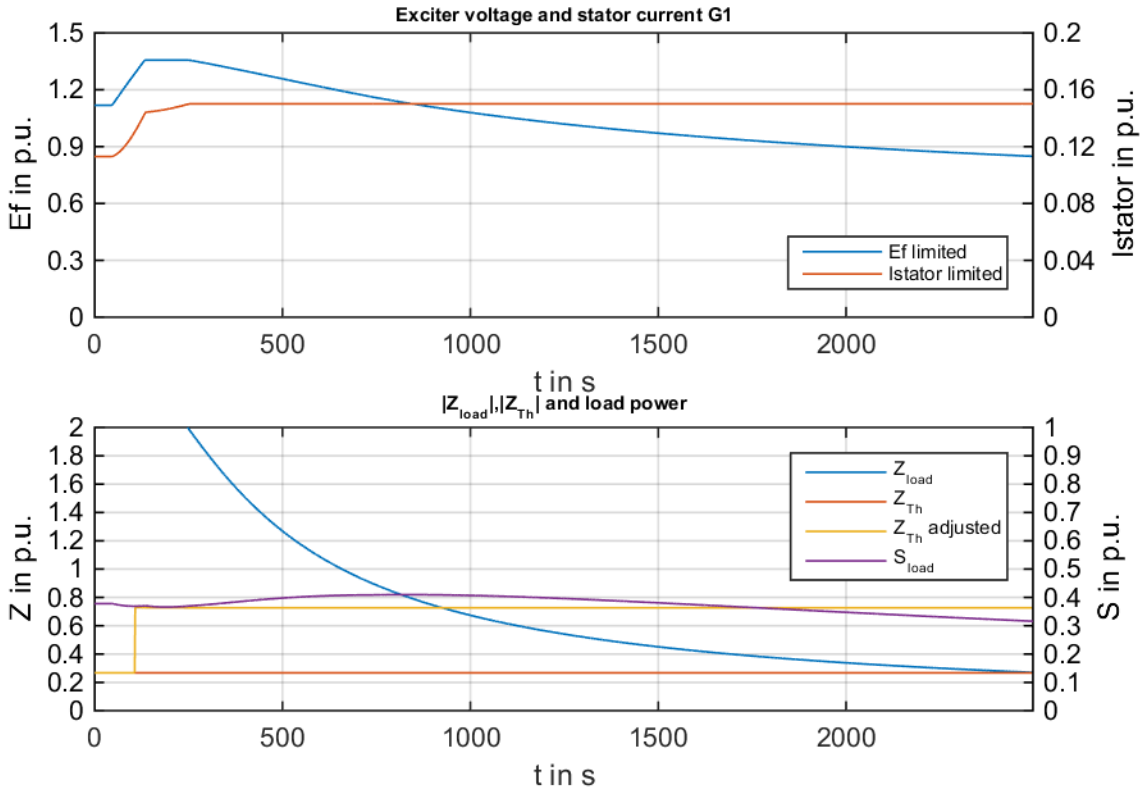

Figure 6-21, P_{load} = 0,2 p.u., 100% resistive load, Q_{Load} increasing

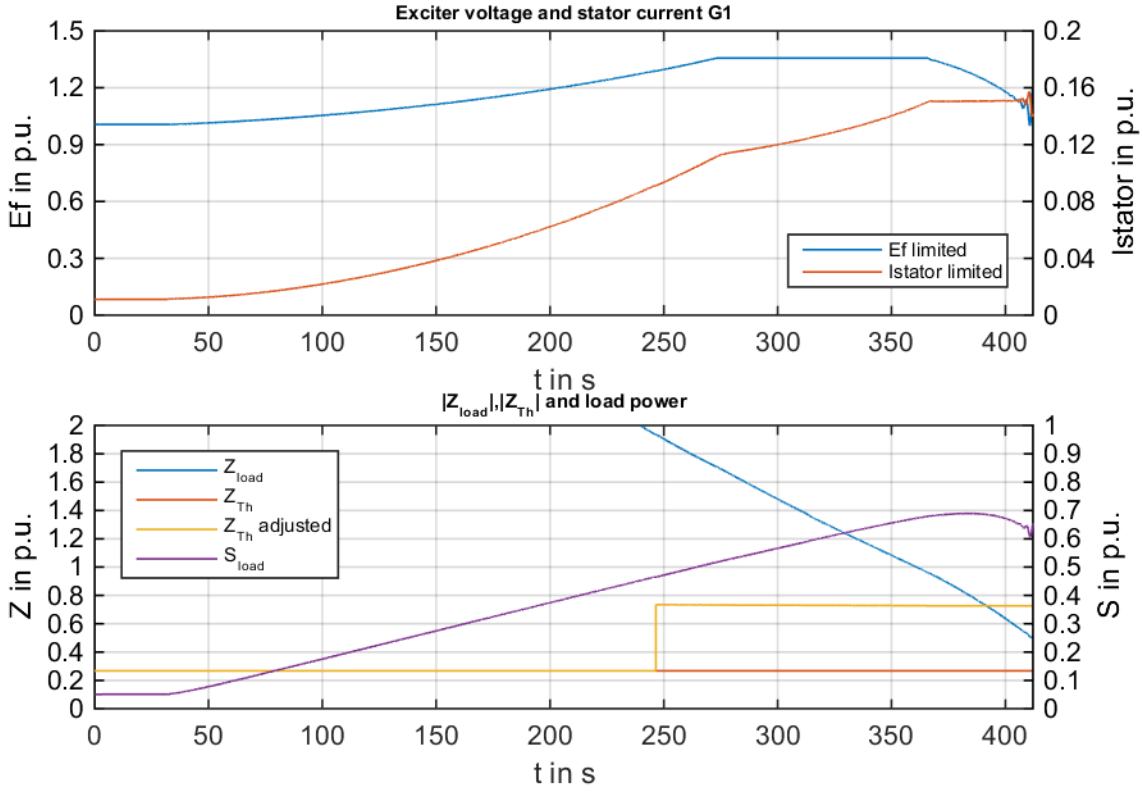

Figure 6-22, P_{SG1} = 0,01 p.u., P_{load} and Q_{load} increasing, 100% controlled load, P_{Load} increasing

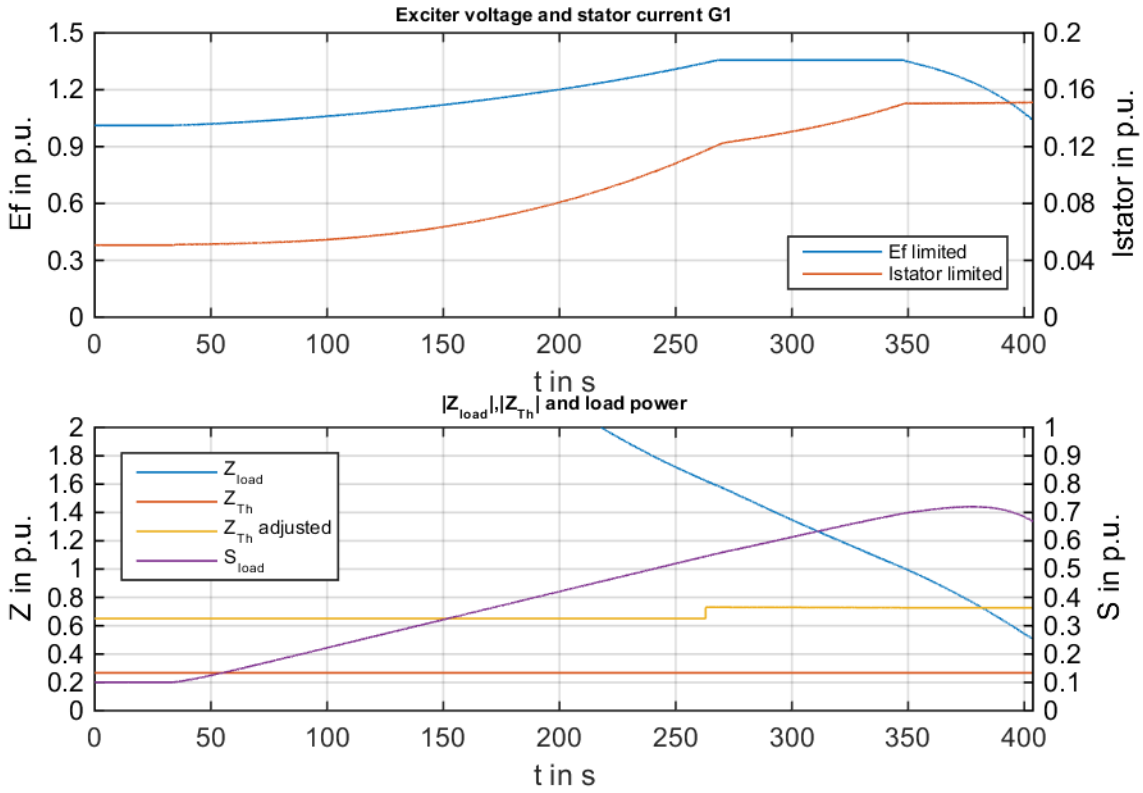

Figure 6-23, P_{SG1} = 0,05 p.u., P_{load} and Q_{load} increasing, 100% controlled load, P_{Load} increasing

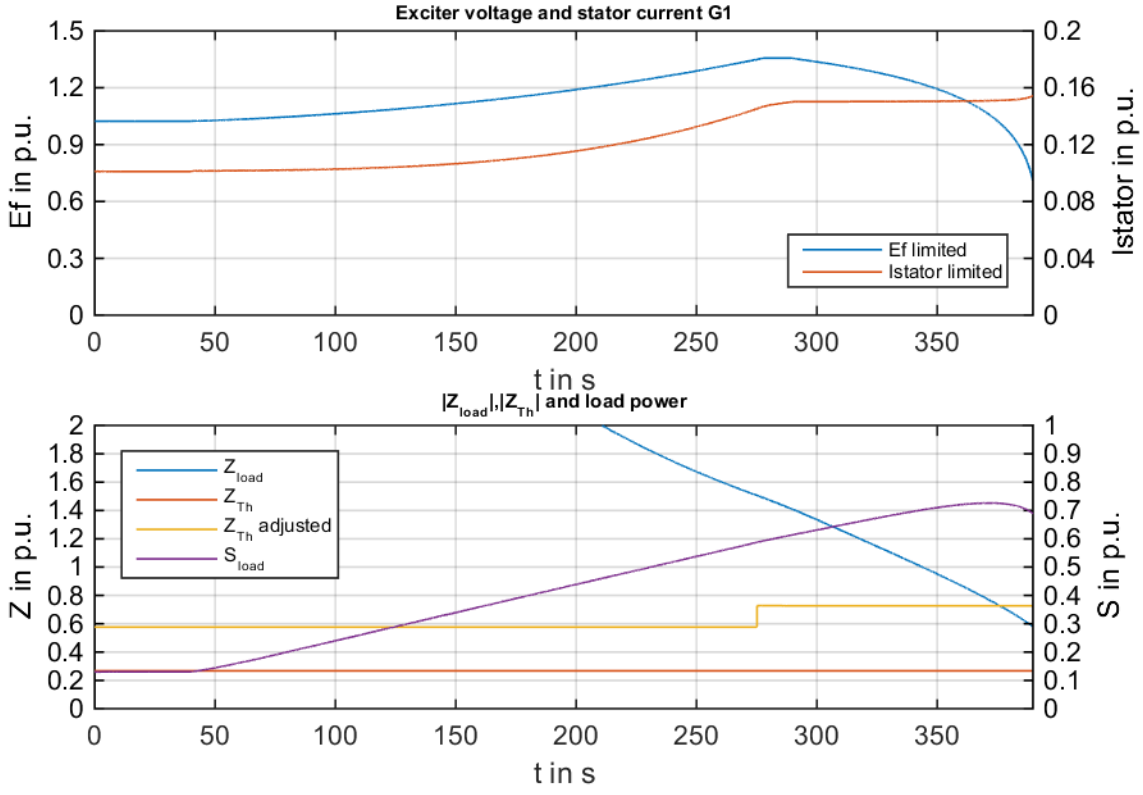

Figure 6-24, P_{SG1} = 0,1 p.u., P_{load} and Q_{load} increasing, 100% controlled load, P_{Load} increasing

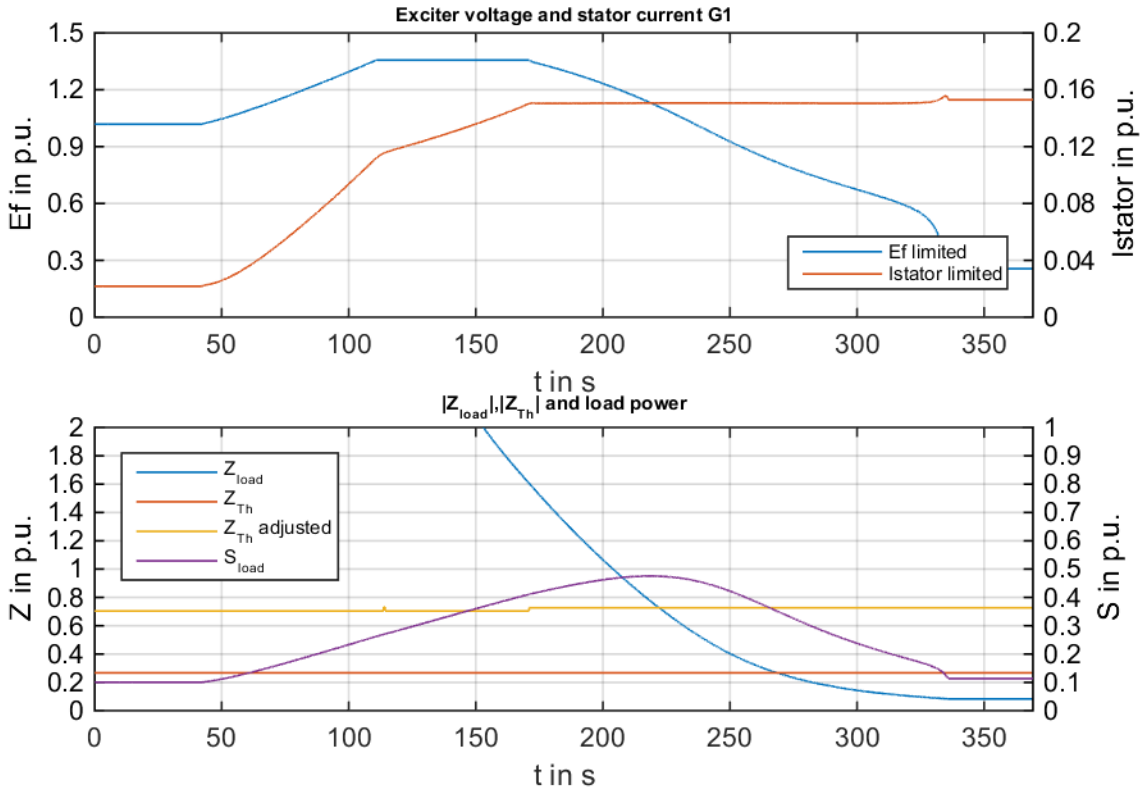

Figure 6-25, P_{SG1} = 0,02 p.u., P_{laod} and Q_{load} increasing, 100% controlled load, P_{Load} and Q_{Load} increasing

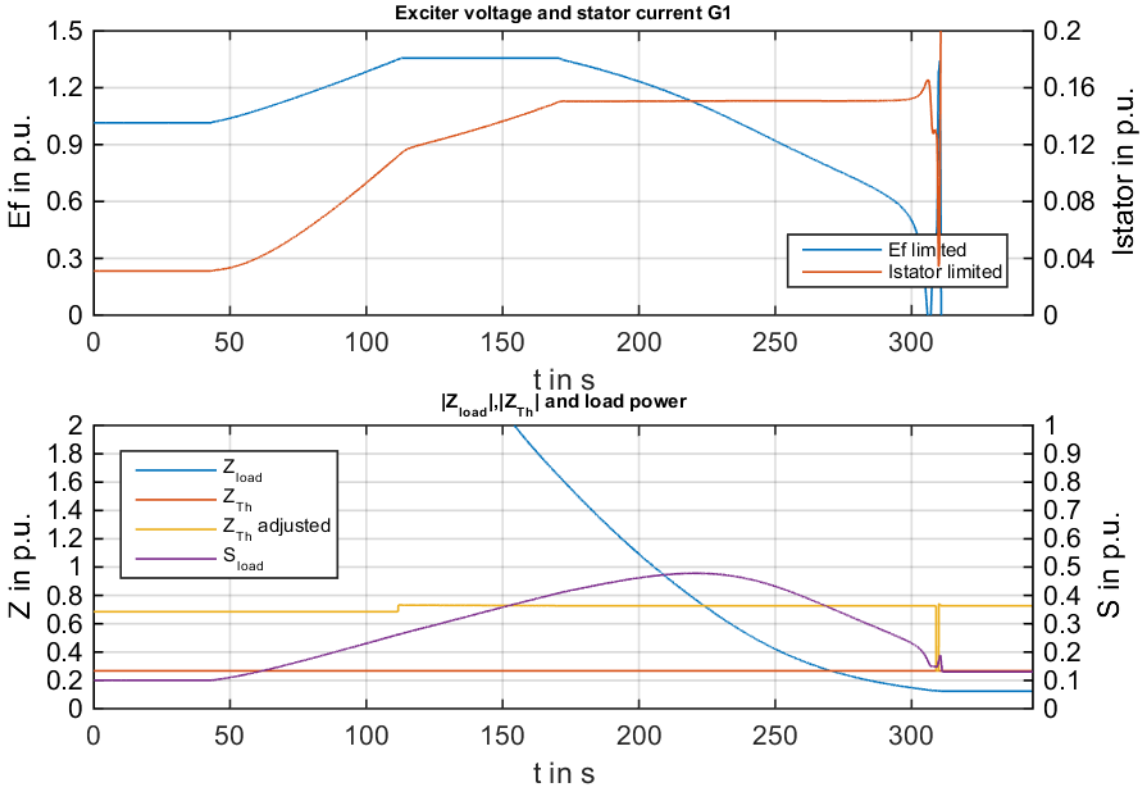

Figure 6-26, P_{SG1} = 0,03 p.u., P_{laod} and Q_{load} increasing, 100% controlled load, P_{Load} and Q_{Load} increasing

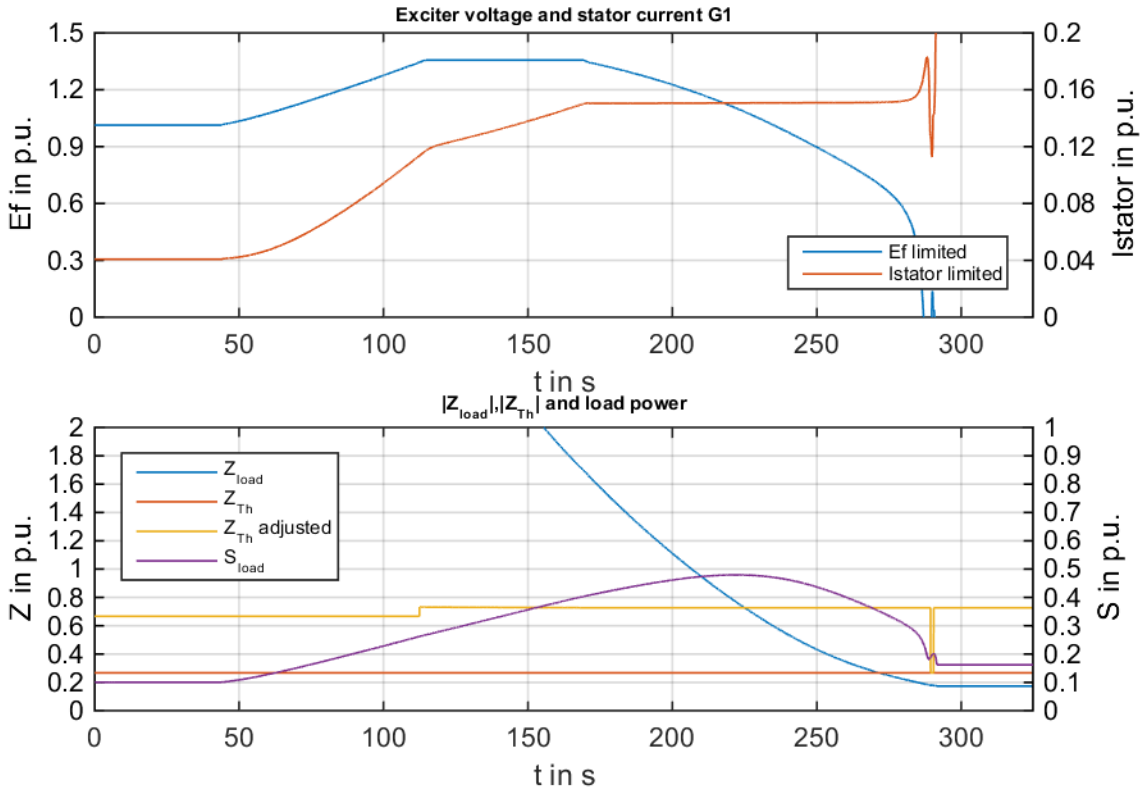

Figure 6-27, P_{SG1} = 0,04 p.u., P_{laod} and Q_{load} increasing, 100% controlled load, P_{Load} and Q_{Load} increasing

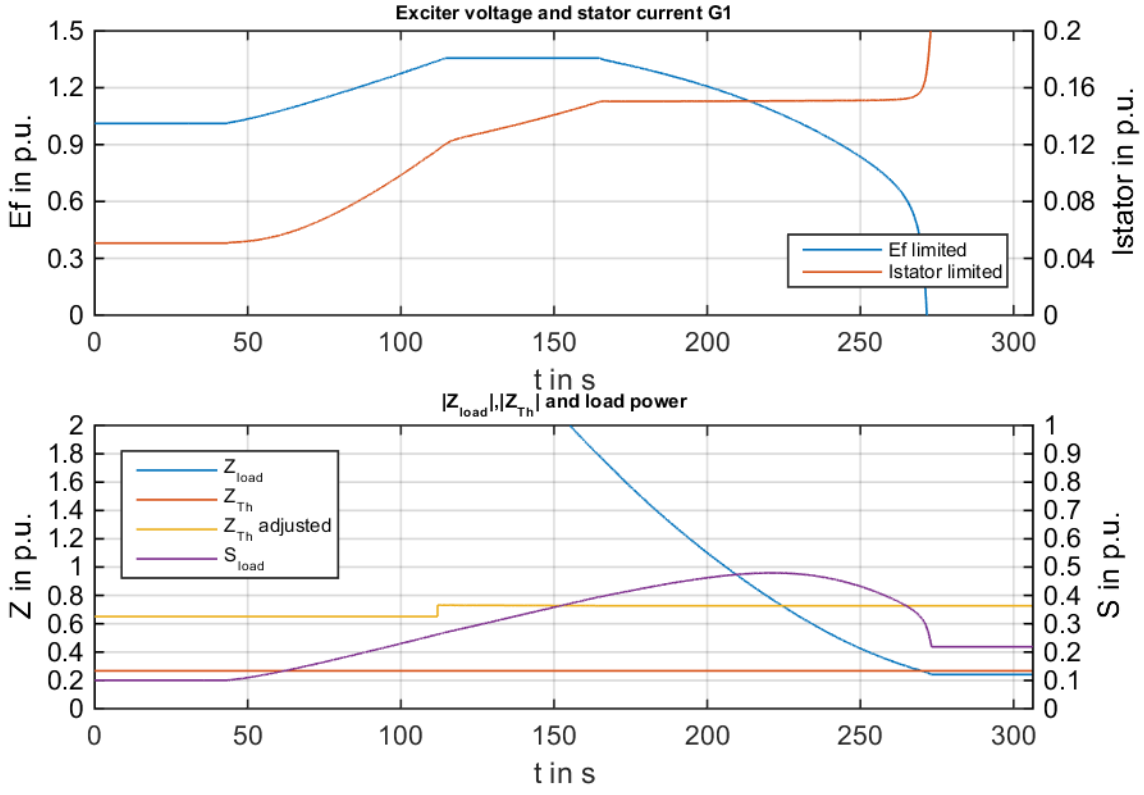

Figure 6-28, P_{SG1} = 0,05 p.u., P_{laod} and Q_{load} increasing, 100% controlled load, P_{Load} and Q_{Load} increasing

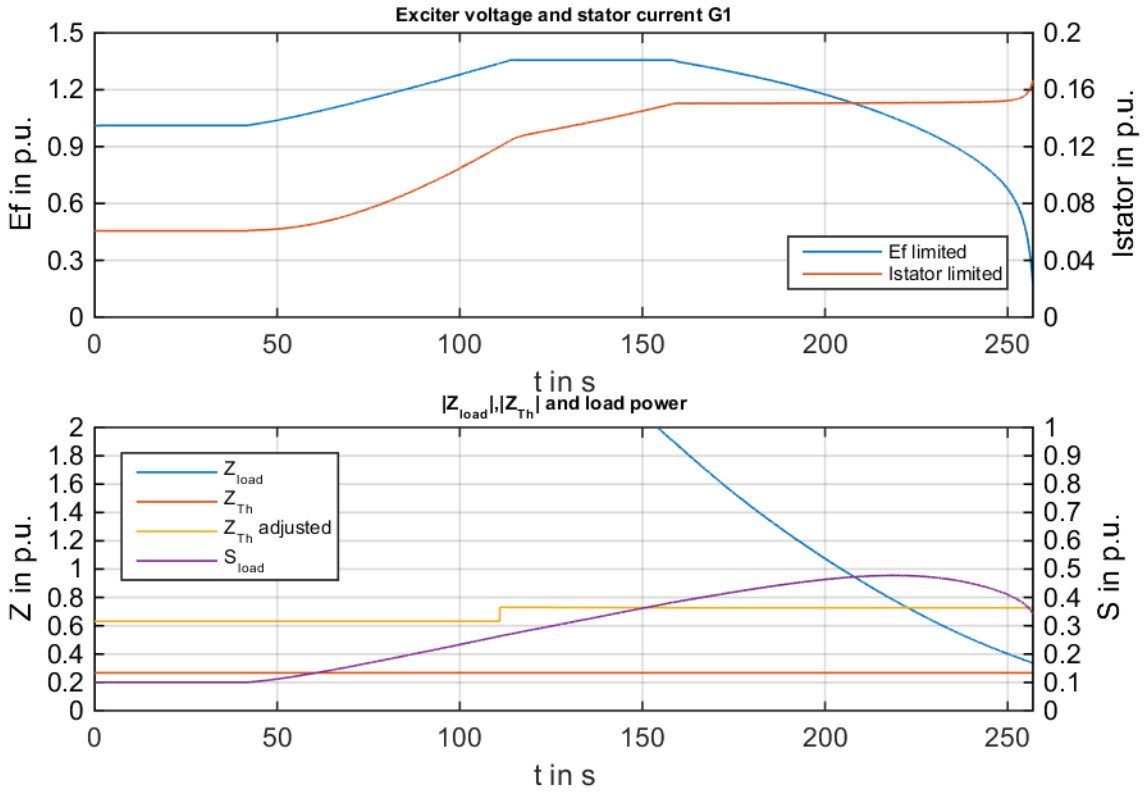

Figure 6-29, P_{SG1} = 0,06 p.u., P_{load} and Q_{load} increasing, 100% controlled load, P_{Load} and Q_{Load} increasing

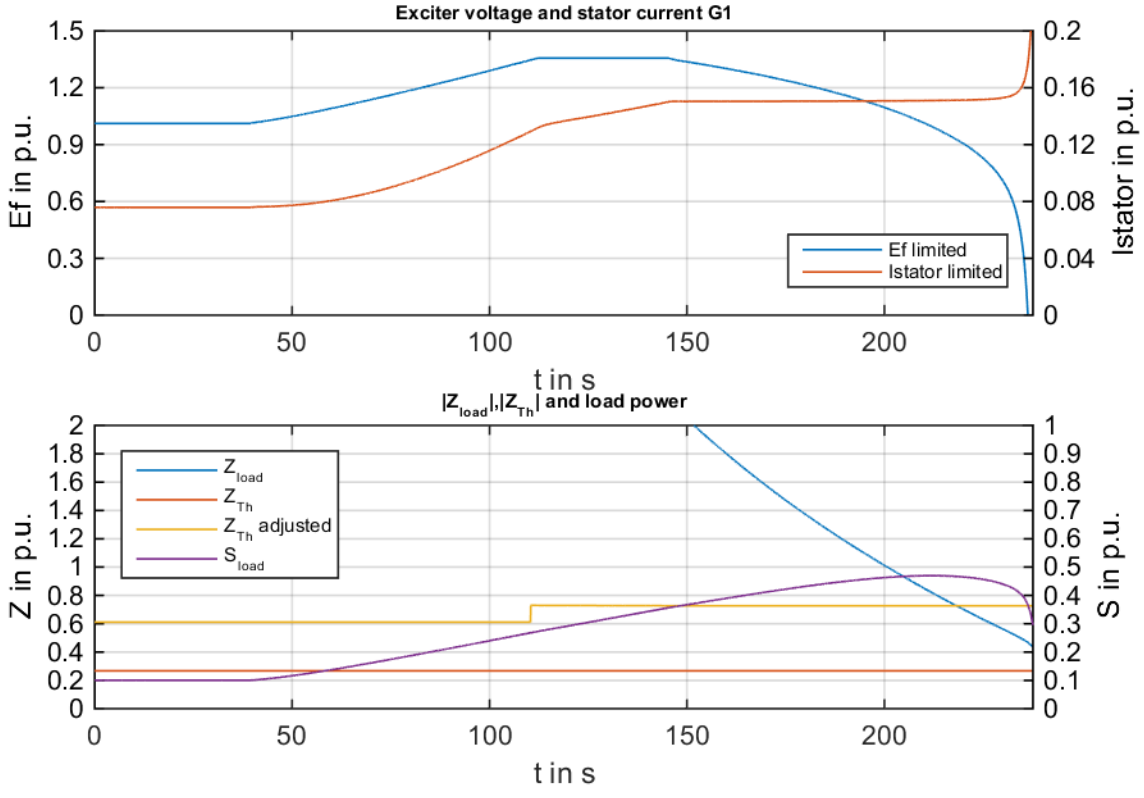

Figure 6-30, P_{SG1} = 0,075 p.u., P_{load} and Q_{load} increasing, 100% controlled load, P_{Load} and Q_{Load} increasing

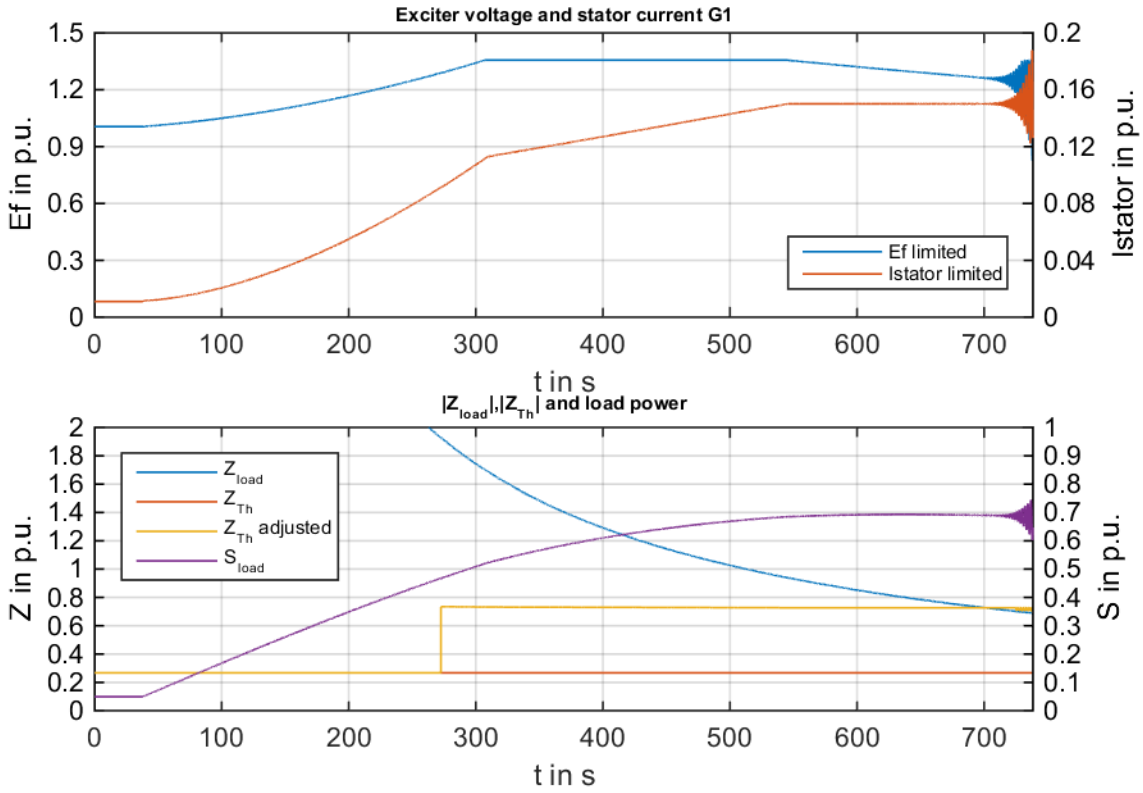

Figure 6-31, P_{SG1} = 0,01 p.u., P_{load} and Q_{load} increasing, 100% resistive load, P_{Load} increasing

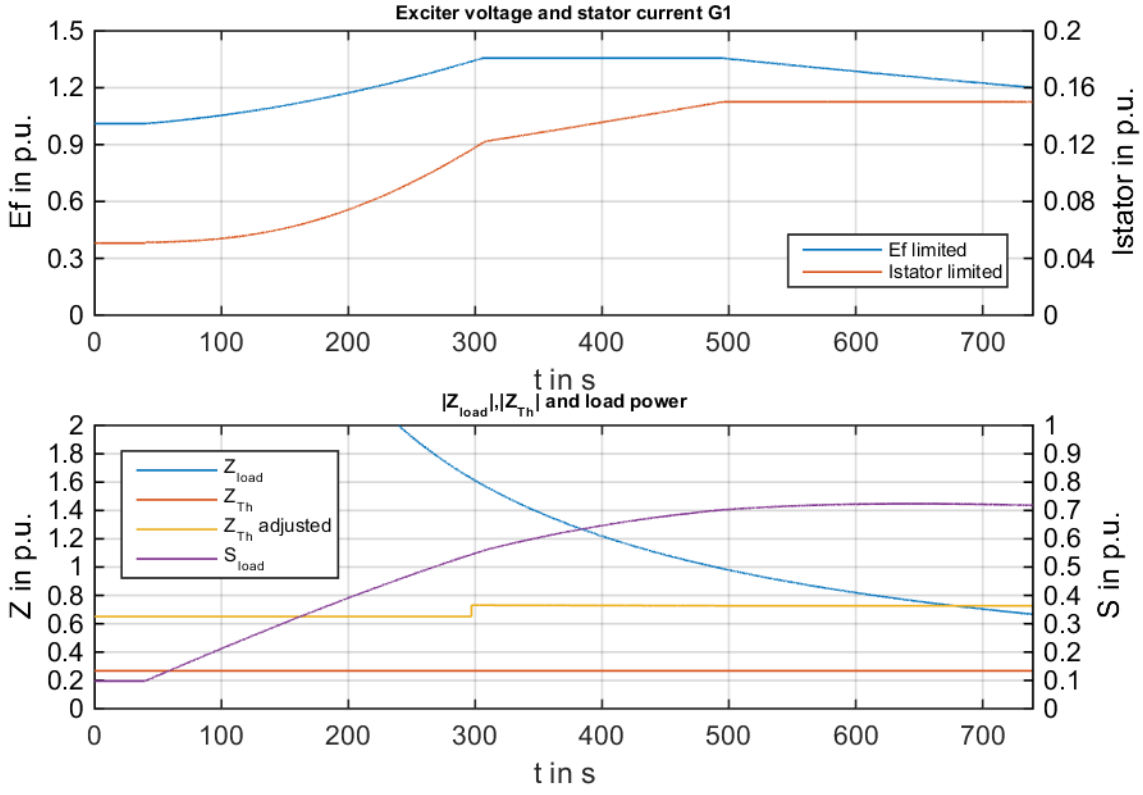

Figure 6-32, P_{SG1} = 0,05 p.u., P_{load} and Q_{load} increasing, 100% resistive load, P_{Load} increasing

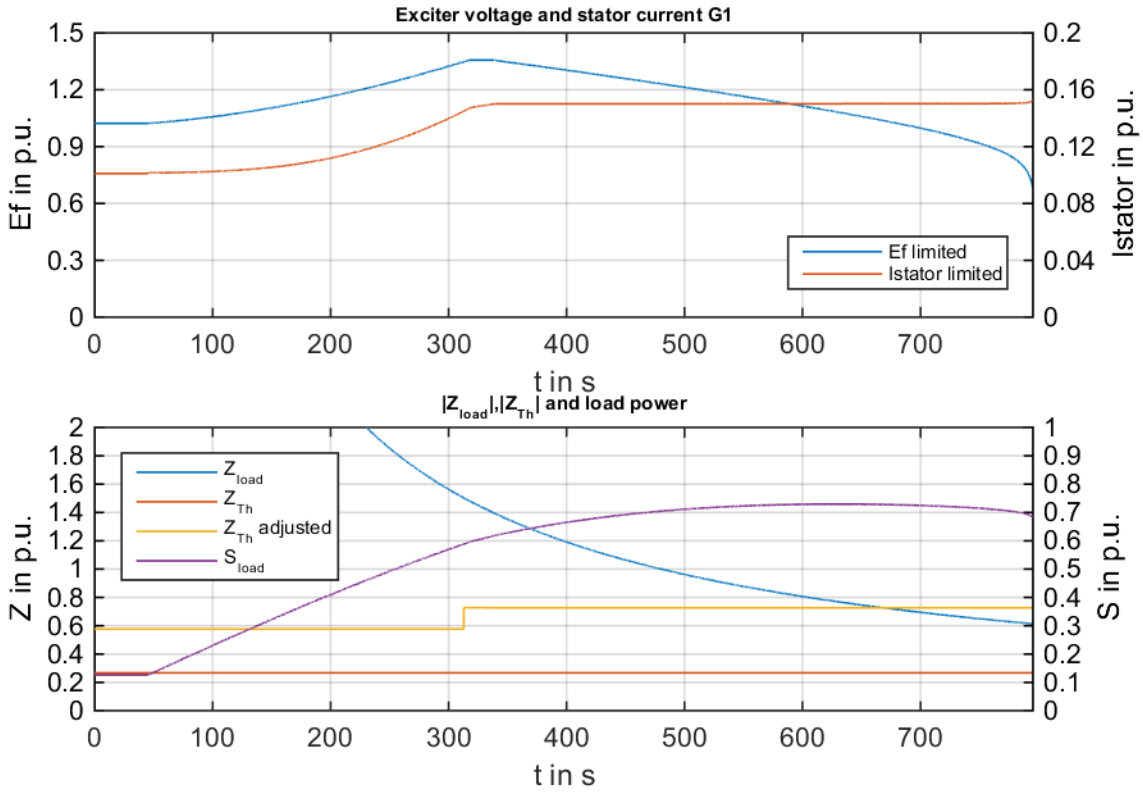

Figure 6-33, P_{SG1} = 0,1 p.u., P_{load} and Q_{load} increasing, 100% resistive load, P_{Load} increasing

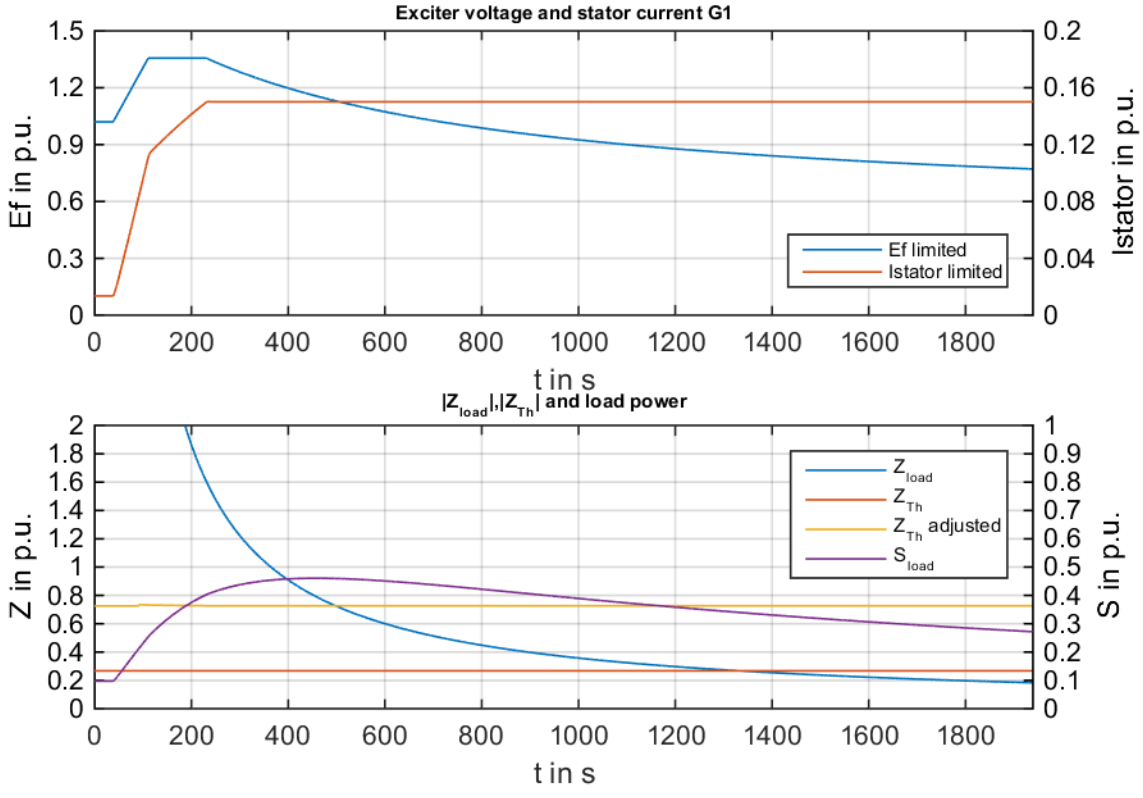

Figure 6-34, P_{SG1} = 0,01 p.u., P_{load} and Q_{load} increasing, 100% resistive load, P_{Load} and Q_{Load} increasing

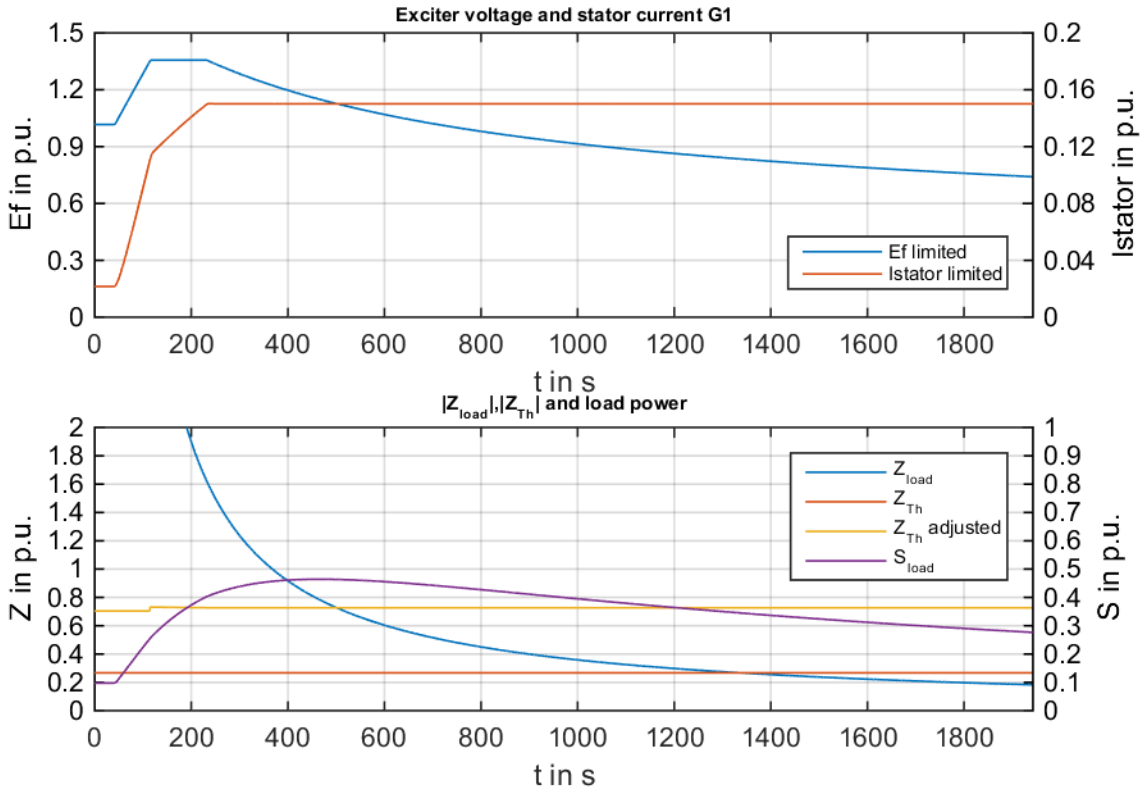

Figure 6-35, P_{SG1} = 0,02 p.u., P_{laod} and Q_{load} increasing, 100% resistive load, P_{Load} and Q_{Load} increasing

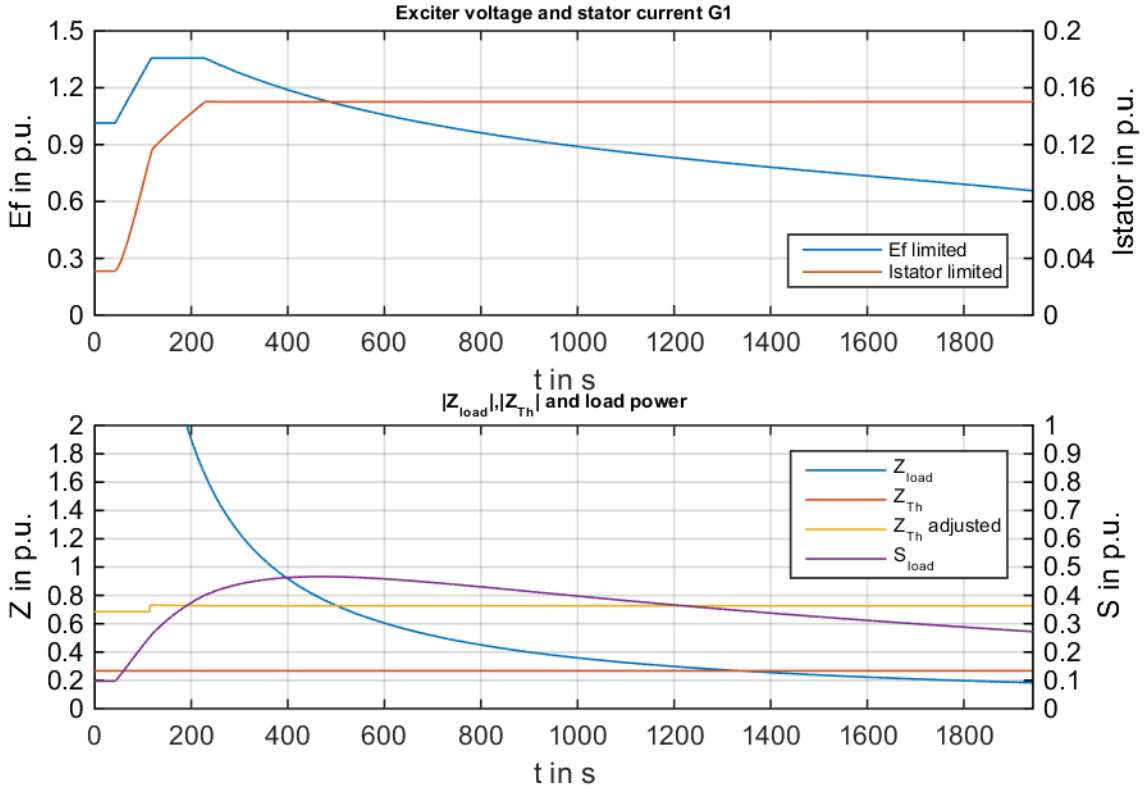

Figure 6-36, P_{SG1} = 0,03 p.u., P_{laod} and Q_{load} increasing, 100% resistive load, P_{Load} and Q_{Load} increasing

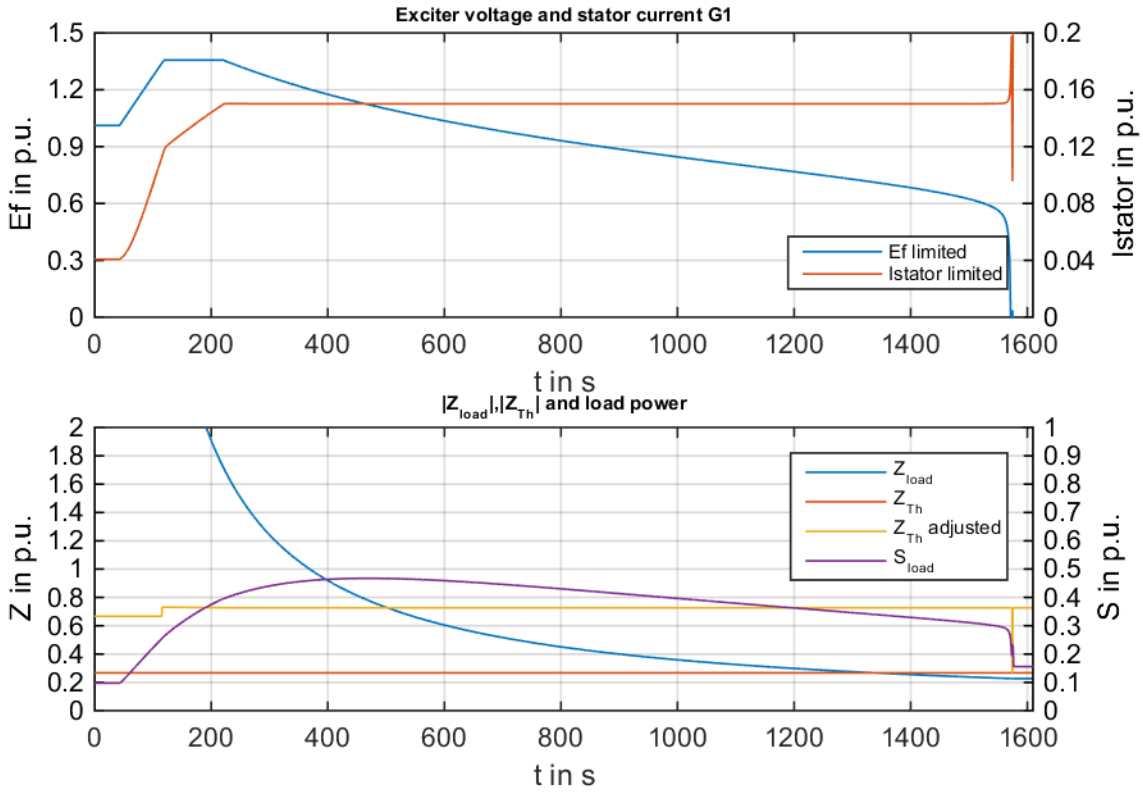

Figure 6-37, P_{SG1} = 0,04 p.u., P_{load} and Q_{load} increasing, 100% resistive load, P_{Load} and Q_{Load} increasing

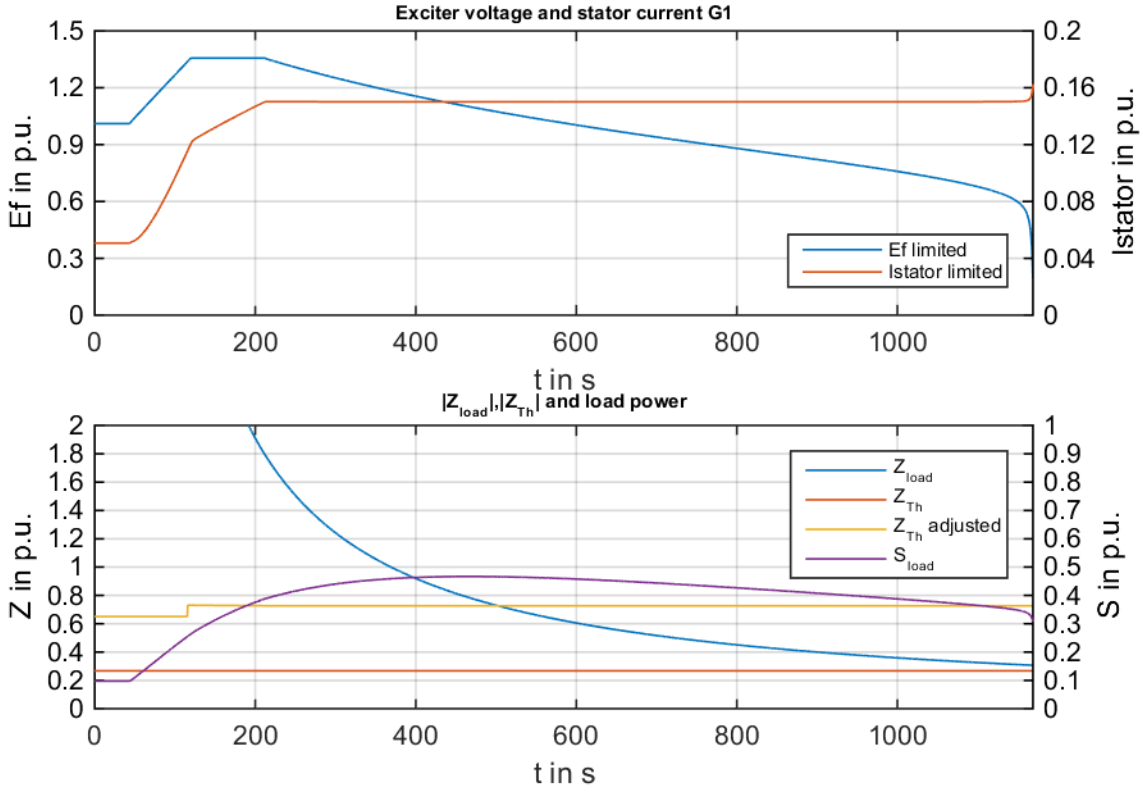

Figure 6-38, P_{SG1} = 0,05 p.u., P_{load} and Q_{load} increasing, 100% resistive load, P_{Load} and Q_{Load} increasing

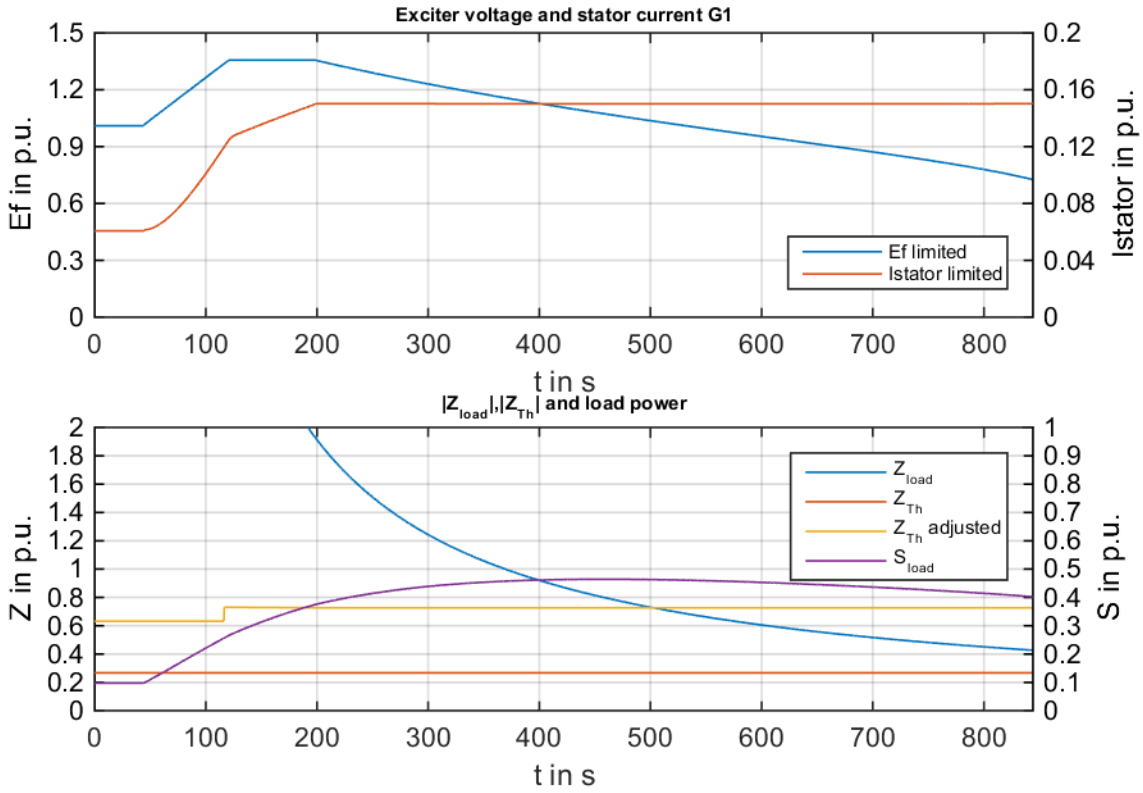

Figure 6-39, P_{SG1} = 0,06 p.u., P_{load} and Q_{load} increasing, 100% resistive load, P_{Load} and Q_{Load} increasing

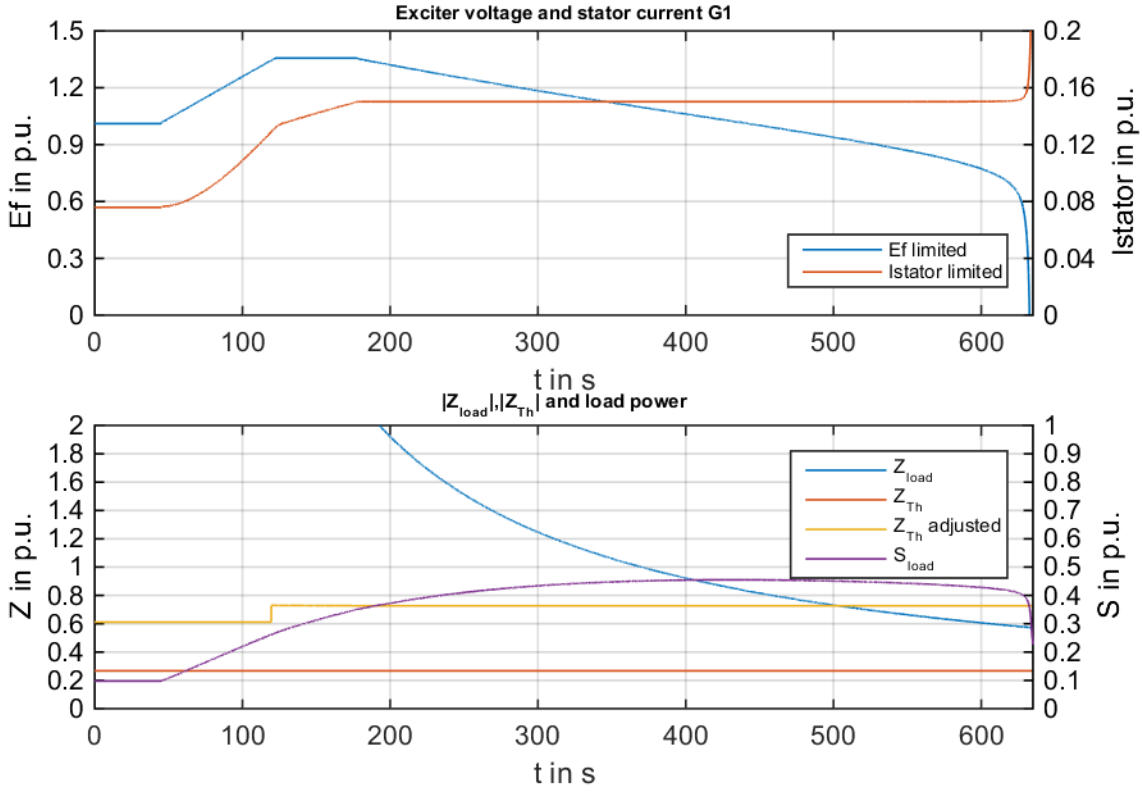

Figure 6-40, P_{SG1} = 0,075 p.u., P_{load} and Q_{load} increasing, 100% resistive load, P_{Load} and Q_{Load} increasing

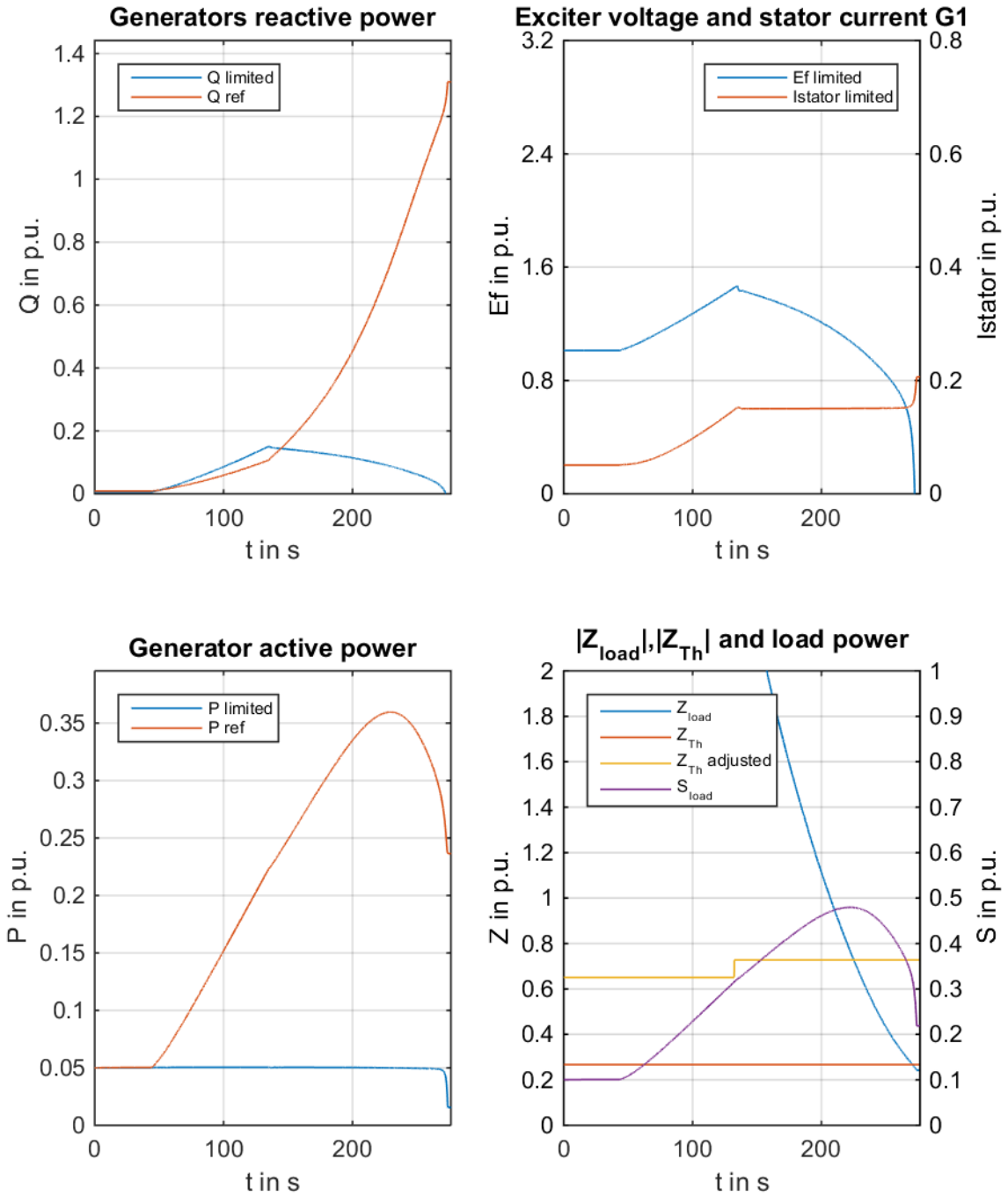

Figure 6-41, $I_{stator,max,SG1}$ = 0,15 p.u., $E_{f,max,SG1}$ = 1,5 p.u., P_{SG1} = 0,05 p.u., P_{Load} and Q_{Load} increased

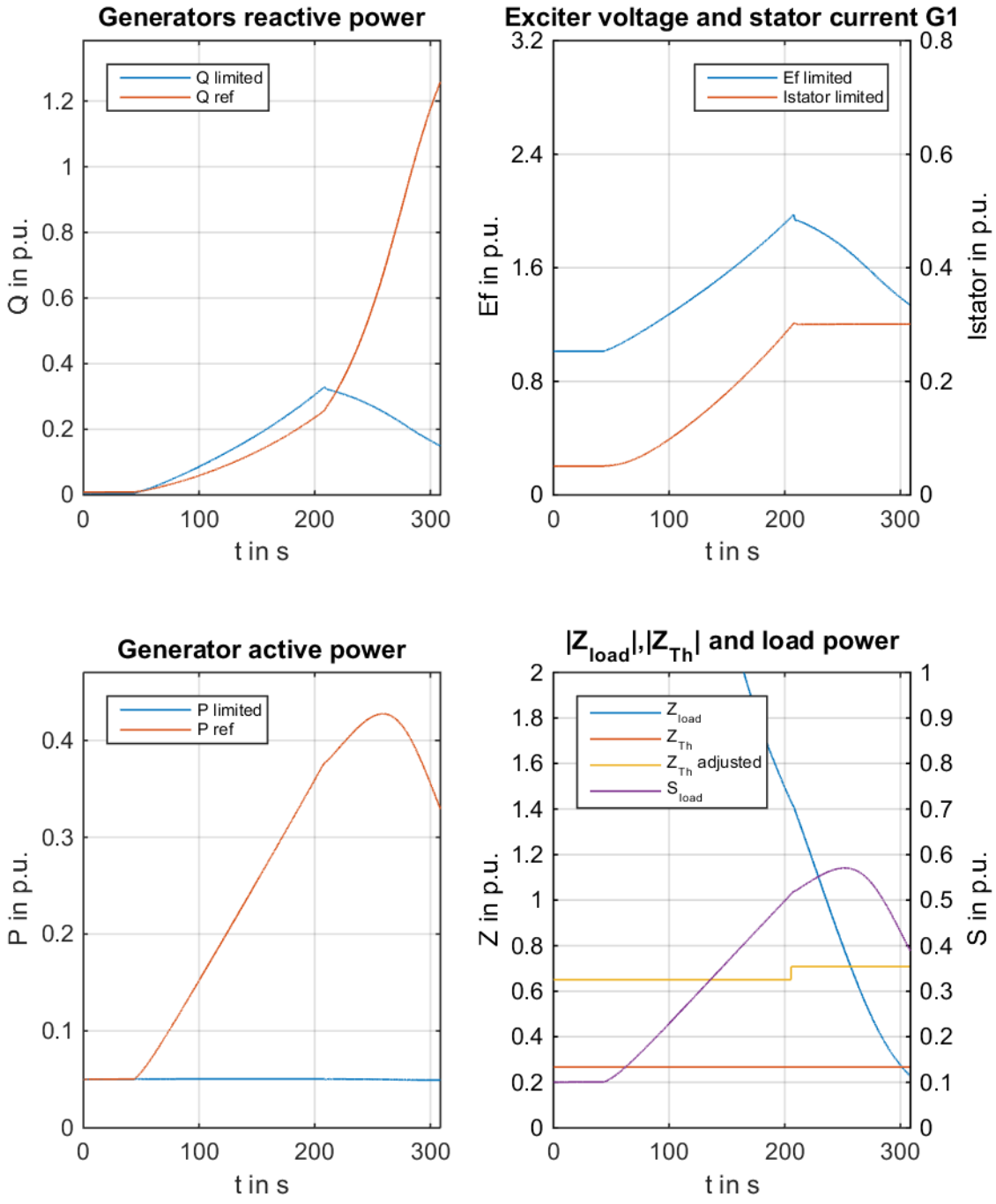

Figure 6-42, $I_{stator,max,SG1}$ = 0,3 p.u., $E_{f,max,SG1}$ = 2,5 p.u., P_{SG1} = 0,05 p.u., P_{Load} and Q_{Load} increased